Year : 2021

Comprehensive characterization of bone properties in knee osteoarthritis using computed tomography

Babel Hugo

Babel Hugo, 2021, Comprehensive characterization of bone properties in knee osteoarthritis using computed tomography

Originally published at : Thesis, University of Lausanne

Posted at the University of Lausanne Open Archive http://serval.unil.ch
Document URN : urn:nbn:ch:serval-BIB_42FB61DB5EAC8

UNIL | Université de Lausanne
Faculté de biologie et de médecine

Département de l'Appareil Locomoteur, Swiss BioMotion Lab

Comprehensive characterization of bone properties in knee osteoarthritis using computed tomography

Thèse de doctorat ès sciences de la vie (PhD)

présentée à la

Faculté de biologie et de médecine
de l'Université de Lausanne

par

Hugo BABEL

M. Sc. in Computational Sciences and Engineering
Ecole Polytechnique Fédérale, Lausanne

Jury

Prof. Grégoire Millet	Président
Prof. Brigitte Jolles-Haeberli	Directrice de thèse
Dr Julien Favre	Co-directeur de thèse
Prof. Bruno Vande Berg	Expert
Dr Jeroen Geurts	Expert
Prof. Henning Müller	Expert

Lausanne
(2021)

UNIL | Université de Lausanne
Faculté de biologie et de médecine

Département de l'Appareil Locomoteur, Swiss BioMotion Lab

Comprehensive characterization of bone properties in knee osteoarthritis using computed tomography

Thèse de doctorat ès sciences de la vie (PhD)

présentée à la

Faculté de biologie et de médecine
de l'Université de Lausanne

par

Hugo BABEL

M. Sc. in Computational Sciences and Engineering
Ecole Polytechnique Fédérale, Lausanne

Jury

Prof. Grégoire Millet	Président
Prof. Brigitte Jolles-Haeberli	Directrice de thèse
Dr Julien Favre	Co-directeur de thèse
Prof. Bruno Vande Berg	Expert
Dr Jeroen Geurts	Expert
Prof. Henning Müller	Expert

Lausanne
(2021)

UNIL | Université de Lausanne
Faculté de biologie et de médecine

Ecole Doctorale
Doctorat ès sciences de la vie

Imprimatur

Vu le rapport présenté par le jury d'examen, composé de

Président·e	Monsieur	Prof.	Grégoire	**Millet**
Directeur·trice de thèse	Madame	Prof.	Brigitte	**Jolles-Haeberli**
Co-directeur·trice	Monsieur	Dr	Julien	**Favre**
Expert·e·s	Monsieur	Prof.	Bruno	**Vande Berg**
	Monsieur	Dr	Jeroen	**Geurts**
	Monsieur	Prof.	Henning	**Müller**

le Conseil de Faculté autorise l'impression de la thèse de

Monsieur Hugo Louis Babel

Master of Science in computational science and engineering,
EPFL - Ecole Polytechnique Fédérale de Lausanne, Suisse

intitulée

Comprehensive characterization of bone properties in knee osteoarthritis using computed tomography

Date de l'examen : 1er avril 2021

Date d'émission de l'imprimatur : Lausanne, le 15 avril 2021

pour le Doyen
de la Faculté de biologie et de médecine

Prof. Niko GELDNER
Directeur de l'Ecole Doctorale

Sitting quietly, doing nothing, Spring comes and the grass rows, by itself.

- Basho

Abstract

Knee osteoarthritis (OA) is a major public health burden and improving disease management will in part depend on the development of enhanced imaging techniques. Knee OA has long been described as simple disruption of cartilage, but is now considered as a disease of the whole joint. As such, a research priority for knee OA is the assessment of all tissues involved in its pathogenesis. In particular, bone alterations have been recognized for their contribution to the pathogenesis of OA, but their exact role is unclear due to current imaging limitations. Notably, the current methods to assess bone properties such as subchondral bone mineral density (sBMD) rely on imaging modalities and analyses that do not support the characterization of spatial variations. As such, implementing computational anatomy algorithms to characterize bone data could improve our understanding of the bone's role in the pathogenesis of OA. Furthermore, recent models in integrated OA research have stressed the role of relationships between components of the knee in maintaining joint homeostasis. Assessing the spatial relationships between components could provide crucial *in vivo* evidence supporting these models. The objective of this thesis was therefore to propose computational anatomy methods allowing a more comprehensive assessment of bone alterations, as well as their spatial relationship to cartilage thickness (CTh), a biomarker for cartilage health. The evaluation of the algorithms' reproducibility indicated their suitability for research and clinical applications. The assessment of sBMD and CTh in knees of various OA severity indicated a coherent pattern of local variations, while the assessment of the relationship provided *in vivo* support for integrated OA models. Overall, this thesis work provided novel bone data, as well as methods that could provide a more comprehensive assessment of the joint status through the characterization of spatial variations in tissue properties.

Résumé

La gonarthrose représente actuellement un problème majeur de santé publique, et l'amélioration de sa prise en charge dépendra en partie de la capacité à améliorer les techniques d'imagerie. Si cette maladie a longtemps été décrite comme une simple destruction du cartilage, elle est maintenant considérée comme une maladie complexe affectant l'ensemble de l'articulation. Une priorité actuelle de la recherche dans ce domaine est l'évaluation de tous les tissus impliqués dans son développement. Les altérations osseuses, en particulier, sont reconnues comme contribuant à la pathogenèse de la maladie, mais leur rôle exact n'est pas clair en raison de limitations actuelles. En particulier, l'évaluation des propriétés de l'os, telle que la densité minérale osseuse sous-chondrale (sBMD), repose sur des modalités d'imagerie et des analyses qui restreignent l'analyse des variations spatiales. Toutefois, l'implémentation d'algorithmes d'anatomie computationnelle permettant l'analyse *in vivo* des propriétés osseuses pourrait aider à clarifier le rôle de l'os dans l'arthrose du genou. De plus, des études physiopathologiques montrent un intérêt croissant pour les relations entre composantes articulaires. La caractérisation de la relation spatiale entre composantes pourrait fournir une confirmation *in* vivo de ces modèles. L'objectif de cette thèse était donc de proposer de nouvelles méthodes permettant d'améliorer la caractérisation des altérations osseuses et de leur relation spatiale avec l'épaisseur du cartilage (CTh), un biomarqueur de la santé du cartilage. L'évaluation du sBMD et du CTh a révélé un pattern cohérent de variations spatiales lié à la gravité de la gonarthrose, tandis que l'évaluation de la relation a fourni un soutien in vivo pour les modèles d'arthrose. Dans l'ensemble, ce travail de thèse a fourni de nouvelles données sur l'os, ainsi que des méthodes qui pourraient améliorer l'évaluation de l'état de l'articulation grâce à la caractérisation des variations spatiales des tissus articulaires.

Acknowledgments

My first thanks go to **Dr Julien Favre**, without whom I would not be the scientist I am today, to **Prof. Jolles-Haeberli**, without whom the Swiss BioMotion Lab (SBML) would not exist, and to **Dr Patrick Omoumi**, for his expertise. My thanks go to **Prof. Grégoire Millet**, **Prof. Bruno Vande Berg**, **Dr. Jeroen Geurts** and **Prof. Henning Müller** for being members of my thesis jury and sharing parts of this journey with me.

Second, deep and sincere thanks to all current colleagues and friends of the SBML: **Baptiste**, **Johann**, **Killian**, **Margaux**, **Shannon**. I have had the privilege of facing all four elements and sharing great moments with you during these past five years.

I would also like to extend my thanks to all the people with whom I have shared mud, snow, dust, rain, storm, sweat, blood, tears… and beautiful landscapes and moments.

Lastly, my gratitude goes to my parents, **Jacques** and **Rachel,** for their unconditional support over the years, and for my sister, **Lucie**, for pushing me to strive.

A mon grand-père, à qui je n'aurai jamais pu vraiment expliquer comment les chirurgiens utilisaient mes équations en salle d'opération.

List of abbreviations

CT	Computed Tomography
CTh	Cartilage Thickness
DXA	Dual-energy X-Ray Absorptiometry
K/L	Kellgren-Lawrence
MRI	Magnetic Resonance Imaging
ROI	Region Of Interest
OA	Osteoarthritis
sBMD	subchondral Bone Mineral Density

List of figures

Content

I Introduction

I.1 Background and motivation

Osteoarthritis (OA) is amongst the leading causes of disability in the world, affecting over 300 million adults around the globe [1-3]. Knee OA, the most common form of OA, is a public health burden as well as a main contributor of pain and impaired mobility in working age adults and the elderly, resulting in a significant decrease in quality of life [4-10]. Furthermore, the impact of this public health burden is expected to increase due to ageing of the population and elevated prevalence of obesity in most societies [6, 11]. Current therapeutic options are limited in their ability to effectively slow down disease progression and mainly focus on alleviating symptoms [11-15]. As such, there is a need to enhance the understanding of the pathophysiology of OA in order to improve disease management [16]. In particular, this will depend on the development of enhanced imaging techniques for the *in vivo* assessment of joint integrity. Furthermore, while cartilage has long been the principal focus of knee OA research, it is now considered as a disease of the whole joint, and pathological features of OA are present in all joint components [16-19].

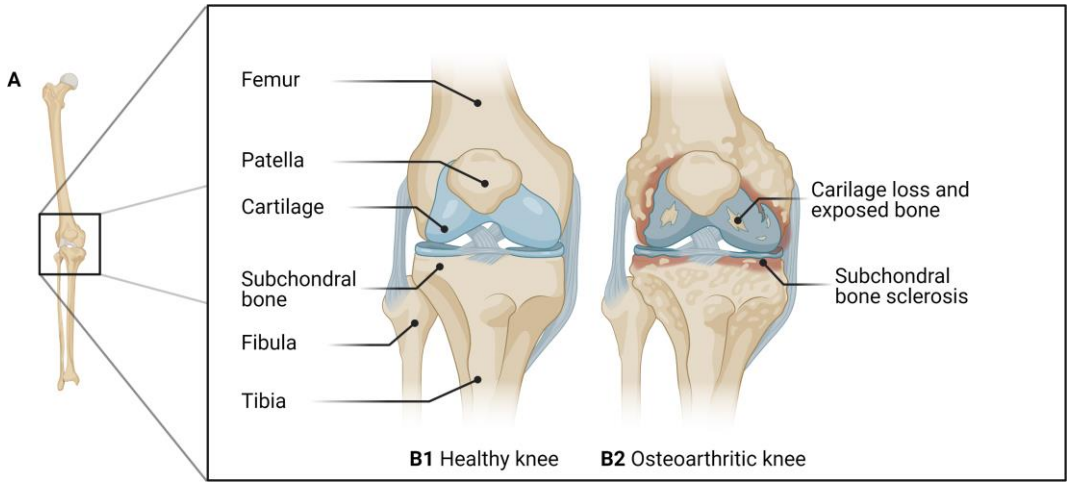

Figure 1 – Representation of a healthy and typical osteoarthritic knee. (A) Right limb of a typical healthy knee (B1) and osteoarthritic knee (B2). Created with BioRender.com

I.2 Bone in knee OA

Bone alterations are a hallmark of knee OA and a central element of the assessment of the radiographic severity of the disease through the Kellgren-Lawrence (K/L) grade [20, 21]. Bone alterations have been recognized for their contribution to the initiation and progression of OA [22, 23]. Indeed, the subchondral bone (Figure 1), located immediately beneath the articular cartilage, plays a key role in distributing forces generated by locomotion and in protecting the knee joint [22, 24]. As such, bone is highly responsive to loading and adapts in ways that maintain conformation of the joint and prevent stress concentrations [22, 25]. The adaptive capabilities of the subchondral bone follow Wolff's law, which states that bone will adapt in response to the loading under which it is subjected [26]. The adaptation of the structural and functional properties of the subchondral bone is achieved through the cellular processes of modeling and remodeling [19, 27].

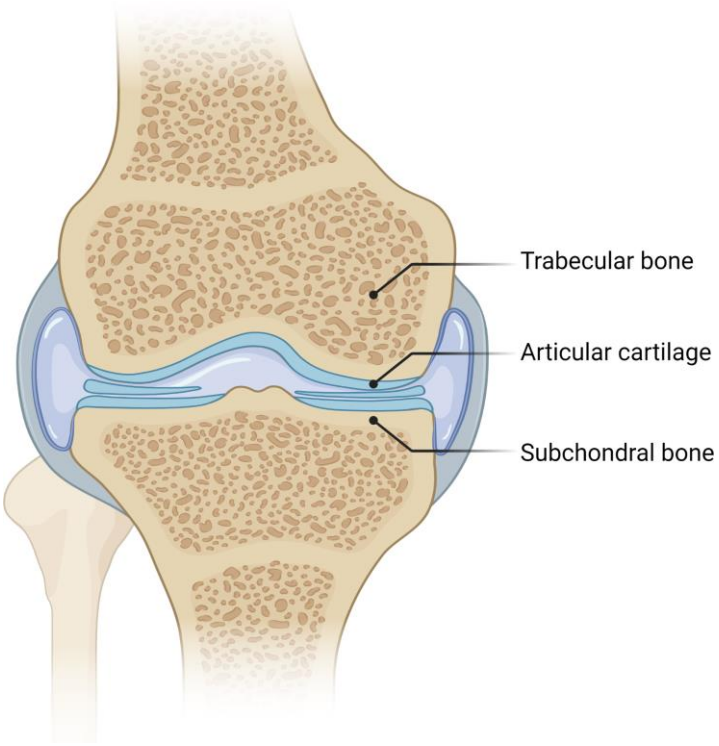

Figure 2 – Bone and cartilage in the knee joint. Created with BioRender.com

The subchondral bone is organized into anatomically distinct components with unique architectural, biological, and mechanical properties (Figure 2) [19, 25, 28]. Adjacent to the cartilage, the subchondral bone plate forms a 0.1-1 mm thick plate-like structure, merging into a structural network of trabecular bone [19, 25, 29-31]. These two bone components play different roles, with the subchondral bone plate providing a hard structural support and the subchondral trabecular bone providing elasticity for shock absorption during joint loading [22]. Changes in each component may affect the health of the joint distinctly and play different roles in knee OA [28, 32]. Specifically, subchondral bone alterations during the course of OA include increased subchondral bone plate thickness, alterations in trabecular bone mass and architecture, osteophytes at the joint margins, as well as bone attrition and bone cysts [19]. In particular, changes in the density and architecture of the subchondral bone environment have a profound effect on both the initiation and progression of cartilage degeneration [33, 34]. Subchondral bone may thus be a potentially

interesting target for OA treatment, due to the prominence of OA-related changes in this component [24, 25, 34]. However, the exact role of subchondral bone in the pathogenesis of OA remains unclear, highlighting the importance of and it is essential to have evaluation tools to define the state of bone [19]. While medical imaging could be used to acquire *in vivo* bone data, most of our understanding of subchondral bone changes in OA comes from *ex vivo* and *in vitro* data, or focuses on end-stage knees [19, 35]. As such, there is a need to obtain *in vivo* bone data in the human knee at various stages of OA [35, 36].

Traditionally, *in vivo* assessment of bone properties in the knee has been mainly achieved using dual-energy X-ray absorptiometry (DXA) [37-41]. However, the sensitivity of DXA to comprehensively characterize bone alterations in the context of OA is limited. Indeed, the two-dimensional nature and low spatial resolution of DXA prohibits the assessment of local variations in bone properties [42]. Furthermore, DXA is unable to distinguish cortical from trabecular bone in the knee, such that DXA has a limited sensitivity to detect changes in trabecular bone [35]. Three-dimensional imaging modalities, such as computed tomography (CT), have been proposed as an alternative to DXA and have the potential to measure important bone parameters *in vivo*, such as subchondral bone mineral density (sBMD) [35, 42-45].

Additionally, in order to conduct a comprehensive three-dimensional assessment of the bone, an anatomical correspondence must be established to remove individual morphological variations, as bones naturally differ in size and shape and further undergo remodeling during the development of OA [46]. Traditionally, this correspondence has been achieved by averaging quantitative measurements inside regions of interest (ROIs) defined based on anatomical or geometrical landmarks [35, 42, 43]. While useful, this ROI-based approach presents a number of limitations. First, average values limit the assessment of spatial variations in the knee joint and may thus reduce the sensitivity to detect

alterations. Indeed, bone properties vary continuously in the femur and the tibia, without intrinsic boundaries [35, 47, 48]. Second, the geometrical or anatomical construction of these ROIs does not match patterns of OA-related alterations as there is evidence that tissue alterations vary spatially within knees of similar disease severity [49].

Establishing a global anatomical correspondence between bones can be achieved using computational anatomy [44]. These methods, initially developed for brain analysis, combine rigid and non-rigid registration to standardize anatomical structures (Figure 3) [44, 50]. More recently, computational anatomy algorithms have been successfully used in the proximal femur for the three-dimensional analysis of bone properties, including sBMD, and the association of spatial patterns with clinical outcomes [44, 51-55]. While such algorithms could provide crucial *in vivo* data to improve our understanding of the role of bone in OA, there is a paucity of computational anatomy methods for the proximal tibia and the distal femur.

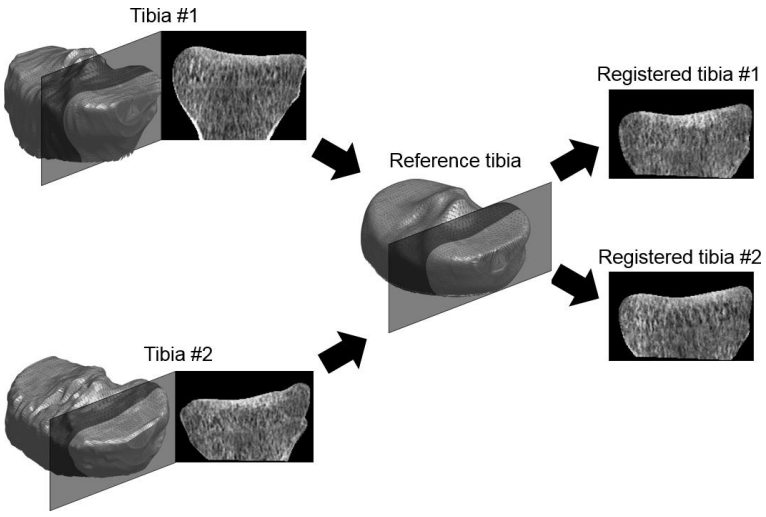

Figure 3 – Illustration of a computational anatomy method for the proximal tibia The surface of individual tibias can be anatomically standardized to a reference tibia, alongside the individual distribution of voxel intensities within the knee.

I.3 Relationships between joint components involved in knee OA

Recent models in integrated OA research have suggested that joint components involved in OA should be considered in the context of the whole joint rather than separately, recognizing the interconnection between these components [56, 57]. In these integrated OA models, joint health depends both on the relationships between its components and on their capacity for mutual adaptation to maintain a healthy homeostasis. In the homeostatic state, articular structures are mutually adapted in what could be described as "healthy" relationships among joint components. Lacking this adaptation, homeostasis is disrupted and these relationships progressively deteriorate, leading to the initiation and progression of the disease [57]. Our understanding of the disease could certainly be improved by considering the relationships between tissue parameters of interest in the pathogenesis of OA. However, integrated knee OA research is an emerging field and further *in vivo* data is needed to confirm the model of mutual adaptation between joint components in non-OA knees as well as its alteration in OA knees [57]. In particular, this could provide valuable data regarding the nature and chronology of alterations within joint components affected by OA as well as implications for the relationships between these joint components. Furthermore, while some relationships have been characterized in non-OA as well as moderate and severe OA, there remains a paucity of studies assessing such relationships in knee spanning all OA severities [58-69].

One such pertinent relationship is between the subchondral bone and articular cartilage, termed the osteochondral unit. Indeed, this functional unit is thought to play a key role in the initiation and progression of the disease, and synergies between the subchondral bone plate, trabecular bone, and articular cartilage support the functional loading of the joint [23, 70, 71]. In addition, there is evidence of physiological interactions as well as biomechanical coupling between bone and cartilage that is conditioned by gait mechanics, with some

authors even suggesting that therapeutic interventions should target both tissues [19, 36, 72-74]. While there is evidence of a greater role played by the bone-cartilage relationship in the pathogenesis of OA than previously thought, the precise mechanisms underlying this interaction and its alteration with knee OA remain unclear, presenting the need for *in vivo* data in the human joint [18, 36, 75, 76].

Although there remains a paucity of studies characterizing bone and cartilage properties within the same knees [65, 68], an inversion of the relationship between cartilage thickness (CTh) and sBMD has recently been reported between non-OA and severe OA femurs [65]. In this study, denser bone was positively associated with thicker cartilage in non-OA knees and negatively associated in radiographic severe OA knees, providing a characterization of the relationship between sBMD and CTh at both endpoints of the disease. However, in order to better understand alterations of these parameters and of their relationship with knee OA development, there is a need to characterize these parameters at all severity stages of the disease. In addition, while the results of this study focused on the magnitude of sBMD and CTh and within ROIs, there is evidence of spatial variations in sBMD and CTh [29, 35, 42, 43, 49, 77-82]. As such, there is an interest to investigate the spatial relationship between these two tissues, as exploiting spatial variations and correlations in tissue parameters could enable the detection of subtle OA-related alterations [83, 84]. In particular, this would enable the characterization of the spatial association between sBMD and CTh within each knee, and the relationship of this association to the OA severity.

Lastly, it is now recognized that the complexity of OA requires the analysis and evaluation of various tissue properties achievable only with multi-modal imaging [85, 86]. Particularly, specific methods are required to establish an anatomical correspondence between images of the same joint acquired using different imaging modalities or obtained with the same modality but using different acquisition parameters [87]. Similarly to

anatomical correspondences between different knees, this standardization has often relied on regions of interest, thus limiting possible analyses and their sensitivity [37, 68, 88, 89]. Other approaches commonly used include the intensity-based global registration of the knee images acquired with different protocols, voxel intensity-based methods, and feature-based registration [87, 90-94]. The analysis of spatial variations in tissue properties usually yield three-dimensional models of the tissues of interest following image segmentations. In particular, these three-dimensional models could be positioned in multiple image sequences based on features specific to the acquisition protocols to allow coordinated measures across multiple parameters and imaging modalities.

I.4 Statement of purpose and aims

The overall aim of this thesis work was to develop new methods to quantify bone properties in the knee joint and to improve the overall understanding of bone alterations with OA disease progression and the relation of these alterations to cartilage properties. To reach these objectives, the thesis is built around two axes:

1. **Development of new image processing methods to analyze tissue properties**

   The first part of this thesis work aimed to introduce computational anatomy methods to allow the comprehensive characterization of spatial variations in bone properties in the distal femur and proximal tibia.

2. **Characterization of bone properties and their relationship with cartilage properties within knees of diverse OA severities**

   The second part of this thesis work aimed to characterize spatial patterns in sBMD and their association with CTh at various stages of medial knee OA severity. In particular, this thesis focused on medial femorotibial OA, the most prevalent form of knee OA [95]

Overall, the aims of this thesis work present a more comprehensive approach to understanding the role of bone alterations and their relationship to cartilage in the pathogenesis of OA.

II
Results

II.1 Summary of the findings

As part of the first axis of this thesis, a computational anatomy method was proposed to establish an anatomical correspondence between proximal tibias, using a combination of rigid and non-rigid registration (Section II.2). This method was then extended to the distal femur and evaluated on cadaveric knees, showing adequate reliability and reproducibility to be used in research and clinical applications (Section II.3). In addition, an expert-supervised multi-modal registration method was proposed (Section II.4), allowing the import of femoral and tibial bones into various imaging modalities of interest in OA and other musculoskeletal pathologies.

In the second axis of this thesis, the relationship between sBMD and CTh was first analyzed by identifying the location of densest BMD and thickest CTh within non-OA femurs. The results indicated a positive correlation along the principal axis of motion of the joint (Section II.5). This spatial association between sBMD and CTh was subsequently characterized in knees of various OA severity (Section II.6). The positive spatial relationship found in non-OA knees decreased progressively with groups of sequential OA severity and became negative in severe OA knees.

The computational anatomy methods presented in this thesis (Section II.2 and II.3) were used to standardize sBMD and CTh to reference models of the distal femur and proximal tibia (Section II.7) and to characterize spatial patterns in CTh, sBMD, and their spatial relationship. The analysis showed distinct patterns forming a coherent succession with

increasing OA severity, including a progressive decrease of the spatial association between sBMD and CTh.

II.2 A registration method for three-dimensional analysis of bone mineral density in the proximal tibia

Babel, H., Wägeli, L., Sonmez, B., Thiran, J. P., Omoumi, P., Jolles, B. M., & Favre, J. (2020). A Registration Method for Three-Dimensional Analysis of Bone Mineral Density in the Proximal Tibia. Journal of Biomechanical Engineering, 143(1).

II.2.a Abstract

Although alterations in bone mineral density (BMD) at the proximal tibia have been suggested to play a role in various musculoskeletal conditions, their pathophysiological implications and their value as markers for diagnosis remain unclear. Improving our understanding of proximal tibial BMD requires novel tools for three-dimensional (3D) analysis of BMD distribution. Three-dimensional imaging is possible with computed tomography (CT), but computational anatomy algorithms are missing to standardize the quantification of 3D proximal tibial BMD, preventing distribution analyses. The objectives of this study were to develop and assess a registration method, suitable with routine knee CT scans, to allow the standardized quantification of 3D BMD distribution in the proximal tibia. Secondly, as an example of application, the study aimed to characterize the distribution of BMD below the tibial cartilages in healthy knees. A method was proposed to register both the surface (vertices) and the content (voxels) of proximal tibias. The method combines rigid transformations to account for differences in bone size and position in the scanner's field of view and to address inconsistencies in the portion of the tibial shaft included in routine CT scan, with a non-rigid transformation locally matching the proximal tibias. The method proved to be highly reproducible and provided a comprehensive description of the relationship between bone depth and BMD. Specifically it reported significantly higher BMD in the first 6mm of bone than deeper in the proximal tibia. In

conclusion, the proposed method offers promising possibilities to analyze BMD and other properties of the tibia in 3D.

II.2.b Personal contribution

Conceptualization, methodology, software, validation, formal analysis, investigation, resources, data curation, writing – original draft preparation, writing – review and editing, visualization, project administration.

II.3 Three-dimensional quantification of bone mineral density in the distal femur and proximal tibia based on computed tomography: in vitro evaluation of an extended standardization method

Babel, H., Omoumi, P., Cosendey, K., Cadas, H., Jolles, B. M., & Favre, J. (2021). Three-Dimensional Quantification of Bone Mineral Density in the Distal Femur and Proximal Tibia Based on Computed Tomography: In Vitro Evaluation of an Extended Standardization Method. Journal of Clinical Medicine, 10(1), 160.

II.3.a Abstract

While alterations in bone mineral density (BMD) are of interest in a number of musculoskeletal conditions affecting the knee, their analysis is limited by a lack of tools able to take full advantage of modern imaging modalities. This study introduced a new method, combining computed tomography (CT) and computational anatomy algorithms, to produce standardized three-dimensional BMD quantification in the distal femur and proximal tibia. The method was evaluated on ten cadaveric knees CT-scanned twice and processed following three different experimental settings to assess the influence of different scans and operators. The median reliability (intraclass correlation coefficient (ICC)) ranged from 0.96 to 0.99 and the median reproducibility (precision error (RMSSD)) ranged from 3.97 to 10.75 mg/cc for the different experimental settings. In conclusion, this paper presented a method to standardize three-dimensional knee BMD with excellent reliability and adequate reproducibility to be used in research and clinical applications. The perspectives offered by this novel method are further reinforced by the fact it relies on conventional CT scan of the knee. The standardization method introduced in this work is not limited to BMD and could be adapted to quantify other bone parameters in three dimensions based on CT images or images acquired using different modalities.

II.3.b Personal contribution

Conceptualization, methodology, software, validation, formal analysis, investigation, resources, data curation, writing – original draft preparation, writing – review and editing, visualization, project administration.

II.4 An Expert-Supervised Registration Method for Multi-Parameter Description of the Knee Joint Using Complementary Imaging Protocols

Original article in preparation for publication

II.4.a Abstract

Knee osteoarthritis being a disease of the entire joint, our pathophysiological understanding could improve with the characterization of the relationships among knee components. Diverse acquisition protocols for magnetic resonance imaging (MRI) and computed tomography (CT) allow capturing numerous parameters of the knee. However, a lack of methods for coordinated measurement of multiple parameters hinders global analyses. This study aimed to design an expert-supervised registration method to facilitate multi-parameter description using complementary acquisition protocols. The method is based on three-dimensional tissue models positioned in the images sets of interest using manually placed attraction points. Two datasets, with ten knees CT-scanned twice and ten knees imaged by CT and MRI, were used to assess the method when registering the distal femur and proximal tibia. The median inter-operator registration errors, quantified using the mean absolute distance and Dice index, were lower than 0.44 mm and higher than 0.97 units, respectively. These values differed by less than 0.1 mm and 0.1 units compared to the errors obtained with gold standard methods. In conclusion, an expert-supervised registration method was introduced. Its capacity to register the distal femur and proximal tibia supports further developments for multi-parameter description of healthy and osteoarthritic knee joints, among other applications.

II.4.b Personal contributions

Conceptualization, methodology, software, validation, formal analysis, investigation, resources, data curation, writing – original draft preparation, writing – review and editing, visualization, project administration.

II.5 New insight on the subchondral bone and cartilage functional unit: Bone mineral density and cartilage thickness are spatially correlated in non-osteoarthritic femoral condyles

Babel, H., Omoumi, P., Andriacchi, T. P., Jolles, B. M., & Favre, J. (2020). New insight on the subchondral bone and cartilage functional unit: Bone mineral density and cartilage thickness are spatially correlated in non-osteoarthritic femoral condyles. Osteoarthritis and Cartilage Open, 2(3), 100079.

II.5.a Abstract

Objective: This study aimed to improve our understanding of the relationship between bone and cartilage by characterizing the morphological coupling between these mechanosensitive tissues exposed to the same mechanical environment within each knee. Specifically, it reanalyzed a prior dataset to test the hypothesis that the locations of thickest cartilage and densest subchondral bone are correlated in non-osteoarthritic femoral condyles.

Method: Anatomically standardized maps of cartilage thickness (CTh) and subchondral bone mineral density (sBMD) were calculated for 50 non-osteoarthritic distal femurs based on computed tomography arthrography examinations. The locations of thickest CTh and densest sBMD were identified in the load-bearing region of the medial and lateral compartments, and correlation analyses were performed to quantify the associations between these locations, with inclusion of age, gender, femoral bone size and femorotibial angle as cofounding variables. Paired Student's t-tests were also performed to compare CTh and sBMD locations.

Results: Locations of thickest CTh and densest sBMD were positively correlated along the anteroposterior direction in both compartments ($r \geq 0.45$, $p \leq 0.001$). Furthermore, thickest CTh was more posterior than densest sBMD in the medial ($p = 0.014$) and lateral

($p < 0.001$) compartments, and more lateral than densest sBMD in the lateral compartment ($p < 0.001$). On average, these location differences were of 1.3, 5.3 and 2.1% of the subchondral bone size.

Conclusion: The positive spatial relationship between the locations of thickest CTh and densest sBMD supports the idea of a functional cartilage/subchondral bone unit with morphological coupling conditioned by the individual loading pattern.

II.5.b Personal contribution

Conceptualization, methodology, software, validation, formal analysis, investigation, resources, data curation, writing – original draft preparation, writing – review and editing, visualization, project administration.

II.6 Decreased adaptation of cartilage thickness (CTh) and bone mineral density (sBMD) spatial variations in osteoarthritic versus non-osteoarthritic knees

Brief report in preparation for publication

II.6.a Abstract

Objective: This study aimed to characterize the spatial relationship between cartilage thickness (CTh) and subchondral bone mineral density (sBMD) for non-osteoarthritic (OA) knees and knees spanning all medial OA severities.

Methods: Anatomically standardized maps of CTh and sBMD were calculated for 51 non-OA (Kellgren and Lawrence (K/L) scores 0-1) and 60 knees of varying severities (K/L 2-4). In addition to the spatial association quantified using Lee's *L*, average CTh and sBMD values were calculated within the load-bearing regions of the femorotibial compartment. Pairwise differences between consecutive groups of increasing OA severity were assessed using Wilcoxon rank-sum tests.

Results: The spatial association between medial CTh and sBMD progressively decreased from positive ($L \geq 0.70$) in non-OA knees, to negative in K/L 4 knees ($L \leq -0.42$), with all differences between groups of sequential severity achieving statistical significance (adjusted $p \leq 0.04$). Average CTh and sBMD measurements exhibited an inconsistent trend of decreasing CTh and increasing sBMD with increasing OA severity which seldom achieved statistical significance.

Conclusion: The study showed a strong positive association between CTh and sBMD in non-OA knees, and a progressive reversal of the relationship with increasing OA severity in the medial femorotibial compartment. In addition, assessing the relationship instead of isolated components presented more consistent patterns. The *in vivo* data bring support to

pathophysiological models of OA based on the disruption of homoeostasis, and highlight the promising potential of assessing spatial variations and relationships to evaluate the osteochondral health and differentiate between disease states.

II.6.b Personal contribution

Conceptualization, methodology, software, validation, formal analysis, investigation, resources, data curation, writing – original draft preparation, writing – review and editing, visualization, project administration.

II.7 Comprehensive description of CTh, sBMD and their association using 3D anatomically standardized maps

Work in progress.

II.7.a Abstract

Purpose: The objective of this study was to characterize spatial variations in cartilage thickness (CTh) and subchondral bone mineral density (sBMD) in knee spanning all osteoarthritis (OA) severities.

Methods: Computed tomography arthrography examinations for 49 non-OA (Kellgren and Lawrence (K/L) scores 0-1) and 77 knees of varying medial OA severity (K/L 2 to 4) were segmented to create three-dimensional bone and cartilage models. Every point of the subchondral bone surface was given a CTh and sBMD value, as well as a measure of the local spatial adaptation (Lee's L_i between CTh and sBMD). The bone models were then anatomically standardized to a reference knee using computational anatomy algorithms. Differences maps and statistical parametric mapping were used to compare the non-OA and the three OA subgroups.

Results: The analysis showed distinct patterns of CTh, sBMD and L_i forming a coherent succession from the non-OA to the K/L 4 subgroups. The femorotibial patterns included thinner medial cartilage, thicker medial and lateral cartilage, higher medial sBMD, and lower Li medially and laterally. Notably, the adaptation between CTh and sBMD progressively decreased from globally positive in non-OA knees to locally negative in K/L 2-4 knees.

Conclusions: This study used computational anatomy algorithms to simultaneously assess spatial patterns in CTh, sBMD, and the relationship between these properties. The

methods were shown to be reproducible, and offer promising possibilities to improve our understanding of bone alterations in the context of integrated OA research.

II.7.b Personal contribution

Conceptualization, methodology, software, validation, formal analysis, investigation, resources, data curation, writing – original draft preparation, writing – review and editing, visualization, project administration.

III
Discussion

Improving the understanding of OA pathogenesis is a key step in developing future effective strategies for disease prevention and treatment. This understanding requires the consideration of the joint in its entirety, precisely understanding not only the role of the individual knee components but also of the relationships between components of the disease [17, 57]. Despite the critical role of bone in the initiation and progression of knee OA, there is a paucity of *in vivo* data regarding bone properties [35, 36]. This thesis aimed to provide new methods to comprehensively characterize bone properties and their alterations with OA, as well as to apply these methods to provide *in vivo* data on alterations in sBMD and their relationship with CTh at various stages of knee OA.

A detailed discussion for each study is provided in annex. The aim of the following sections is to summarize the key results, to broaden the reflection and to provide a more global interpretation of the findings and their implications. Lastly, the limitations of the thesis are discussed, along with possible future research directions.

III.1 Computational anatomy algorithms for the in vivo assessment of bone properties

In the first part of this thesis (Sections II.2, II.3), computational anatomy algorithms were introduced to standardize bone properties in the distal femur and proximal tibia. These algorithms, compatible with routine knee CT scans, depend neither on the acquisition parameters nor on bone size, offering potential application to other imaging modalities. In

addition, the *in silico*, *ex vivo*, and *in vivo* evaluations of the proposed methods ensure their suitability for future clinical and research uses.

The application of the presented procedures to knees of diverse OA severities allowed the characterization of spatial patterns in sBMD related to the radiographic severity of OA (Section II.7). Specifically, higher sBMD in the external aspect of the femorotibial compartment was observed in K/L 2, 3 and 4 compared to the non-OA subgroups. Interestingly, assessing spatial variations in CTh in the same knees suggested that sBMD and CTh alterations did not occur in the same areas, as thinner cartilage was observed more laterally than the locations of higher sBMD in K/L 2 and 3 knees. A possible explanation for these results could come from the differential adaptation of cartilage and bone, in particular to a changing loading environment [19, 96-101]

In contrast to previous studies investigating bone properties within the knee joint using ROIs [35, 42, 43, 92], the methods proposed in this thesis allow the assessment of location-specific patterns. This is particularly important, as ROIs are poorly associated with disease severity, limiting their usefulness in assessing the condition of the joint, and spatial variations in tissue properties were shown to be more sensitive than ROIs [83, 84, 102-104]. Additionally, the low sensitivity of ROIs and redundancy of information between adjacent mean measurements have led to the identification of subsets of measurements, which result in the obfuscation of data from regions in which tissue alterations related to OA are observed [49, 105]. For instance, while ROI-based analyses are usually limited to the femorotibial load-bearing regions [106], the comprehensive analysis of tissue properties provides a broader view of OA-related alterations, including in the posterior aspect of the femoral condyles or in the lateral compartment where alterations were shown to occur [49, 107].

III.2 *In vivo* assessment of the relationship between sBMD and CTh

The second part of this thesis focused on the *in vivo* assessment of the relationship between sBMD and CTh. This assessment was performed inter- and intra-knee for non-OA knees, and intra-knee for OA knees (Figure 3). In non-OA knees, the correlation between the locations of densest sBMD and thickest CTh showed the presence of a positive spatial relationship between sBMD and CTh within the group of knees (Figure 3.A). A measure of bivariate spatial association, Lee's *L*, was then used to globally assess the spatial adaptation between sBMD and CTh within the load-bearing regions of the femorotibial compartments (Figure 3.B) [108]. The positive relationship found within non-OA knees confirmed the inter-knee observations and provided an intra-knee characterization of the spatial relationship. Lastly, a local version of the bivariate measure Lee's L_i, was used to locally assess the spatial adaptation between sBMD and CTh in the neighborhood of each point of the bone-cartilage interface (Figure 3.C), thus allowing the assessment of spatial variations in the intra-knee relationship.

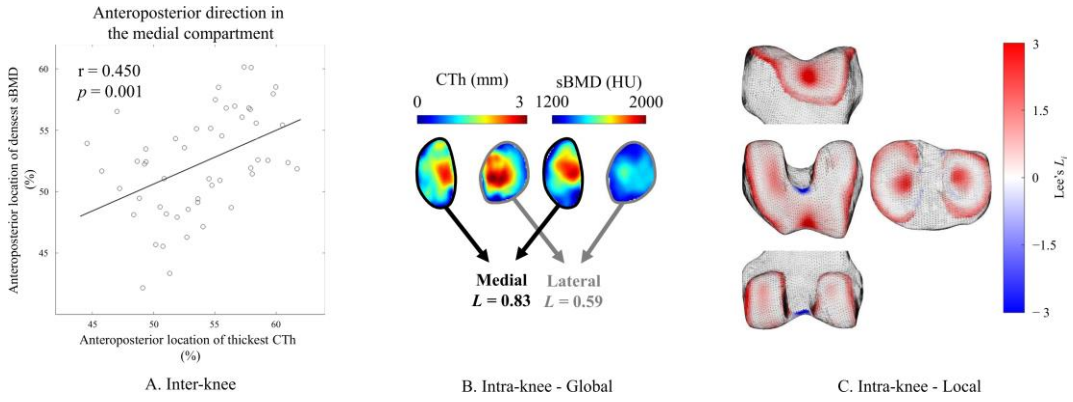

Figure 4 – Summary of the spatial relationship results in non-OA knees. **A**: scatter plot of the location of densest sBMD with respect to the location of thickest CTh along the anteroposterior direction in the medial femoral condyle. **B**: Quantification of the global spatial relationship (Lee's *L*) between sBMD and CTh in the tibial compartments. **C**: Average distribution of the local spatial relationship (Lee's L_i) in the non-OA group.

The intra-knee assessment of the sBMD-CTh relationship in intermediate and severe OA knees indicated a progressive reversal of the relationship with increasing radiographic

severity from a positive relationship in non-OA knees to a negative association in severe OA knees. Interestingly, the reversal of the relationship exhibited local spatial patterns (Section II.7) that were not captured when assessing the relationship within the medial femorotibial compartment (Section II.6). Specifically, the results indicated a local inversion of the relationship quantified using Lee's L_i in K/L 3 knees, while the global negative relationship, quantified using Lee's L, became predominant only in K/L 4 knees. Furthermore, while the global analysis of the relationship within the lateral femorotibial compartment indicated a quasi-constant positive association, the local analysis indicated a decrease in adaptation resulting in a local negative relationship in severe OA knees.

As such, this study presented novel ways to assess the status of the osteochondral unit *in vivo* and highlighted the interest in assessing the relationship between sBMD and CTh. In contrast to separate analyses of sBMD and CTh, differences between consecutive OA grades were found more consistently when assessing the relationship between these two parameters in the medial femorotibial compartment (Section II.6). This is notably due to large variations in sBMD and CTh within knees of similar OA severity [102, 109]. While some studies have tried to account for the individual variations within individual tissues, assessing the relationship between sBMD and CTh allows a natural standardization of inter- and intra-knee variations by exploiting spatial variations rather than magnitudes [42, 67, 104, 110]. Furthermore, the assessment of spatial variations in the relationship allowed the identification of local decreases in adaptation within the lateral femorotibial compartment (Section II.7), which were not detected in either sBMD or CTh maps of the same knees. In particular, this suggests that evaluating the relationship could be more sensitive than individual components and could become a powerful tool to assess the condition of the osteochondral unit as well as to differentiate disease states.

The results of Section II.5-II.7 support the theory that the mechanical environment shared by cartilage and bone in healthy knees results in a coordinated adaptation consisting of thicker cartilage growth and denser bone in areas of greater loading [19, 63, 72, 111]. Additionally, the progressive reversal of the sBMD-CTh relationship supports OA pathophysiology models based on the disruption of homeostasis between articular components [57].

III.3 Limitations

While this thesis offers new insights into bone alterations in knee OA, it also comes with a number of limitations that future research should address to consolidate and broaden this work.

First, the comprehensive characterization of bone properties focused on sBMD and its relationship with CTh. A number of other bone properties are of interest in the pathogenesis of OA and could be assessed using CT imaging [46, 112-115]. While not implemented in this thesis work, the proposed methods could be applied to other properties (see Section III.4 for a more detailed discussion). In particular, their assessment could form the basis for an even more comprehensive characterization of bone properties by aggregating bone data from various sources.

Second, the analysis of OA-related differences relied on a radiographic definition of OA using the K/L grade [20, 21]. However, this radiographic severity has its limitations, including its reliability, an underlying assumption of a linear radiographic progression of OA, an emphasis on the presence of osteophytes as well as poor correlation with OA-related symptom changes [116-123]. Nevertheless, this grading is the gold standard for assessing OA severity currently used for both clinical and research purposes [123, 124].

Third, the design for all *in vivo* study data was retrospective and cross-sectional. Much could be gained by following patients to assess longitudinal changes in sBMD, CTh, and their relationship associated to the initiation and progression of OA. However, the slow progression of the OA disease along with the ethical and safety considerations of exposing otherwise healthy patients to repeated CT radiation highlight the value of a cross-sectional approach as a first step to improving the understanding of the role of bone in the pathogenesis of OA [125-127].

Fourth, while the computational anatomy methods proposed in this work rely on bone surfaces and are thus independent of CT calibration, the *in vivo* bone data was acquired on uncalibrated CT scans. In particular, the attenuation measurements could be biased by non-mineral components of bone such as fat and blood vessels, which are taken into account [45]. Future studies should calibrate the CT data using a calibration phantom as performed in the *ex vivo* evaluation of the methods. However, all examinations were performed on the same scanner using the same acquisition parameters to minimize biases. As such, the absence of calibration should have little effect on the reported patterns but limits data comparisons with studies from other research facilities.

Lastly, the current work relied on semi-manual segmentation that, while remaining a gold standard, is a time-consuming process [128-132]. In particular, the current processing time, from segmentation to anatomical standardization, is not compatible with clinics or applications to large number of knees. This should, however, not be seen as a limitation, as automatic segmentation methods have been proposed for the knee [133].

III.4 Future perspectives

In its entirety, the work presents novel insights into bone properties in the context of the whole joint, in non-OA knees, and in knees at various stages of medial knee OA.

First, the methods implemented in the first part of this thesis open the door to a number of applications providing further quantitative data regarding not only bone and cartilage, but also other tissues undergoing pathological changes with OA. Indeed, in addition to sBMD and CTh, they could be applied to other bone properties (Figure 5), such as bone texture and microarchitecture, osteophytes, and bone shape [46, 112-115, 134, 135] ; to other tissue properties, such as T2 and T1rho relaxation times of cartilage [136-139]; to other pathologies in which femorotibial alterations in knee properties are of interest, such as meniscal damage and repair, osteoporosis, osteogenesis imperfecta, and fractures [37-39, 140-148].

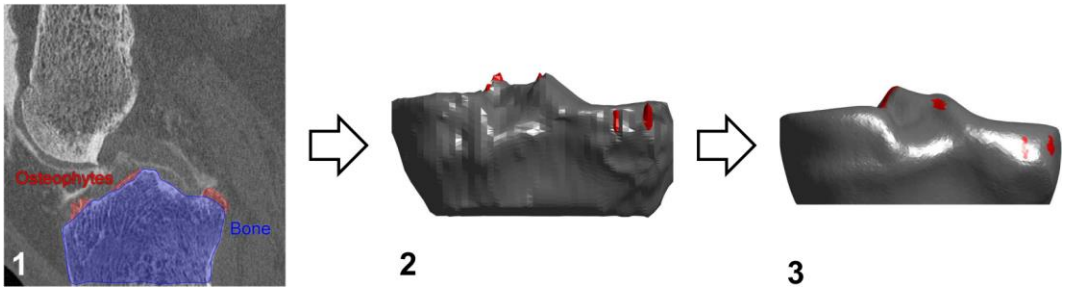

Figure 5 – Example of future possible application to characterize the location of osteophytes by applying the methods proposed in this work [114]. The osteophytes and tibial bone are segmented (**1**) resulting in three-dimensional meshes (**2**). The osteophyte locations are then embedded in the tibial bone mesh, which is registered to the reference tibia (**3**).

In addition to *in vivo* properties assessed via CT, the computational anatomy algorithms presented here could be combined with the expert-supervised multi-modal registration procedure to provide an anatomically standardized assessment of other pathological features of OA across multiple imaging modalities and sequences [149]. In particular, the assessment of alterations to the physiological content of cartilage is of interest in knee OA as a potential target for the earlier detection of pathological changes [150, 151], and MR sequences such as T2 and T1rho can provide *in vivo* data related to proteoglycan and collagen content as well as the integrity of the extracellular matrix [136-139]. However, while the characterization of cartilage composition mainly relies on ROIs [152-154], the

methods proposed in this thesis could allow the assessment of spatial variations in cartilage composition.

Second, application of the proposed methods to other parameters could in turn allow the assessment of relationships between *in vivo* parameters acquired through quantitative imaging [149]. More broadly, addressing osteoarthritis as a disease of the whole joint will require an in-depth analysis of individual components as well as of the relationships between components involved in the initiation and progression of the disease [155]. For instance, the relationship between mechanical loading and tissue properties is of interest in integrated OA research [57]. Indeed, walking mechanics is a key factor in knee OA, constituting the main mechanical stimulation experienced by the knee [56, 96, 97]. However, while spatial correlations between biomechanics and cartilage properties have been reported [63, 67, 153, 154, 156], the assessment of the relationship between bone properties and loading suffers from similar limitations than the assessment of bone [57-59, 66, 69]. Therefore, the methods presented in this thesis work could be applied to provide a more comprehensive assessment of the relationship between sBMD, CTh, and the mechanical environment of the knee joint.

Furthermore, while ROI-based measures of tissue properties exhibit a non-monotonic pattern with increasing OA severity [109, 157-159], the coherent succession of sBMD and CTh patterns reported in this work could be used to score the condition of the osteochondral unit by removing inter-knee variations [160]. For instance, dimensionality reduction techniques [151, 161-165] could be used to identify patterns associated with the initiation and progression of knee OA and to score the condition of a tissue with respect to the severity of the disease or to clinical outcomes in individual components [135, 166-168]. In particular, the development of a score could help harness the potential of spatial variations to improve our understanding of the pathogenesis of OA by providing tools to efficiently

assess the condition of individual components. Specifically, such methods could prove to be more sensitive to OA-related changes than current evaluations [167]. More broadly, the scoring of individual components could be extended to multiple tissues and imaging modalities, for instance using the expert-supervised multi-modal registration proposed in this thesis work, to provide a comprehensive characterization of the joint. Indeed, the methods could be used to create a snapshot of the condition of individual components, of the relationships between components as well as of the joint status, and to assess their evolution over time. Furthermore, the aggregation of large quantities of data could be used to train machine learning algorithms. In particular, spatial variations in multiple tissue properties could be used to improve machine learning algorithms applied to knee OA [84, 169], which seldom rely on quantitative imaging data [155, 169].

III.5 Conclusion

Overall, this work proposed new tools for the comprehensive assessment of individual knee tissue properties and the spatial relationship between tissue properties, and provided an evaluation of the methods for future applications in research and clinics. Applying the proposed method to knees of various OA severity allowed the characterization of spatial patterns in bone and cartilage properties and underscored the potential of these methods by providing *in vivo* bone and cartilage data. In addition, the *in vivo* characterization of the relationship between sBMD and CTh provided evidence supporting the theory of the osteochondral unit as well as integrated OA research. Extending the tools to other variables of interest in the pathogenesis of OA and assessing the spatial relationships between specific pairs could, in turn, provide a comprehensive *in vivo* assessment of joint integrity. More broadly, improving our understanding of the pathogenesis of the disease could help improve disease management and alleviate the burden of knee OA.

IV
Bibliography

1. Safiri, S., et al., *Global, regional and national burden of osteoarthritis 1990-2017: a systematic analysis of the Global Burden of Disease Study 2017.* Ann Rheum Dis, 2020. **79**(6): p. 819-828.
2. Cisternas, M.G., et al., *Alternative Methods for Defining Osteoarthritis and the Impact on Estimating Prevalence in a US Population-Based Survey.* Arthritis Care Res (Hoboken), 2016. **68**(5): p. 574-80.
3. Vos, T., et al., *Global, regional, and national incidence, prevalence, and years lived with disability for 328 diseases and injuries for 195 countries, 1990–2016: a systematic analysis for the Global Burden of Disease Study 2016.* The Lancet, 2017. **390**(10100): p. 1211-1259.
4. Vos, T., et al., *Years lived with disability (YLDs) for 1160 sequelae of 289 diseases and injuries 1990–2010: a systematic analysis for the Global Burden of Disease Study 2010.* The Lancet, 2012. **380**(9859): p. 2163-2196.
5. Grotle, M., et al., *Prevalence and burden of osteoarthritis: results from a population survey in Norway.* J Rheumatol, 2008. **35**(4): p. 677-84.
6. Turkiewicz, A., et al., *Current and future impact of osteoarthritis on health care: a population-based study with projections to year 2032.* Osteoarthritis Cartilage, 2014. **22**(11): p. 1826-32.
7. Rabenda, V., et al., *Direct and indirect costs attributable to osteoarthritis in active subjects.* J Rheumatol, 2006. **33**(6): p. 1152-8.
8. Reginster, J.Y., *The prevalence and burden of arthritis.* Rheumatology (Oxford), 2002. **41 Supp 1**(suppl_1): p. 3-6.
9. Guccione, A.A., et al., *The effects of specific medical conditions on the functional limitations of elders in the Framingham Study.* Am J Public Health, 1994. **84**(3): p. 351-8.
10. Hubertsson, J., et al., *Risk of sick leave and disability pension in working-age women and men with knee osteoarthritis.* Ann Rheum Dis, 2013. **72**(3): p. 401-5.
11. Hunter, D.J., et al., *Developing strategic priorities in osteoarthritis research: Proceedings and recommendations arising from the 2017 Australian Osteoarthritis Summit.* BMC Musculoskelet Disord, 2019. **20**(1): p. 74.
12. Michael, J.W., K.U. Schluter-Brust, and P. Eysel, *The epidemiology, etiology, diagnosis, and treatment of osteoarthritis of the knee.* Dtsch Arztebl Int, 2010. **107**(9): p. 152-62.
13. Felson, D.T., *Osteoarthritis of the knee.* New England Journal of Medicine, 2006. **354**(8): p. 841-848.
14. Matthews, G.L. and D.J. Hunter, *Emerging drugs for osteoarthritis.* Expert Opin Emerg Drugs, 2011. **16**(3): p. 479-91.
15. Felson, D.T., *Osteoarthritis: priorities for osteoarthritis research: much to be done.* Nat Rev Rheumatol, 2014. **10**(8): p. 447-8.
16. Conaghan, P.G., et al., *Osteoarthritis research priorities: a report from a EULAR ad hoc expert committee.* Ann Rheum Dis, 2014. **73**(8): p. 1442-5.
17. Loeser, R.F., et al., *Osteoarthritis: a disease of the joint as an organ.* Arthritis Rheum, 2012. **64**(6): p. 1697-707.
18. Felson, D.T. and T. Neogi, *Osteoarthritis: is it a disease of cartilage or of bone?* Arthritis Rheum, 2004. **50**(2): p. 341-4.
19. Goldring, S.R. and M.B. Goldring, *Changes in the osteochondral unit during osteoarthritis: structure, function and cartilage-bone crosstalk.* Nat Rev Rheumatol, 2016. **12**(11): p. 632-644.
20. Kellgren, J. and J. Lawrence, *Radiological assessment of osteo-arthrosis.* Annals of the rheumatic diseases, 1957. **16**(4): p. 494.
21. Felson, D.T., et al., *Defining radiographic osteoarthritis for the whole knee.* Osteoarthritis and Cartilage, 1997. **5**(4): p. 241-250.

22. Stewart, H.L. and C.E. Kawcak, *The Importance of Subchondral Bone in the Pathophysiology of Osteoarthritis.* Front Vet Sci, 2018. **5**: p. 178.
23. Radin, E.L. and R.M. Rose, *Role of subchondral bone in the initiation and progression of cartilage damage.* Clin Orthop Relat Res, 1986(213): p. 34-40.
24. Castaneda, S., et al., *Subchondral bone as a key target for osteoarthritis treatment.* Biochem Pharmacol, 2012. **83**(3): p. 315-23.
25. Burr, D.B. and M.A. Gallant, *Bone remodelling in osteoarthritis.* Nat Rev Rheumatol, 2012. **8**(11): p. 665-73.
26. Wolff, J., *Das gesetz der transformation der knochen.* A Hirshwald, 1892. **1**: p. 1-152.
27. Goldring, M.B. and S.R. Goldring, *Articular cartilage and subchondral bone in the pathogenesis of osteoarthritis.* Ann N Y Acad Sci, 2010. **1192**: p. 230-7.
28. Burr, D.B., *Anatomy and physiology of the mineralized tissues: role in the pathogenesis of osteoarthrosis.* Osteoarthritis Cartilage, 2004. **12 Suppl A**: p. S20-30.
29. Olah, T., et al., *Topographic modeling of early human osteoarthritis in sheep.* Science Translational Medicine, 2019. **11**(508): p. eaax6775.
30. Kroker, A., et al., *Quantitative in vivo assessment of bone microarchitecture in the human knee using HR-pQCT.* Bone, 2017. **97**: p. 43-48.
31. Bhatla, J., et al., *Differences in subchondral bone plate and cartilage thickness between women with anterior cruciate ligament reconstructions and uninjured controls.* 2018. **26**(7): p. 929-939.
32. Burr, D.B., *The importance of subchondral bone in the progression of osteoarthritis.* J Rheumatol Suppl, 2004. **70**(70): p. 77-80.
33. Bobinac, D., et al., *Changes in articular cartilage and subchondral bone histomorphometry in osteoarthritic knee joints in humans.* Bone, 2003. **32**(3): p. 284-90.
34. Funck-Brentano, T. and M. Cohen-Solal, *Subchondral bone and osteoarthritis.* Curr Opin Rheumatol, 2015. **27**(4): p. 420-6.
35. Bennell, K.L., et al., *Tibial subchondral trabecular volumetric bone density in medial knee joint osteoarthritis using peripheral quantitative computed tomography technology.* Arthritis Rheum, 2008. **58**(9): p. 2776-85.
36. Findlay, D.M. and J.S. Kuliwaba, *Bone–cartilage crosstalk: a conversation for understanding osteoarthritis.* Bone research, 2016. **4**: p. 16028.
37. Lo, G.H., et al., *Meniscal damage associated with increased local subchondral bone mineral density: a Framingham study.* Osteoarthritis Cartilage, 2008. **16**(2): p. 261-7.
38. van der Wal, R.J.P., et al., *Two-year follow-up of bone mineral density changes in the knee after meniscal allograft transplantation: Results of an explorative study.* Knee, 2018. **25**(6): p. 1091-1099.
39. Bousson, V., et al., *Trabecular bone score (TBS): available knowledge, clinical relevance, and future prospects.* Osteoporos Int, 2012. **23**(5): p. 1489-501.
40. Hulet, C., et al., *Distribution of bone mineral density at the proximal tibia in knee osteoarthritis.* Calcif Tissue Int, 2002. **71**(4): p. 315-22.
41. Lo, G.H., et al., *The ratio of medial to lateral tibial plateau bone mineral density and compartment-specific tibiofemoral osteoarthritis.* Osteoarthritis Cartilage, 2006. **14**(10): p. 984-90.
42. Omoumi, P., et al., *Quantitative regional and sub-regional analysis of femoral and tibial subchondral bone mineral density (sBMD) using computed tomography (CT): comparison of non-osteoarthritic (OA) and severe OA knees.* Osteoarthritis Cartilage, 2017. **25**(11): p. 1850-1857.
43. Johnston, J.D., B.A. Masri, and D.R. Wilson, *Computed tomography topographic mapping of subchondral density (CT-TOMASD) in osteoarthritic and normal knees: methodological development and preliminary findings.* Osteoarthritis Cartilage, 2009. **17**(10): p. 1319-26.
44. Carballido-Gamio, J. and D.P. Nicolella, *Computational anatomy in the study of bone structure.* Curr Osteoporos Rep, 2013. **11**(3): p. 237-45.
45. Bousson, V., et al., *CT imaging for the investigation of subchondral bone in knee osteoarthritis.* Osteoporos Int, 2012. **23 Suppl 8**: p. S861-5.
46. Hunter, D., et al., *Longitudinal validation of periarticular bone area and 3D shape as biomarkers for knee OA progression? Data from the FNIH OA Biomarkers Consortium.* Annals of the rheumatic diseases, 2016. **75**(9): p. 1607-1614.
47. Johnston, J.D., et al., *A comparison of conventional maximum intensity projection with a new depth-specific topographic mapping technique in the CT analysis of proximal tibial subchondral bone density.* Skeletal Radiol, 2010. **39**(9): p. 867-76.
48. Carballido-Gamio, J., et al., *Proximal femoral density distribution and structure in relation to age and hip fracture risk in women.* J Bone Miner Res, 2013. **28**(3): p. 537-46.

49. Favre, J., et al., *Anatomically Standardized Maps Reveal Distinct Patterns of Cartilage Thickness With Increasing Severity of Medial Compartment Knee Osteoarthritis.* J Orthop Res, 2017. **35**(11): p. 2442-2451.
50. Grenander, U. and M.I. Miller, *Computational anatomy: An emerging discipline.* Quarterly of Applied Mathematics, 1998. **56**(4): p. 617-694.
51. Li, W., et al. *Hip fracture risk estimation based on principal component analysis of QCT atlas: a preliminary study*. in *Medical Imaging 2009: Biomedical Applications in Molecular, Structural, and Functional Imaging*. 2009. International Society for Optics and Photonics.
52. Li, W., et al., *Voxel-based modeling and quantification of the proximal femur using inter-subject registration of quantitative CT images.* Bone, 2007. **41**(5): p. 888-95.
53. Li, W., et al., *Identify fracture-critical regions inside the proximal femur using statistical parametric mapping.* Bone, 2009. **44**(4): p. 596-602.
54. Bredbenner, T.L., et al., *Fracture risk predictions based on statistical shape and density modeling of the proximal femur.* J Bone Miner Res, 2014. **29**(9): p. 2090-100.
55. Marangalou, J.H., et al., *Inter-individual variability of bone density and morphology distribution in the proximal femur and T12 vertebra.* Bone, 2014. **60**: p. 213-220.
56. Andriacchi, T.P., et al., *A systems view of risk factors for knee osteoarthritis reveals insights into the pathogenesis of the disease.* Ann Biomed Eng, 2015. **43**(2): p. 376-87.
57. Edd, S.N., et al., *Modeling knee osteoarthritis pathophysiology using an integrated joint system (IJS): a systematic review of relationships among cartilage thickness, gait mechanics, and subchondral bone mineral density.* Osteoarthritis Cartilage, 2018. **26**(11): p. 1425-1437.
58. Hudson, D., T. Royer, and J. Richards, *Bone mineral density of the proximal tibia relates to axial torsion in the lower limb.* Gait Posture, 2007. **26**(3): p. 446-51.
59. Hurwitz, D.E., et al., *Dynamic knee loads during gait predict proximal tibial bone distribution.* J Biomech, 1998. **31**(5): p. 423-30.
60. Blazek, K., et al., *Age and obesity alter the relationship between femoral articular cartilage thickness and ambulatory loads in individuals without osteoarthritis.* J Orthop Res, 2014. **32**(3): p. 394-402.
61. Koo, S. and T.P. Andriacchi, *A comparison of the influence of global functional loads vs. local contact anatomy on articular cartilage thickness at the knee.* J Biomech, 2007. **40**(13): p. 2961-6.
62. Koo, S., J.H. Rylander, and T.P. Andriacchi, *Knee joint kinematics during walking influences the spatial cartilage thickness distribution in the knee.* J Biomech, 2011. **44**(7): p. 1405-9.
63. Scanlan, S.F., J. Favre, and T.P. Andriacchi, *The relationship between peak knee extension at heel-strike of walking and the location of thickest femoral cartilage in ACL reconstructed and healthy contralateral knees.* J Biomech, 2013. **46**(5): p. 849-54.
64. Babel, H., et al., *New insight on the subchondral bone and cartilage functional unit: bone mineral density and cartilage thickness are spatially correlated in non-osteoarthritic femoral condyles.* Osteoarthritis Cartilage Open, 2020: p. 100079.
65. Omoumi, P., et al., *Relationships between cartilage thickness and subchondral bone mineral density in non-osteoarthritic and severely osteoarthritic knees: In vivo concomitant 3D analysis using CT arthrography.* Osteoarthritis Cartilage, 2019. **27**(4): p. 621-629.
66. Thorp, L.E., et al., *Bone mineral density in the proximal tibia varies as a function of static alignment and knee adduction angular momentum in individuals with medial knee osteoarthritis.* Bone, 2006. **39**(5): p. 1116-1122.
67. Erhart-Hledik, J.C., J. Favre, and T.P. Andriacchi, *New insight in the relationship between regional patterns of knee cartilage thickness, osteoarthritis disease severity, and gait mechanics.* J Biomech, 2015. **48**(14): p. 3868-75.
68. Cao, Y., et al., *Cross-sectional and longitudinal associations between systemic, subchondral bone mineral density and knee cartilage thickness in older adults with or without radiographic osteoarthritis.* Ann Rheum Dis, 2014. **73**(11): p. 2003-9.
69. Wada, M., et al., *Relationships among bone mineral densities, static alignment and dynamic load in patients with medial compartment knee osteoarthritis.* Rheumatology (Oxford), 2001. **40**(5): p. 499-505.
70. Madry, H., F.P. Luyten, and A. Facchini, *Biological aspects of early osteoarthritis.* Knee Surg Sports Traumatol Arthrosc, 2012. **20**(3): p. 407-22.
71. Gomoll, A.H. and J. Farr, *The osteochondral unit*, in *Cartilage Restoration*. 2014, Springer. p. 9-15.
72. Imhof, H., et al., *Subchondral bone and cartilage disease: a rediscovered functional unit.* Invest Radiol, 2000. **35**(10): p. 581-8.

73. Andriacchi, T.P., S. Koo, and S.F. Scanlan, *Gait mechanics influence healthy cartilage morphology and osteoarthritis of the knee.* J Bone Joint Surg Am, 2009. **91 Suppl 1**: p. 95-101.
74. Karsdal, M., et al., *The coupling of bone and cartilage turnover in osteoarthritis: opportunities for bone antiresorptives and anabolics as potential treatments?* Annals of the rheumatic diseases, 2013: p. annrheumdis-2013-204111.
75. Karsdal, M.A., et al., *The coupling of bone and cartilage turnover in osteoarthritis: opportunities for bone antiresorptives and anabolics as potential treatments?* Ann Rheum Dis, 2014. **73**(2): p. 336-48.
76. Lories, R.J. and F.P. Luyten, *The bone-cartilage unit in osteoarthritis.* Nat Rev Rheumatol, 2011. **7**(1): p. 43-9.
77. Terukina, M., et al., *Analysis of the thickness and curvature of articular cartilage of the femoral condyle.* Arthroscopy, 2003. **19**(9): p. 969-73.
78. Cohen, Z.A., et al., *Knee cartilage topography, thickness, and contact areas from MRI: in-vitro calibration and in-vivo measurements.* Osteoarthritis Cartilage, 1999. **7**(1): p. 95-109.
79. Cohen, Z.A., et al., *Templates of the cartilage layers of the patellofemoral joint and their use in the assessment of osteoarthritic cartilage damage.* Osteoarthritis and Cartilage, 2003. **11**(8): p. 569-579.
80. Li, G., et al., *The cartilage thickness distribution in the tibiofemoral joint and its correlation with cartilage-to-cartilage contact.* Clin Biomech (Bristol, Avon), 2005. **20**(7): p. 736-44.
81. Armstrong, S.J., R.A. Read, and R. Price, *Topographical Variation within the Articular-Cartilage and Subchondral Bone of the Normal Ovine Knee-Joint - a Histological Approach.* Osteoarthritis and Cartilage, 1995. **3**(1): p. 25-33.
82. Phillips, A., et al., *Topographic Bone Density of the Radius and Ulna in Greyhounds and Labrador Retrievers With and Without Medial Coronoid Process Disease.* Veterinary Surgery, 2015. **44**(2): p. 180-190.
83. Favre, J., et al., *Patterns of femoral cartilage thickness are different in asymptomatic and osteoarthritic knees and can be used to detect disease-related differences between samples.* J Biomech Eng, 2013. **135**(10): p. 101002-10.
84. Pedoia, V., et al., *Diagnosing osteoarthritis from T2 maps using deep learning: an analysis of the entire Osteoarthritis Initiative baseline cohort.* Osteoarthritis and cartilage, 2019. **27**(7): p. 1002-1010.
85. Hayashi, D., F.W. Roemer, and A. Guermazi, *Recent advances in research imaging of osteoarthritis with focus on MRI, ultrasound and hybrid imaging.* Clin Exp Rheumatol, 2018. **36 Suppl 114**(5): p. 43-52.
86. Peterfy, C.G., et al., *MRI protocols for whole-organ assessment of the knee in osteoarthritis.* Osteoarthritis Cartilage, 2006. **14 Suppl A**: p. A95-111.
87. Oliveira, F.P. and J.M. Tavares, *Medical image registration: a review.* Comput Methods Biomech Biomed Engin, 2014. **17**(2): p. 73-93.
88. Lo, G.H., et al., *Bone marrow lesions in the knee are associated with increased local bone density.* Arthritis Rheum, 2005. **52**(9): p. 2814-21.
89. Williams, A., C.S. Winalski, and C.R. Chu, *Early articular cartilage MRI T2 changes after anterior cruciate ligament reconstruction correlate with later changes in T2 and cartilage thickness.* J Orthop Res, 2017. **35**(3): p. 699-706.
90. Li, X., et al., *In vivo T(1rho) and T(2) mapping of articular cartilage in osteoarthritis of the knee using 3 T MRI.* Osteoarthritis Cartilage, 2007. **15**(7): p. 789-97.
91. Carballido-Gamio, J., et al., *Spatial analysis of magnetic resonance T1rho and T2 relaxation times improves classification between subjects with and without osteoarthritis.* Med Phys, 2009. **36**(9): p. 4059-67.
92. Lowitz, T., et al., *Bone marrow lesions identified by MRI in knee osteoarthritis are associated with locally increased bone mineral density measured by QCT.* Osteoarthritis Cartilage, 2013. **21**(7): p. 957-64.
93. Li, X., et al., *Spatial distribution and relationship of T1ρ and T2 relaxation times in knee cartilage with osteoarthritis.* Magnetic Resonance in Medicine: An Official Journal of the International Society for Magnetic Resonance in Medicine, 2009. **61**(6): p. 1310-1318.
94. Pluim, J.P.W., J.B.A. Maintz, and M.A. Viergever, *Mutual-information-based registration of medical images: a survey.* IEEE transactions on medical imaging, 2003. **22**(8): p. 986-1004.
95. Felson, D.T., et al., *High prevalence of lateral knee osteoarthritis in Beijing Chinese compared with Framingham Caucasian subjects.* Arthritis & Rheumatism, 2002. **46**(5): p. 1217-1222.

96. Andriacchi, T.P., et al., *A framework for the in vivo pathomechanics of osteoarthritis at the knee.* Annals of Biomedical Engineering, 2004. **32**(3): p. 447-457.
97. Andriacchi, T.P. and J. Favre, *The Nature of In Vivo Mechanical Signals That Influence Cartilage Health and Progression to Knee Osteoarthritis.* Current rheumatology reports, 2014. **16**(11): p. 463.
98. Saari, T., et al., *Knee kinematics in medial arthrosis. Dynamic radiostereometry during active extension and weight-bearing.* Journal of Biomechanics, 2005. **38**(2): p. 285-292.
99. Hunter, D.J., L. Sharma, and T. Skaife, *Alignment and osteoarthritis of the knee.* JBJS, 2009. **91**(Supplement_1): p. 85-89.
100. Sharma, L., et al., *The role of knee alignment in disease progression and functional decline in knee osteoarthritis.* Jama, 2001. **286**(2): p. 188-195.
101. Sharma, L., *The role of varus and valgus alignment in knee osteoarthritis.* Arthritis & Rheumatism, 2007. **56**(4): p. 1044-1047.
102. Frobell, R.B., et al., *Femorotibial subchondral bone area and regional cartilage thickness: a cross-sectional description in healthy reference cases and various radiographic stages of osteoarthritis in 1,003 knees from the Osteoarthritis Initiative.* Arthritis Care Res (Hoboken), 2010. **62**(11): p. 1612-23.
103. Le Graverand, M.P., et al., *Change in regional cartilage morphology and joint space width in osteoarthritis participants versus healthy controls: a multicentre study using 3.0 Tesla MRI and Lyon-Schuss radiography.* Ann Rheum Dis, 2010. **69**(1): p. 155-62.
104. Buck, R.J., et al., *Does the use of ordered values of subregional change in cartilage thickness improve the detection of disease progression in longitudinal studies of osteoarthritis?* Arthritis Rheum, 2009. **61**(7): p. 917-24.
105. Buck, R.J., et al., *An efficient subset of morphological measures for articular cartilage in the healthy and diseased human knee.* Magn Reson Med, 2010. **63**(3): p. 680-90.
106. Wirth, W. and F. Eckstein, *A technique for regional analysis of femorotibial cartilage thickness based on quantitative magnetic resonance imaging.* IEEE Trans Med Imaging, 2008. **27**(6): p. 737-44.
107. Omoumi, P., et al., *Cartilage can be thicker in advanced osteoarthritic knees: a tridimensional quantitative analysis of cartilage thickness at posterior aspect of femoral condyles.* The British journal of radiology, 2018. **91**(xxxx): p. 20170729.
108. Lee, S.-I., *Developing a bivariate spatial association measure: an integration of Pearson's r and Moran's I.* Journal of geographical systems, 2001. **3**(4): p. 369-385.
109. Hellio Le Graverand, M.P., et al., *Subregional femorotibial cartilage morphology in women--comparison between healthy controls and participants with different grades of radiographic knee osteoarthritis.* Osteoarthritis Cartilage, 2009. **17**(9): p. 1177-85.
110. Chehab, E.F., et al., *Baseline knee adduction and flexion moments during walking are both associated with 5 year cartilage changes in patients with medial knee osteoarthritis.* Osteoarthritis Cartilage, 2014. **22**(11): p. 1833-9.
111. Turner, C., *Three rules for bone adaptation to mechanical stimuli.* Bone, 1998. **23**(5): p. 399-407.
112. MacKay, J.W., et al., *Association of subchondral bone texture on magnetic resonance imaging with radiographic knee osteoarthritis progression: data from the Osteoarthritis Initiative Bone Ancillary Study.* Eur Radiol, 2018. **28**(11): p. 4687-4695.
113. Showalter, C., et al., *Three-dimensional texture analysis of cancellous bone cores evaluated at clinical CT resolutions.* Osteoporosis International, 2006. **17**(2): p. 259-266.
114. Babel, H., et al. *The Location Of Tibial Osteophytes Is Patient-Specific In Severe Osteoarthritis*. in *Orthopaedic Proceedings*. 2018. The British Editorial Society of Bone & Joint Surgery.
115. Neogi, T. and D.T. Felson, *Osteoarthritis: Bone as an imaging biomarker and treatment target in OA.* Nat Rev Rheumatol, 2016. **12**(9): p. 503-4.
116. Kohn, M.D., A.A. Sassoon, and N.D. Fernando, *Classifications in Brief: Kellgren-Lawrence Classification of Osteoarthritis.* Clin Orthop Relat Res, 2016. **474**(8): p. 1886-93.
117. Riddle, D.L., W.A. Jiranek, and J.R. Hull, *Validity and reliability of radiographic knee osteoarthritis measures by arthroplasty surgeons.* Orthopedics, 2013. **36**(1): p. e25-32.
118. Scott Jr, W.W., et al., *Reliability of grading scales for individual radiographic features of osteoarthritis of the knee. The Baltimore longitudinal study of aging atlas of knee osteoarthritis.* Investigative radiology, 1993. **28**(6): p. 497-501.
119. Sheehy, L. and T.D.V. Cooke, *Radiographic assessment of leg alignment and grading of knee osteoarthritis: A critical review.* World, 2015. **2**.

120. Wright, R.W. and M. Group, *Osteoarthritis Classification Scales: Interobserver Reliability and Arthroscopic Correlation.* J Bone Joint Surg Am, 2014. **96**(14): p. 1145-1151.
121. Tiulpin, A., et al., *Automatic Knee Osteoarthritis Diagnosis from Plain Radiographs: A Deep Learning-Based Approach.* Sci Rep, 2018. **8**(1): p. 1727.
122. Spector, T.D. and C. Cooper, *Radiographic assessment of osteoarthritis in population studies: whither Kellgren and Lawrence?* Osteoarthritis Cartilage, 1993. **1**(4): p. 203-6.
123. Roemer, F.W., et al., *The role of imaging in osteoarthritis.* Best Pract Res Clin Rheumatol, 2014. **28**(1): p. 31-60.
124. Guermazi, A., et al., *Imaging in osteoarthritis.* Rheumatic Disease Clinics of North America, 2008. **34**(3): p. 645-687.
125. Emrani, P.S., et al., *Joint space narrowing and Kellgren–Lawrence progression in knee osteoarthritis: an analytic literature synthesis.* Osteoarthritis and Cartilage, 2008. **16**(8): p. 873-882.
126. Brenner, D.J. and E.J. Hall, *Computed tomography—an increasing source of radiation exposure.* New England Journal of Medicine, 2007. **357**(22): p. 2277-2284.
127. Littman, B.H. and S.A. Williams, *The ultimate model organism: progress in experimental medicine.* Nature Reviews Drug Discovery, 2005. **4**(8): p. 631-638.
128. Ahn, C., et al., *Fully automated, level set-based segmentation for knee MRIs using an adaptive force function and template: data from the osteoarthritis initiative.* Biomed Eng Online, 2016. **15**(1): p. 99.
129. Tack, A., A. Mukhopadhyay, and S. Zachow, *Knee menisci segmentation using convolutional neural networks: data from the Osteoarthritis Initiative.* Osteoarthritis and Cartilage, 2018. **26**(5): p. 680-688.
130. Kapur, T., et al. *Model-based segmentation of clinical knee MRI*. in *Proc. IEEE Int'l Workshop on Model-Based 3D Image Analysis*. 1998.
131. Dam, E.B., et al., *Automatic segmentation of high- and low-field knee MRIs using knee image quantification with data from the osteoarthritis initiative.* J Med Imaging (Bellingham), 2015. **2**(2): p. 024001.
132. Shim, H., et al., *Knee cartilage: efficient and reproducible segmentation on high-spatial-resolution MR images with the semiautomated graph-cut algorithm method.* Radiology, 2009. **251**(2): p. 548-56.
133. Taddei, F., et al., *Subject-specific finite element models of long bones: an in vitro evaluation of the overall accuracy.* Journal of biomechanics, 2006. **39**(13): p. 2457-2467.
134. Depeursinge, A., et al., *Three-dimensional solid texture analysis in biomedical imaging: review and opportunities.* Med Image Anal, 2014. **18**(1): p. 176-96.
135. Neogi, T., et al., *Magnetic resonance imaging-based three-dimensional bone shape of the knee predicts onset of knee osteoarthritis: data from the osteoarthritis initiative.* Arthritis Rheum, 2013. **65**(8): p. 2048-58.
136. Mosher, T.J. and B.J. Dardzinski. *Cartilage MRI T 2 relaxation time mapping: overview and applications*. in *Seminars in musculoskeletal radiology*. 2004.
137. David-Vaudey, E., et al., *T2 relaxation time measurements in osteoarthritis.* Magn Reson Imaging, 2004. **22**(5): p. 673-82.
138. Akella, S.V., et al., *Proteoglycan-induced changes in T1ρ-relaxation of articular cartilage at 4T.* Magnetic resonance in medicine, 2001. **46**(3): p. 419-423.
139. Liess, C., et al., *Detection of changes in cartilage water content using MRI T2-mapping in vivo.* Osteoarthritis and cartilage, 2002. **10**(12): p. 907-913.
140. Bayar, A., et al., *Regional bone density changes in anterior cruciate ligament deficient knees: a DEXA study.* Knee, 2008. **15**(5): p. 373-7.
141. van Meer, B.L., et al., *Bone mineral density changes in the knee following anterior cruciate ligament rupture.* Osteoarthritis Cartilage, 2014. **22**(1): p. 154-61.
142. Edwards, W.B., T.J. Schnitzer, and K.L. Troy, *Bone mineral and stiffness loss at the distal femur and proximal tibia in acute spinal cord injury.* Osteoporos Int, 2014. **25**(3): p. 1005-15.
143. Garland, D.E., et al., *Osteoporosis after spinal cord injury.* J Orthop Res, 1992. **10**(3): p. 371-8.
144. Shi, M., et al., *Effect of bisphosphonates on periprosthetic bone loss after total knee arthroplasty: a meta-analysis of randomized controlled trials.* BMC Musculoskelet Disord, 2018. **19**(1): p. 177.
145. Winther, N., et al., *Changes in bone mineral density of the proximal tibia after uncemented total knee arthroplasty. A prospective randomized study.* Int Orthop, 2016. **40**(2): p. 285-94.

146. Henderson, R.C., et al., *The relationship between fractures and DXA measures of BMD in the distal femur of children and adolescents with cerebral palsy or muscular dystrophy.* J Bone Miner Res, 2010. **25**(3): p. 520-6.
147. Petersen, M.M., et al., *Changes in bone mineral density of the distal femur following uncemented total knee arthroplasty.* J Arthroplasty, 1995. **10**(1): p. 7-11.
148. Petersen, M.M., et al., *Late changes in bone mineral density of the proximal tibia following total or partial medial meniscectomy. A randomized study.* J Orthop Res, 1996. **14**(1): p. 16-21.
149. Bowes, M.A., et al., *Osteoarthritic bone marrow lesions almost exclusively colocate with denuded cartilage: a 3D study using data from the Osteoarthritis Initiative.* Ann Rheum Dis, 2016. **75**(10): p. 1852-7.
150. Guermazi, A., et al., *Compositional MRI techniques for evaluation of cartilage degeneration in osteoarthritis.* Osteoarthritis Cartilage, 2015. **23**(10): p. 1639-53.
151. Ashinsky, B.G., et al., *Predicting Early Symptomatic Osteoarthritis in the Human Knee Using Machine Learning Classification of Magnetic Resonance Images From the Osteoarthritis Initiative.* Journal of Orthopaedic Research, 2017. **35**(10): p. 2243-2250.
152. Edd, S.N., et al., *Comprehensive description of T2 value spatial variations in non-osteoarthritic femoral cartilage using three-dimensional registration of morphological and relaxometry data.* Knee, 2019. **26**(3): p. 555-563.
153. Van Rossom, S., et al., *Knee Cartilage Thickness, T1rho and T2 Relaxation Time Are Related to Articular Cartilage Loading in Healthy Adults.* PLoS One, 2017. **12**(1): p. e0170002.
154. Van Rossom, S., et al., *Topographical Variation of Human Femoral Articular Cartilage Thickness, T1rho and T2 Relaxation Times Is Related to Local Loading during Walking.* Cartilage, 2019. **10**(2): p. 229-237.
155. Jamshidi, A., J.P. Pelletier, and J. Martel-Pelletier, *Machine-learning-based patient-specific prediction models for knee osteoarthritis.* Nat Rev Rheumatol, 2019. **15**(1): p. 49-60.
156. Favre, J., et al., *Baseline ambulatory knee kinematics are associated with changes in cartilage thickness in osteoarthritic patients over 5 years.* J Biomech, 2016. **49**(9): p. 1859-1864.
157. Buck, R.J., et al., *Osteoarthritis may not be a one-way-road of cartilage loss--comparison of spatial patterns of cartilage change between osteoarthritic and healthy knees.* Osteoarthritis Cartilage, 2010. **18**(3): p. 329-35.
158. Reichenbach, S., et al., *Does cartilage volume or thickness distinguish knees with and without mild radiographic osteoarthritis? The Framingham Study.* Ann Rheum Dis, 2010. **69**(1): p. 143-9.
159. Eckstein, F., et al., *Rates of change and sensitivity to change in cartilage morphology in healthy knees and in knees with mild, moderate, and end-stage radiographic osteoarthritis: results from 831 participants from the Osteoarthritis Initiative.* Arthritis Care Res (Hoboken), 2011. **63**(3): p. 311-9.
160. Favre, J., B. Fasel, and T.P. Andriacchi, *Pattern in Femoral Cartilage Thickness Map Allows Subtle Scoring of Medial Compartment Knee Osteoarthritis Severity.* Osteoarthritis and Cartilage, 2013. **21**: p. S231-S232.
161. Tenenbaum, J.B., V. de Silva, and J.C. Langford, *A global geometric framework for nonlinear dimensionality reduction.* Science, 2000. **290**(5500): p. 2319-23.
162. Van der Maaten, L. and G. Hinton, *Visualizing data using t-SNE.* Journal of machine learning research, 2008. **9**(11).
163. Pearson, K., *LIII. On lines and planes of closest fit to systems of points in space.* The London, Edinburgh, and Dublin Philosophical Magazine and Journal of Science, 1901. **2**(11): p. 559-572.
164. Hastie, T., et al., *The elements of statistical learning: data mining, inference and prediction.* The Mathematical Intelligencer, 2005. **27**(2): p. 83-85.
165. Archer, K.J. and A.A. Williams, *L 1 penalized continuation ratio models for ordinal response prediction using high-dimensional datasets.* Statistics in Medicine, 2012. **31**(14): p. 1464-1474.
166. Barr, A.J., et al., *The relationship between three-dimensional knee MRI bone shape and total knee replacement—a case control study: data from the Osteoarthritis Initiative.* Rheumatology, 2016. **55**(9): p. 1585-1593.
167. Dube, B., et al., *The relationship between two different measures of osteoarthritis bone pathology, bone marrow lesions and 3D bone shape: data from the Osteoarthritis Initiative.* Osteoarthritis and cartilage, 2018. **26**(10): p. 1333-1337.
168. Lynch, J.T., et al., *Statistical shape modelling reveals large and distinct subchondral bony differences in osteoarthritic knees.* Journal of Biomechanics, 2019. **93**: p. 177-184.
169. Kokkotis, C., et al., *Machine learning in knee osteoarthritis: A review.* Osteoarthritis and Cartilage Open, 2020: p. 100069.

V
Annex

A Registration Method for Three-Dimensional Analysis of Bone Mineral Density in the Proximal Tibia

Hugo Babel[1]
Swiss BioMotion Lab,
Department of Musculoskeletal Medicine,
Lausanne University Hospital and
University of Lausanne (CHUV-UNIL),
Lausanne CH-1011, Switzerland
e-mail: hugo.babel@chuv.ch

Loïc Wägeli
Swiss BioMotion Lab,
Department of Musculoskeletal Medicine,
Lausanne University Hospital and
University of Lausanne (CHUV-UNIL),
Lausanne CH-1011, Switzerland
e-mail: loic.waegeli@alumni.epfl.ch

Berke Sonmez
Swiss BioMotion Lab,
Department of Musculoskeletal Medicine,
Lausanne University Hospital and
University of Lausanne (CHUV-UNIL),
Lausanne CH-1011, Switzerland
e-mail: berkearalsonmez@gmail.com

Jean-Philippe Thiran
Signal Processing Laboratory,
Ecole Polytechnique Fédérale Lausanne (EPFL),
Lausanne CH-1015, Switzerland;
Service of Diagnostic and Interventional Radiology,
Lausanne University Hospital and
University of Lausanne (CHUV-UNIL),
Lausanne CH-1011, Switzerland
e-mail: jean-philippe.thiran@epfl.ch

Patrick Omoumi[2]
Service of Diagnostic and Interventional Radiology,
Lausanne University Hospital and
University of Lausanne (CHUV-UNIL),
Lausanne CH-1011, Switzerland
e-mail: patrick.omoumi@chuv.ch

Brigitte M. Jolles[2]
Swiss BioMotion Lab,
Department of Musculoskeletal Medicine,
Lausanne University Hospital and
University of Lausanne (CHUV-UNIL),
Lausanne CH-1011, Switzerland;
Institute of Microengineering,
Ecole Polytechnique Fédérale Lausanne (EPFL),
Lausanne CH-1015, Switzerland
e-mail: brigitte.jolles-haeberli@chuv.ch

Julien Favre[2]
Swiss BioMotion Lab,
Department of Musculoskeletal Medicine,
Lausanne University Hospital and
University of Lausanne (CHUV-UNIL),
Lausanne CH-1011, Switzerland
e-mail: julien.favre@chuv.ch

Although alterations in bone mineral density (BMD) at the proximal tibia have been suggested to play a role in various musculoskeletal conditions, their pathophysiological implications and their value as markers for diagnosis remain unclear. Improving our understanding of proximal tibial BMD requires novel tools for three-dimensional (3D) analysis of BMD distribution. Three-dimensional imaging is possible with computed tomography (CT), but computational anatomy algorithms are missing to standardize the quantification of 3D proximal tibial BMD, preventing distribution analyses. The objectives of this study were to develop and assess a registration method, suitable with routine knee CT scans, to allow the standardized quantification of 3D BMD distribution in the proximal tibia. Second, as an example of application, the study aimed to characterize the distribution of BMD below the tibial cartilages in healthy knees. A method was proposed to register both the surface (vertices) and the content (voxels) of proximal tibias. The method combines rigid transformations to account for differences in bone size and position in the scanner's field of view and to address inconsistencies in the portion of the tibial shaft included in routine CT scan, with a nonrigid transformation locally matching the proximal tibias. The method proved to be highly reproducible and provided a comprehensive description of the relationship between bone depth and BMD. Specifically it reported significantly higher BMD in the first 6 mm of bone than deeper in the proximal tibia. In conclusion, the proposed method offers promising possibilities to analyze BMD and other properties of the tibia in 3D. [DOI: 10.1115/1.4048335]

1 Introduction

Alterations in bone mineral density (BMD) at the proximal tibia have been suggested to play a role in various conditions, including meniscal damage and repair [1,2], injury and reconstruction of the anterior cruciate ligament [3,4], bone fracture [5,6], arthroplasty [7,8], and osteoarthritis [9,10]. However, even though proximal tibial BMD has been studied for decades, there is a need to better understand its pathophysiological implication, its potential as a target for therapeutic interventions and its value as a marker for diagnosis. Improving our understanding in this regard will especially require the design of new methods to standardize the quantification of three-dimensional (3D) distribution of BMD, similarly to what has been proposed to study BMD in the proximal femur notably in relation to osteoporosis and arthroplasty [11–14]. In fact, standardizing the reporting of 3D BMD across individuals and/or time points will allow performing comprehensive analyses of spatial variations in BMD [12,15]. Furthermore, standardized description of 3D BMD constitutes a necessary initial step to conduct more advanced evaluations, for example, of bone structure through texture analyses [16–18].

In vivo, proximal tibial BMD has been mainly measured using dual X-ray absorptiometry (DXA). While this technique contributed to important data [1–4,6–10], the two-dimensional projection nature of DXA images limits the range of possible analyses. Therefore, researchers have started using computed tomography (CT) for 3D BMD measurement, including at the proximal tibia [5,19–22]. Nevertheless, in these prior tibial studies, BMD was described by averaging BMD over a few rather large regions of interest (ROI) defined by geometric guidelines based on anatomical features identified on each tibia. While this ROI-based

[1]Corresponding author.
[2]Contributed equally to this work

Manuscript received October 28, 2019; final manuscript received August 24, 2020; published online September 29, 2020. Assoc. Editor: Spencer P. Lake.

approach is valuable to report consistent local BMD measures independently of the individual tibia shapes, it is hardly compatible with 3D analyses of BMD distribution. In fact, analyzing 3D distribution with this approach would require thousands of smaller ROI and it would be difficult ensuring consistent locations of such ROI using geometric guidelines.

Actually, to truly assess 3D BMD distribution a different approach, known as computational anatomy, is necessary to standardize the data [23,24]. In this case, a registration procedure is used to establish a global anatomical correspondence between two bones in the form of a mathematical transformation. When the application requires the analysis of one or more groups of bones, a reference bone can be registered to all the bones of interest, therefore establishing a 3D correspondence among all of them despite individualities in their shapes [23]. Similarly, for longitudinal studies, a bone can be registered to itself, thus compensating for the spatial variations in data acquisition and for the possible changes in bone shape over time. The transformation typically includes a combination of translation, rotation, and scaling to overlay the bones, followed by nonlinear operations to morph the bones [23]. The transformations are usually calculated by reducing cost functions based either on the differences in CT voxel intensities or on the distance between bone surfaces. Although intensity-based methods are frequently used in medical imaging, they are not recommended for the current application because the intensity of the CT voxels is heterogeneous inside the tibias, with possibly different spatial distribution among bones [12]. Therefore, determining the registration transformations by minimizing the differences in relative voxel intensities does not guaranty an anatomical correspondence. Consequently, the state-of-the-art to analyze 3D BMD distribution suggests to CT scan the bones, segment the images to build 3D bone models and use registration algorithms based on surfaces matching. Methods have been developed to standardize the 3D BMD in the proximal femur following this state-of-the-art procedure and reported promising results [12–14]. However, although there is clear clinical and scientific needs to better understand proximal tibial 3D BMD distribution [1–4,7–10], no comparable method has been proposed for the tibia. It could seem that the methods developed for the femur could be applied as is for the tibia. Yet, the shape of the proximal tibia, with less anatomical features and a higher level of symmetry, requires the design of specific methods. For example, special strategies are necessary to determine the scaling along the longitudinal axis with routine CT scans of the knee that include only a small and inconsistent portion of the tibial shaft.

The primary objectives of this study were to develop and assess a registration method, suitable with routine knee CT scans, to allow standardized quantification of 3D BMD distribution in the proximal tibia. In practice, BMD is first measured in unit of CT intensity (Hounsfield unit) and then a calibration procedure can be used to express the BMD in mg/cm^3 [25,26]. The method designed in this study aimed to be applicable to both uncalibrated and calibrated BMD measures. Second, as an example of application, the study aimed to characterize the distribution of BMD below the medial and lateral tibial cartilages. Indeed, bone is a mechanosensitive tissue that adapts to its mechanical environment [27], resulting in a varying BMD with respect to bone depth. While prior ROI-based studies indicated lower BMD in deeper ROIs [20,28], the patterns of BMD diminution with respect to bone depth have never been reported.

2 Materials and Methods

2.1 Experimental Setup. A convenience set of 23 CT scans of healthy knees, namely, without imaging sign of fracture, disease or surgery, was selected from the institution's database for this study approved by the institutional review board (61 ± 6 years old, 30% male, 44% left). The sample size was based on previous, comparable computational anatomy methods for the proximal femur [11,29,30]. These tibias included at least 2.0 cm, and no more than 3.5 cm, of bone below the cartilages. This range of bone lengths, which is standard in routine CT examination of the knee, was sufficient to characterize the BMD distribution below the cartilages as the interest mostly lies in the first 2 cm of bone [1,4,20]. Scans were acquired in a routine clinical practice setting, as part of a diagnostic workup for suspected meniscocartilaginous lesions, with the patients lying on the back with the knee of interest extended. A contrast material was injected in the synovial fluid shortly before scanning for clinical purposes independent of this research. The injection has no impact on this study, as the contrast material did not propagate to the bone. Examinations were performed on a 40 row detector helical CT scanner (Somatom Definition AS; Siemens Healthcare, Forchheim, Germany), using the following acquisition parameters: tube voltage, 120 kVp; reference tube current–time product, 350 mAs with the application of a dose modulation protocol (Care Dose 4D; Siemens Healthcare); bone convolution kernel (U70u), voxel size of 0.3 × 0.3 × 0.3 mm. In this study, uncalibrated images were used, meaning that the BMD was measured in CT voxel intensity unit [25,26].

The tibial bone mesh was created following methods previously described [22,31]. Briefly, the contour of the tibia was segmented semi-manually in each CT image using custom software based on B-splines, and then the segmentations were combined across images to build a 3D triangular mesh models of the tibial bone (Fig. 1). During the segmentation procedure, the bone contour was coded differently if the bone was covered by cartilage (subchondral bone) or not. This coding allowed identifying the medial and lateral subchondral areas (and the corresponding vertices) in the 3D mesh model, as illustrated in Fig. 1. Finally, a bone membership mask identifying the CT voxels located within the boundaries of the tibial bone mesh was calculated. Depending on the knees, the tibial bone mesh included between 25 and 40 thousand vertices, out of which between 4 and 9 thousand corresponded to subchondral bone. Additionally, the mask of the 23 knees included between 1.5 and 4.0 million voxels of tibial bone.

2.2 Registration. The following sections (Secs. 2.2.1–2.2.4) detail the procedure to register a moving tibia to a fixed tibia. This procedure involves two phases: the matching of the surface (mesh) of the two bones (Secs. 2.2.1–2.2.3) and then the matching of the voxels inside the tibias by extension of the surface-to-surface transformation (Sec. 2.2.4). The first phase includes three steps (Fig. 2). First, an initial alignment, consisting in a translation, a rotation, and an isotropic scaling, is applied to the moving mesh to account for differences in bone size and for differences in position and orientation in the field of view of the scanner (Sec. 2.2.1). This initial alignment is based on the overlaying of the subchondral areas. During the second step, a translation and a scaling along the longitudinal axis, as well as a scaling in the transverse plane, are applied to the moving mesh to match its transverse bone area profile to the one of the fixed mesh (Sec. 2.2.2). Matching the transverse bone area profile is a new concept introduced in this study to address the difficulties related to the fact that routine CT scans include small and inconsistent portion of the tibial shafts. Finally, the third step consists in deforming the moving mesh locally so that its surface closely matches the surface of the fixed mesh (Sec. 2.2.3).

In the following, the attributes of the moving and fixed meshes are referenced using the "mov" and "fix" abbreviations, respectively. Furthermore, the Euclidian norm of a vector $\boldsymbol{v}$ is denoted $\|\boldsymbol{v}\|$, the scalar product of two vectors $\boldsymbol{v}$ and $\boldsymbol{w}$ denoted $\boldsymbol{v} \cdot \boldsymbol{w}$, and the cross product between two vectors $\boldsymbol{v}$ and $\boldsymbol{w}$ denoted $\boldsymbol{v} \times \boldsymbol{w}$. Additionally, the cardinality of a set V is denoted $|V|$. Moreover, for the sake of clarity, the following sections assume that all tibias are right tibias positioned in the scanner to have their anterior–posterior, medial–lateral, and distal–proximal axes roughly aligned with the x, y, and z CT axes, respectively. Left tibias or tibias scanned with another axes' convention should be

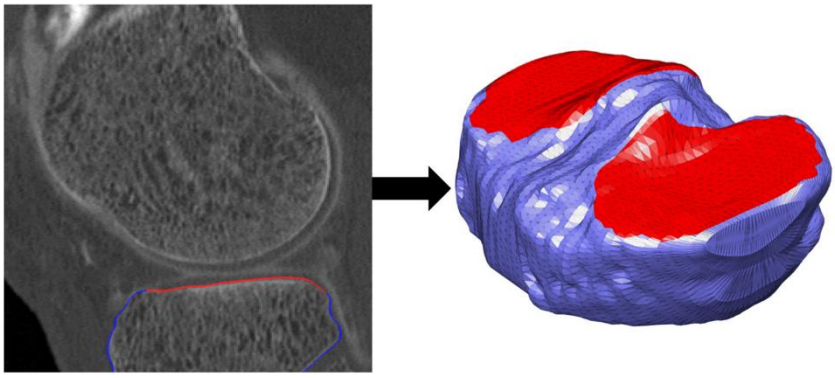

Fig. 1 Illustration of the methods to build a 3D tibial mesh from a CT scan. First (left image), the tibia was segmented in each CT image. During this procedure, the bone contour was coded differently if the bone was covered by cartilage (subchondral bone; red line) or not (blue line). Second (right image), the segmentations were combined across CT images to generate a 3D mesh model with identification of the medial and lateral subchondral areas (red).

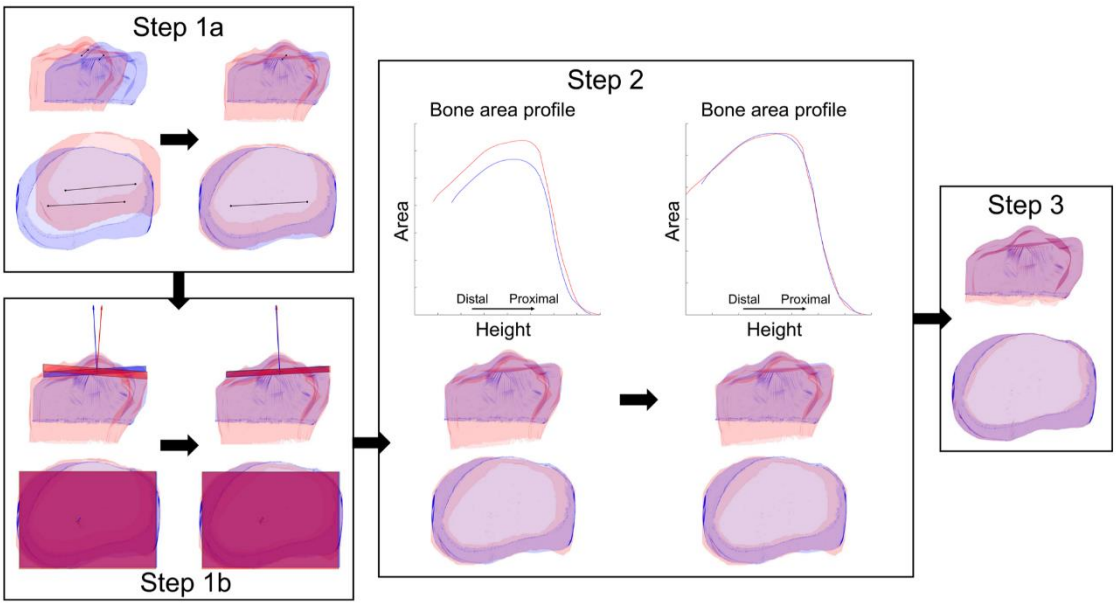

Fig. 2 Illustration of the first phase of the registration procedure which includes three steps (Secs. 2.2.1–2.2.3). The boxes present the moving (red) and fixed (blue) tibial meshes before (left) and after (right) each step. A side (upper plot) and a bottom (lower plot) views of the tibias are provided in each box. Step 1: (*a*) the centers of the medial and lateral subchondral areas and (*b*) the normal of the least squares plane fitted to the subchondral areas of the moving and fixed tibial meshes are aligned. Step 2: the bone area profile of the moving and fixed meshes are calculated (see Fig. 3 for details). The profile of the moving tibia is then matched to the profile of the fixed tibia, and the moving mesh is modified accordingly. Step 3: a nonrigid transformation is applied to the moving mesh to match locally the fixed mesh.

transformed beforehand by mirroring and 90-deg rotation operations.

2.2.1 Phase 1 – Step 1: Initial, Rigid, Transformation to Overlay the Subchondral Bone Areas. The first stage of the method consists in moving, rotating, and scaling the moving mesh to limit the differences between both tibias in terms of bone size and placement in the scanner (Fig. 2). This initial step is achieved by overlaying the subchondral bone areas of the moving mesh on the subchondral bone areas of the fixed mesh.

Let $V = \{\boldsymbol{v}_j\} = \{(x_j, y_j, z_j)^T\}$ be the original 3D position of all mesh vertices of one bone, where each vertex is identified with the j index. Moreover, let V_c be the subset of vertices of the subchondral area in the compartment c, with c being either the medial (med) or the lateral (lat) compartment. The center of the subchondral area in the compartment c, $\boldsymbol{m}_c$, is defined as the average position of all the subchondral vertices in this compartment (1).

$$\boldsymbol{m}_c = \frac{1}{|V_c|} \sum_{\boldsymbol{v}_j \in V_c} \boldsymbol{v}_j \tag{1}$$

Let $\boldsymbol{d}$ be the direction of the axis from the center of the medial subchondral area to the center of the lateral subchondral area (2), and $\widehat{\boldsymbol{d}}$ be the unitary vector associated with $\boldsymbol{d}$ (3).

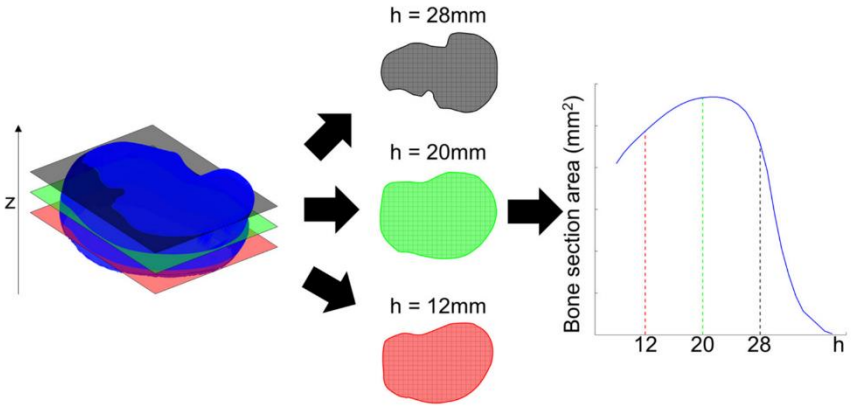

Fig. 3 Illustration of the calculation of the transverse bone area profile (Sec. 2.2.2). Left: A tibial mesh intersected with transverse planes. Center: The bone slices (polygons) corresponding to the intersections. Right: The bone area profile. For sake of clarity, this figure includes only three measures of bone area at heights (*h*) equal to 12, 20, and 28 mm, whereas in reality, the profile is determined by slicing the bone at 1 mm intervals.

$$\boldsymbol{d} = \frac{\boldsymbol{m}_{\text{lat}} - \boldsymbol{m}_{\text{med}}}{\|\boldsymbol{m}_{\text{lat}} - \boldsymbol{m}_{\text{med}}\|} \tag{2}$$

$$\widehat{\boldsymbol{d}} = \frac{\boldsymbol{d}}{\|\boldsymbol{d}\|} \tag{3}$$

Additionally, let $\widehat{\boldsymbol{c}}$ be the unitary coplanar vector of $\widehat{\boldsymbol{d}}_{\text{fix}}$ and $\widehat{\boldsymbol{d}}_{\text{mov}}$ (4).

$$\widehat{\boldsymbol{c}} = \frac{\widehat{\boldsymbol{d}}_{\text{mov}} - (\widehat{\boldsymbol{d}}_{\text{fix}} \cdot \widehat{\boldsymbol{d}}_{\text{mov}})\widehat{\boldsymbol{d}}_{\text{fix}}}{\|\widehat{\boldsymbol{d}}_{\text{mov}} - (\widehat{\boldsymbol{d}}_{\text{fix}} \cdot \widehat{\boldsymbol{d}}_{\text{mov}})\widehat{\boldsymbol{d}}_{\text{fix}}\|} \tag{4}$$

With the variables above, it is possible to calculate the change of basis matrix between the moving and fixed tibias, C, (5) and, then, the rotation matrix R (6) that rotates and scales the vector $\boldsymbol{d}_{\text{mov}}$ such that $\boldsymbol{d}_{\text{mov}}R = \boldsymbol{d}_{\text{fix}}$.

$$C = \begin{bmatrix} \widehat{\boldsymbol{d}}_{\text{fix}} & \widehat{\boldsymbol{c}} & -\widehat{\boldsymbol{d}}_{\text{fix}} \times \widehat{\boldsymbol{d}}_{\text{mov}} \end{bmatrix} \tag{5}$$

$$R = \frac{\|\boldsymbol{d}_{\text{fix}}\|}{\|\boldsymbol{d}_{\text{mov}}\|} C \begin{bmatrix} \widehat{\boldsymbol{d}}_{\text{fix}} \cdot \widehat{\boldsymbol{d}}_{\text{mov}} & \|\widehat{\boldsymbol{d}}_{\text{fix}} \times \widehat{\boldsymbol{d}}_{\text{mov}}\| & 0 \\ \|\widehat{\boldsymbol{d}}_{\text{fix}} \times \widehat{\boldsymbol{d}}_{\text{mov}}\| & \widehat{\boldsymbol{d}}_{\text{fix}} \cdot \widehat{\boldsymbol{d}}_{\text{mov}} & 0 \\ 0 & 0 & 1 \end{bmatrix} C^{-1} \tag{6}$$

Next, the original moving vertices $V_{\text{mov}} = \{\boldsymbol{v}_{\text{mov},j}\}$ are updated such that the center of the medial and lateral subchondral areas of the moving tibia are in the same position as the center of the subchondral areas of the fixed tibia. Specifically, a new position $\boldsymbol{v}^{(1a)}_{\text{mov},j}$ is calculated for every original moving vertex $\boldsymbol{v}_{\text{mov},j}$ using (7).

$$\boldsymbol{v}^{(1a)}_{\text{mov},j} = (\boldsymbol{v}_{\text{mov},j} - \boldsymbol{m}_{\text{mov,med}})R + \boldsymbol{m}_{\text{fix,med}} \tag{7}$$

After aligning the centers of the subchondral areas of the moving tibia on those of the fixed tibia, the moving mesh is rotated around the axis joining the center of the medial and lateral subchondral areas in order to have the subchondral areas of the moving tibia parallel to the subchondral areas of the fixed tibia. To this end, let us define the tibial plateau (plat) as the set of all subchondral vertices, such that $V_{\text{plat}} = V_{\text{med}} \cup V_{\text{lat}}$. A least squares plane, defined as $ax + by + cz + d = 0$, can be fitted to the tibial plateau vertices by setting $c = 1$ and solving the linear system in Eq. (8).

$$\begin{bmatrix} \sum_{\boldsymbol{v}_j \in V_{\text{plat}}} (x_j)^2 & \sum_{\boldsymbol{v}_j \in V_{\text{plat}}} x_j y_j & \sum_{\boldsymbol{v}_j \in V_{\text{plat}}} x_j \\ \sum_{\boldsymbol{v}_j \in V_{\text{plat}}} y_j x_j & \sum_{\boldsymbol{v}_j \in V_{\text{plat}}} (y_j)^2 & \sum_{\boldsymbol{v}_j \in V_{\text{plat}}} y_j \\ \sum_{\boldsymbol{v}_j \in V_{\text{plat}}} x_j & \sum_{\boldsymbol{v}_j \in V_{\text{plat}}} y_j & |V_{\text{plat}}| \end{bmatrix} \begin{bmatrix} a \\ b \\ d \end{bmatrix} = -\begin{bmatrix} \sum_{\boldsymbol{v}_j \in V_{\text{plat}}} x_j z_j \\ \sum_{\boldsymbol{v}_j \in V_{\text{plat}}} y_j z_j \\ \sum_{\boldsymbol{v}_j \in V_{\text{plat}}} z_j \end{bmatrix} \tag{8}$$

Let $\widehat{\boldsymbol{n}}$ be the unitary normal vector of the least squares plane $ax + by + z + d = 0$. Then, similarly to above, a rotation P can be applied such that $\widehat{\boldsymbol{n}}^{(1a)}_{\text{mov}}P = \widehat{\boldsymbol{n}}_{\text{fix}}$. The rotation P can be calculated using $\widehat{\boldsymbol{w}}$, the unitary vector coplanar to $\widehat{\boldsymbol{n}}_{\text{fix}}$ and $\widehat{\boldsymbol{n}}^{(1a)}_{\text{mov}}$ (Eq. (9)), and B, the change of basis matrix (Eq. (10)).

$$\widehat{\boldsymbol{w}} = \frac{\widehat{\boldsymbol{n}}^{(1a)}_{\text{mov}} - (\widehat{\boldsymbol{n}}_{\text{fix}} \cdot \widehat{\boldsymbol{n}}^{(1a)}_{\text{mov}})\widehat{\boldsymbol{n}}_{fix}}{\|\widehat{\boldsymbol{n}}^{(1a)}_{\text{mov}} - (\widehat{\boldsymbol{n}}_{\text{fix}} \cdot \widehat{\boldsymbol{n}}^{(1a)}_{\text{mov}})\widehat{\boldsymbol{n}}_{fix}\|} \tag{9}$$

$$B = \begin{bmatrix} \widehat{\boldsymbol{n}}_{\text{fix}} & \widehat{\boldsymbol{n}}_{\text{fix}} \times \widehat{\boldsymbol{n}}^{(1a)}_{\text{mov}} & -\widehat{\boldsymbol{w}} \end{bmatrix} \tag{10}$$

$$P = B \begin{bmatrix} \widehat{\boldsymbol{n}}_{\text{fix}} \cdot \widehat{\boldsymbol{n}}^{(1a)}_{\text{mov}} & 0 & \|\widehat{\boldsymbol{n}}_{\text{fix}} \times \widehat{\boldsymbol{n}}^{(1a)}_{\text{mov}}\| \\ 0 & 1 & 0 \\ -\|\widehat{\boldsymbol{n}}_{\text{fix}} \times \widehat{\boldsymbol{n}}^{(1a)}_{\text{mov}}\| & 0 & \widehat{\boldsymbol{n}}_{\text{fix}} \cdot \widehat{\boldsymbol{n}}^{(1a)}_{\text{mov}} \end{bmatrix} B^{-1} \tag{11}$$

The vertices of the moving tibia $V^{(1a)}_{\text{mov}} = \left\{\boldsymbol{v}^{(1a)}_{\text{mov},j}\right\}$ are then updated to align the least squares plane of the subchondral areas of the moving bone onto those of the fixed bone. Specifically, a new set $V^{(1b)}_{\text{mov}} = \left\{\boldsymbol{v}^{(1b)}_{\text{mov},j}\right\}$ is obtained by calculating a new position for every moving vertex $\boldsymbol{v}^{(1a)}_{\text{mov},j}$ as the following (Eq. (12)).

$$\boldsymbol{v}^{(1b)}_{\text{mov},j} = \left(\boldsymbol{v}^{(1a)}_{\text{mov},j} - \boldsymbol{m}^{(1a)}_{\text{mov,plat}}\right)P + \boldsymbol{m}_{\text{fix,plat}} \tag{12}$$

where $\boldsymbol{m}_{\text{plat}} = 0.5*(\boldsymbol{m}_{\text{lat}} + \boldsymbol{m}_{\text{med}})$ is the midpoint between the center of the medial and lateral subchondral bone areas.

2.2.2 Phase 1—Step 2: Rigid Transformation to Match the Bone Area Profiles. The initial transformation (Sec. 2.2.1) overlaid the proximal part of both bones. While necessary and useful,

this initial step is insufficient to allow proper local deformation of the moving mesh (Sec. 2.2.3) notably because it did not match the bones in the proximal–distal and anterior–posterior directions. Matching the tibias longitudinally is particularly challenging because the small portion of the tibial shafts acquired in routine practice do not include bony landmark that could be used to establish correspondence in the proximal–distal direction. A new metric, the transverse bone area profile, is therefore proposed to address this issue. Indeed, all tibias have a profile of similar shape and matching the moving profile to the fixed profile allows translating and scaling the moving bone along the longitudinal axis, as well as scaling it in the transverse plane, as detailed below.

The bone area profile is defined as the area of the transversal bone sections sampled at 1 mm interval (Fig. 3). Specifically, let $h_{\text{up}} = \lfloor \max_{v_j \in V} z_j \rfloor$ and $h_{\text{low}} = \lceil \min_{v_j \in V} z_j \rceil$ be the upper and lower integer bounds of the z-coordinates of the vertex positions of the mesh. For each integer height $h_i \in \{h_{\text{low}}, \ldots, h_{\text{up}}\}$, the profile $p(h_i)$ is defined as the area of the transverse bone section, calculated by intersecting the bone model and the plane $z = h_i$ using [32], and then measuring the area of the resulting polygon (Fig. 3). At both the upper and lower extremities of the tibia, special cases may arise. At the top, because of the bone shape, the intersection may yield several polygons. In this case, the area of the bone section is defined as the sum of the area of all polygons. At the bottom, a similar situation may occur due to the incomplete scan or segmentation of the bone. In this case, the profile is limited to the lowest height h_i for which the intersection yields only one polygon.

Let p_{fix} and $p^{(1b)}_{\text{mov}}$ be the profiles of the fixed tibia and of the moving tibia after the initial transformation, respectively. The matching of the moving profile to the fixed profile involves three operations that can then be applied to the moving mesh: a translation t_z along the z-axis, a scaling s_z along the z-axis and a scaling s_a of the profile (Fig. 2). The three parameters conditioning these operations are determined using an optimization routine minimizing the distance between the two profiles, as explained below.

First, initial parameters, s^0_a, s^0_z, and t^0_z, are calculated based on the maximum value of the profiles and on the heights at which these maximum values occur. For each tibia, let $h_{\max} = \text{argmax}_{i=h_{\text{low}}}^{h_{\text{up}}} p(h_i)$ be the height of the maximum profile value and let $m = p(h_{\max})$ be the maximum value of the profile. The initial scaling s^0_a of the moving profile is calculated using the following (Eq. (13)).

$$s^0_a = \frac{m_{\text{fix}}}{m^{(1b)}_{\text{mov}}} \tag{13}$$

The initial scaling s^0_z along the z-axis is determined using Eq. (14), by locating the midpoint $h^{(1b)}_{\text{mov,mid}}$ between the top of the tibia h_{up} and the height of the maximum transverse area $h_{\max}$ in the moving (Eq. (15)) and fixed (Eq. (16)) bones.

$$s^0_z = \frac{h_{\text{fix, mid}} - h_{\text{fix,max}}}{h^{(1b)}_{\text{mov,mid}} - h^{(1b)}_{\text{mov,max}}} \tag{14}$$

$$h^{(1b)}_{\text{mov,mid}} = \frac{1}{2}\left(h^{(1b)}_{\text{mov,up}} + h^{(1b)}_{\text{mov,max}}\right) \tag{15}$$

$$h_{\text{fix,mid}} = \max\left(\left\{h_j \in \{h_{\text{fix,low}}, \ldots, h_{\text{fix,up}}\} \,|\, p_{\text{fix}}(h_j) s^0_a p^{(1b)}_{\text{mov}}\left(h^{(1b)}_{\text{mov,mid}}\right)\right\}\right) \tag{16}$$

The initial translation t^0_z along the z-axis is calculated using the following Eq. (17).

$$t^0_z = \frac{h_{\text{fix,max}} - s^0_z h^{(1b)}_{\text{mov,max}}}{s^0_z} \tag{17}$$

Second, a routine is applied to tune s_a, s_z, and t_z in order to optimize the matching of the moving profile to the fixed profile. The routine uses an interior-point algorithm [33], starting with the initial parameters determined above $\left(s^0_a, s^0_z, t^0_z\right)$. The cost function at each iteration of the optimization is calculated as the mean squared error (MSE) between the fixed profile p_{fix} and the temporary moving profile $p^{(t)}_{\text{mov}}$ (Eq. (18)). For more robust estimation, the MSE is only computed over the height range ($\{h^{(t)}_{\text{low}}, \ldots, h^{(t)}_{\text{up}}\}$) that is common to both tibias (Eqs. (19) and (20)).

$$\text{MSE}\left(p^{(t)}\right) = \frac{1}{h^{(t)}_{\text{up}} - h^{(t)}_{\text{low}} + 1} \sum_{h=h^{(t)}_{\text{low}}}^{h^{(t)}_{\text{up}}} \left(p_{\text{fix}}(h) - p^{(t)}_{\text{mov}}(h)\right)^2 \tag{18}$$

$$h^{(t)}_{\text{low}} = \max\left\{h_{\text{fix,low}}, h^{(t)}_{\text{mov,low}}\right\} \tag{19}$$

$$h^{(t)}_{\text{up}} = \min\left\{h_{\text{fix,up}}, h^{(t)}_{\text{mov,up}}\right\} \tag{20}$$

The final optimization parameters $\left(s^{(f)}_a, s^{(f)}_z, t^{(f)}_z\right)$ can then be used to transform the vertices of the moving mesh obtained at the end of step 1 $\left(\boldsymbol{v}^{(1b)}_{\text{mov},j} = \left(x^{(1b)}_j, y^{(1b)}_j, z^{(1b)}_j\right)^T\right)$ into new vertices $\left(\boldsymbol{v}^{(2)}_{\text{mov},j} = \left(x^{(2)}_j, y^{(2)}_j, z^{(2)}_j\right)^T\right)$ such that the mesh associated with these new vertices has a $p^{(f)}_{\text{mov}}$ profile. The operations to obtain the new vertices are presented in Eqs. (21)–(23). In these equations, $\bar{x}$ and $\bar{y}$ correspond to the average x and y coordinates of the bone model vertices.

$$x^{(2)}_j = \sqrt{s^{(f)}_a}\left(x^{(1b)}_j - \bar{x}^{(1b)}\right) + \bar{x}^{(1b)} \tag{21}$$

$$y^{(2)}_j = \sqrt{s^{(f)}_a}\left(y^{(1b)}_j - \bar{y}^{(1b)}\right) + \bar{y}^{(1b)} \tag{22}$$

$$z^{(2)}_j = s^{(f)}_z\left(z^{(1b)}_j + t^{(f)}_z - h^{(f)}_{\text{mov,up}}\right) + h^{(f)}_{\text{mov,up}} \tag{23}$$

2.2.3 Phase 1 – Step 3: Nonrigid Local Transformation to Match the Mesh Surfaces. After the second step, the moving mesh generally overlaps the fixed mesh (Fig. 2). However, since only rigid and semirigid transformations have been applied so far, there remain local differences between both meshes at this stage. A third step is therefore used to ensure that the moving mesh closely matches the fixed mesh everywhere. In this last step, the moving vertices belonging to $V^{(2)}_{\text{mov}}$ obtained after the second step are registered to the fixed mesh using an adaptive stiffness variant of nonrigid ICP [34], resulting in a temporary set of registered vertices which are then used as target coordinates for thin-plate splines [35], yielding a final set of matched vertices $V^{(3)}_{\text{mov}} = \left\{\boldsymbol{v}^{(3)}_{\text{mov},j}\right\}$. Because the length of the meshes varies from bone to bone depending on how the knees were scanned, the moving and fixed meshes are truncated distally in order to have the same length before performing the nonrigid registration. This is done by removing all the vertices of the longer mesh that are below the distal limit of the shorter mesh, without retriangulation.

2.2.4 Phase 2: Registration of the Voxel Centers. The first phase of the registration (steps 1–3 above, Secs. 2.2.1–2.2.3) transformed the surface (i.e., the position of the mesh vertices) of the moving tibia so that it matches the surface of the fixed tibia. This second registration phase consists in applying the surface-to-surface transformations to the voxels inside the moving tibia. This is done by calculating new (matched) position for the center of the moving tibia voxels. Let $C_{\text{mov}} = \{\boldsymbol{c}_{\text{mov},i}\} = \left\{(x_v, y_v, z_v)^T\right\}$ be the original 3D position of all the voxel centers of the moving tibia. These positions, first, undergo the same rigid (Sec. 2.2.1) and semirigid (Sec. 2.2.2) transformations as determined above, resulting in $C^{(1a)}_{\text{mov}}$ after (Eq. (7)), in $C^{(1b)}_{\text{mov}}$ after (Eq. (12)), and in

$C^{(2)}_{mov}$ after (Eqs. (21)–(23)). Then, if necessary, voxel centers are removed from $C^{(2)}_{mov}$ to account for the distal truncation in Sec. 2.2.3. Lastly, the thin-plate splines transformation calculated in Sec. 2.2.3 is applied to the truncated $C^{(2)}_{mov}$, yielding the final matched position of the voxel centers $C^{(3)}_{mov}$.

2.3 Reference Tibial Mesh. The method presented in Sec. 2.2 allows to register any moving tibia to any fixed tibia. In practice, such a method will often involve a reference bone to which one or more bones will be registered. A reference mesh is usually obtained by averaging a group of meshes, which can be done using the method in Sec. 2.2. Specifically, creating a tibial reference mesh based on a group of meshes requires to randomly select one of the individual tibias in the group and match its mesh to the mesh of the remaining tibias as described in Secs. 2.2.1–2.2.3. An initial set of reference vertices is then obtained by averaging the position of the vertices after they have been matched to the remaining bones. Next, an initial reference mesh is calculated using the initial reference vertices [36]. After that, the series of matching, averaging and meshing operations is repeated, but these times with matching the current reference mesh to all the tibial meshes used to create the reference mesh. This series of operations is repeated until the changes in the reference mesh between two successive iterations become negligible.

2.4 Evaluation of the Method

2.4.1 Distance Between the Moving and Fixed Meshes During the Mesh Matching Steps. To assess the efficacy of the three steps of the mesh matching procedure (Secs. 2.2.1–2.2.3), a reference tibial mesh was created using the 23 tibias in this study (Sec. 2.3). It included 22 thousand vertices, 5 thousand of which were coded as subchondral bone. Then, the meshes of 23 tibias were registered to the reference mesh and the distance between the moving and fixed meshes was calculated after each matching step (Secs. 2.2.1–2.2.3). Two metrics were used to quantify the distance. First, the maximal distance between the two meshes was assessed using the Hausdorff distance [37]. Second, the mean closest point distance (MCPD) was calculated to assess the average distance between the two meshes. The MCPD was defined as the maximal value of either the average distance from each vertex of the fixed mesh to the closest vertex of the moving mesh or the average distance from each vertex of the moving mesh to the closest vertex of the fixed mesh. To avoid biasing the evaluation, the moving and fixed meshes were truncated distally to the same length before calculating the distances.

2.4.2 Reproducibility of the Voxel Centers Registration. In agreement with the objective of the registration method to provide an anatomical standardization, the reproducibility assessed to which extent the method provides similar standardized data for bones of different shape, but same relative structure. This was done by deforming the bone mesh and the corresponding voxels of the 23 tibia five times, resulting in 23 sets of six tibias each (the original tibia, plus five deformed tibias). With this, each set included six tibias of different shapes, but all with the same relative position of voxel centers. Next, these 138 tibias were individually registered to the reference tibia, and the position variability of the voxel centers was assessed for each set. This was done first by calculating the mean position over the six tibias and then calculating the average distance between the six positions and the average position, voxel by voxel. Then, the average distance of all the voxels were averaged to have one position variability value per tibia set. To assess the reproducibility of a real data situation, the tibias were deformed using the statistical distribution of the registration parameters. Specifically, the mean μ and standard deviation σ of each parameter needed to register the 23 original tibial meshes to the reference mesh were compiled, and then the tibias were deformed using parameters randomly drawn from a normal distribution $N(\mu, \sigma)$.

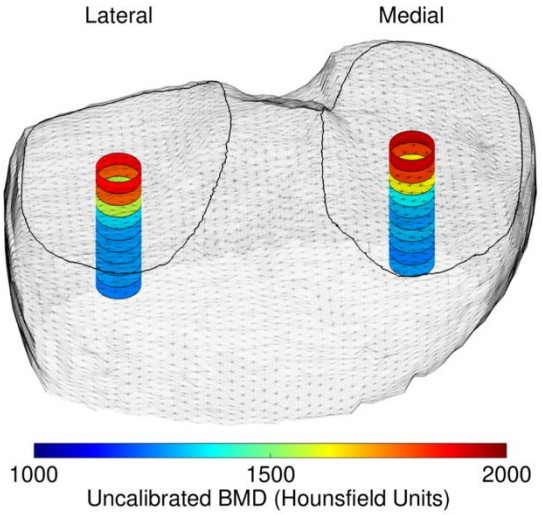

Fig. 4 Illustration of the cylindrical cells used to measure the BMD distribution below the center of the subchondral areas. The cells were defined for the reference tibia as shown in this figure. They are colored according to the average BMD of the 23 tibias (BMD values are reported in Fig. 5).

2.5 Example of Application: BMD Distribution Below the Cartilages

2.5.1 Standardized Quantification. To show the potential of the registration method to quantify 3D tibial BMD, and in line with literature [1,4,20], this work aimed to characterize the variations of BMD below the cartilages. To this end, first, two stacks of ten cells, were embedded in the reference mesh obtained by the averaging of the 23 individual tibias (Sec. 2.3). The stacks were placed beneath the centers of the medial and lateral subchondral bone areas, with each cell being a cylinder of 4 mm radius and 2 mm height (Fig. 4). Then, each of the 23 tibias (mesh and bone voxels) was registered to the reference tibia (Secs. 2.2.1–2.2.4) and the bone voxels were tagged based on the position of their center after registration. Specifically, for each tibia, the voxels belonging to a reference cell were listed. Finally, for each tibia, a BMD value was calculated for each cell by averaging the BMD value of all the voxels belonging to the cell. With this method, a standardized 3D quantification of the uncalibrated BMD below the cartilages was achieved.

2.5.2 Reproducibility Evaluation. The reproducibility of the BMD quantification method in Sec. 2.5.1 was assessed using the 23 sets of six tibias described in Sec. 2.4.2. After registration to the reference tibia, the BMD of the 138 tibias was determined in the 20 cells. Next, a two-way mixed effects intraclass correlation coefficient (ICC) [38] was calculated for the 20 BMD measures of the six tibias within each set. Additionally, the coefficient of variation was calculated for each set and cell, and then averaged over all the cells, leading to an average coefficient of variation for each original tibia (aCV).

2.5.3 Statistical Analysis. To test if BMD differed statistically significantly among bone depths, the BMD of the 23 original tibias measured below the cartilages (Sec. 2.5.1) were compared. Specifically, repeated-measure ANOVA with a Greenhouse–Geisser correction, followed by posthoc paired *t*-tests with a Bonferroni correction for multiple comparisons, were performed separately for the ten measures below the medial cartilage and the

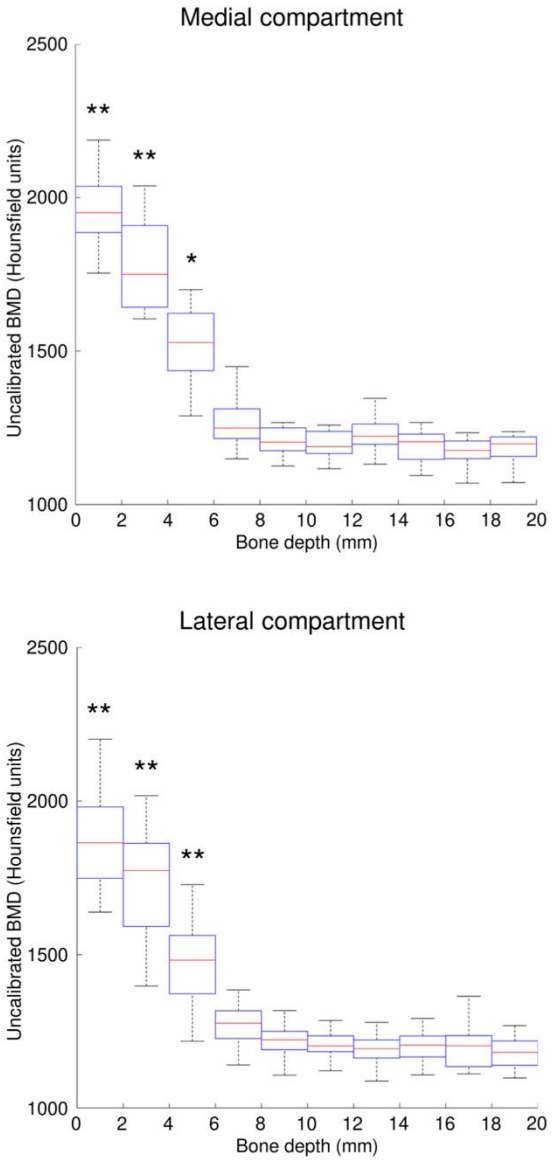

Fig. 5 Boxplot of the BMD of the 23 tibias below the center of the medial (top) and lateral (bottom) subchondral areas. BMD was measured using the cells as illustrated in Fig. 4. The stars indicate cells that were significantly denser than all deeper cells (*: $P < 0.01$; **: $P < 0.001$).

ten measures below the lateral cartilage. An alpha-level set a priori at 5% was considered significant for these tests.

All processing in this study was done with custom software using MATLAB (R2014b, Mathworks, Natick, MA), and all statistical analyses were performed using SPSS version 25 (IBM, Armonk, NY).

3 Results

3.1 Distance Between the Moving and Fixed Meshes During the Mesh Matching Steps. After the first matching step (Sec. 2.2.1), the average (±standard deviation) Hausdorff distance of the 23 tibias was 5.5 ± 1.4 mm and the average MCPD 1.3 ± 0.3 mm. The matching of the bone area profiles (Sec. 2.2.2) decreased both the Hausdorff distance (4.4 ± 1.0 mm) and the MCPD (1.0 ± 0.2 mm). The Hausdorff distance and MCPD further reduced after the nonrigid local transformation (Sec. 2.2.3) to 1.8 ± 1.5 and 0.30 ± 0.03 mm, respectively.

3.2 Reproducibility of the Voxel Centers Registration. The average variability in the position of the voxels after registration was 0.68 ± 0.60 mm, indicating that more than 80% of the voxels were located with variations of four voxels or less. Expressed with respect to the size of the tibia, the reproducibility of 0.68 ± 0.60 mm corresponded to 0.95 ± 0.85% of the medial–lateral diameter (maximum width of the tibia in the frontal plane).

3.3 BMD Distribution Below the Cartilages. The BMD measured below the cartilage with two stacks of ten cells were reproducible, with an average ICC of 0.99 ± 0.01 and average aCV of 1.3 ± 0.4% for the 23 tibias.

The BMD measured below the medial and lateral tibial cartilages are reported in Fig. 5. Consistent patterns were observed among tibias and compartments, with a characteristic drop in the first 6 mm. There were significant differences in BMD between depths (cells) in both the medial ($F(1.510, 33.209) = 283.159$, $p < 0.001$) and lateral ($F(1.999, 45.981) = 285.102$, $p < 0.001$) compartments. Posthoc paired t-tests indicated that, both medially and laterally, the three closest cells to the subchondral area had significantly higher BMD than all the deeper cells ($p < 0.01$).

4 Discussion

This article introduced a registration method for 3D quantification and analysis of the BMD distribution in the proximal tibia. This method is compatible with routine knee CT scans thanks to an innovative technique to match two meshes with different positions, orientations, lengths, and shapes. The registration method, which relies solely on the bone surfaces, is independent of the CT-scan resolution and independent of the sizes of the bones. Furthermore, it requires no images preprocessing, such as cropping.

The method was shown to register proximal tibia reproducibly. First, the average variability of the voxel positions following the anatomical standardization among bones with different shapes, but same relative structure, was well within the ranges considered acceptable for image registration [39], and represented less than 1% of the medial–lateral diameter of the bones. Second, the suitability of the method was further confirmed when it was used to characterize the BMD distribution below the medial and lateral cartilages. Specifically, this example of application reported high reproducibility in local BMD measurement and provided a comprehensive description of the relationship between bone depth and BMD.

To the best of the authors' knowledge, the present method is the first to allow the registration of proximal tibias, both in terms of bone surface (mesh) and content (voxels). A few methods based on the same principle of bone segmentation followed by surface matching were previously proposed for the proximal femur [12–14]. However, the "simpler" shape of the proximal tibia, with a higher level of symmetry and less compelling anatomical features, required the design of a specific method. In particular, a solution was needed for the distal–proximal scaling because this scaling cannot be predicted from the scaling in the other directions and because the length of the tibial shaft varies among acquisitions without simple option to determine it, such as the localization of anatomical landmarks. The transverse bone area profile proposed in this work was shown to be an effective answer to this difficulty. Interestingly, the concept of matching bones based on their area profile is not limited to the proximal tibia. Indeed, it can be used for the registration of other bones, or even other tissues, which are not imaged in their entirety and lack anatomical landmarks.

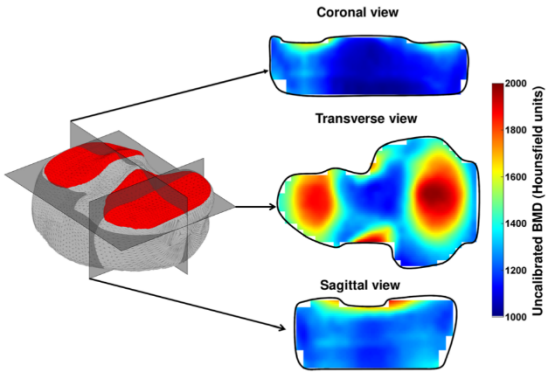

Fig. 6 Another example of application of the registration method where BMD is quantified in the entire proximal tibia. This figure displays the reference tibial mesh (left) and three BMD maps corresponding to the average of the 23 knees (right).

The method proposed in this article opens the door to numerous applications. As an example, it was used to characterize the BMD distribution below the cartilages. However, it can easily be adapted to analyze BMD in different locations and with different resolutions. In fact, filling the reference mesh with cells instead of using two stacks of cells below the cartilages allows quantifying the distribution of BMD in the entire proximal tibia. Figure 6 illustrates such an application of the method with cubic cells of 2 mm sides. This other application also reported an excellent reproducibility (ICC of 0.95 ± 0.02 and aCV $2.5 \pm 2.1\%$). Therefore, combining the results of the evaluations performed for measurements below the cartilage centers and in the entire proximal tibia suggests an excellent reproducibility of the registration method everywhere in the proximal tibia. In addition to the location of interest, the method can also be extended to standardize the assessment of other bone parameters. For instance, modeling the relationships (texture) among voxels, instead of averaging their values, could provide an indirect assessment of bone microarchitecture [40]. Finally, it is worth mentioning that the method is not limited to CT scans, and that it would work just as well with magnetic resonance images.

It is important to stress the fact that the proposed registration method requires tibias imaged from the intercondilar tubercule to at least 2.0 cm below the cartilages. This minimal height is necessary to match the bone profile area and thus to calculate the proximal–distal scaling (Sec. 2.2.2). This requirement should however not be seen as a limitation as the present method was precisely designed to analyze the first few centimeters of bone below the cartilages and therefore to be applied to images with enough bone height. Nevertheless, alternatives methods already exist to quantify smaller depth of bone below the cartilages [19,22]. It is also important to mention that the number of voxel centers per unit of volume (i.e., the voxel centers density) could vary after registration. For example, registering a smaller bone to a larger bone will decrease the voxel center density. Therefore, when planning to use the proposed registration method, like with any registration method, it is important to consider not only the initial voxel centers density (imaging resolution), but also the density changes that could occur with the registration. In fact, this remark of acquiring adequate images for the analysis of interest is not limited to the resolution. It extends to the other acquisition parameters, such as reconstruction algorithms and X-ray settings. But again, the selection of the appropriate parameters is not conditioned by the proposed surface-based registration method, but by the future applications (research questions or clinical applications).

This study has a few limitations, which should be discussed. First, it included only healthy subjects, meaning that the method will need to be evaluated on other populations in subsequent research. Second, while the reproducibility was shown to be excellent in two examples of applications, future uses of the method could require additional validation if the applications differ significantly from the applications considered in this work. Furthermore, since this study focused on the registration method, which is not tied to a particular segmentation method, the reproducibility with respect to different segmentations was not investigated. However, the reproducibility of knee segmentation methods reported previously suggest that the segmentation should have little effect on the registration [41,42]. Third, uncalibrated BMD was reported in this study due to data availability. Nevertheless, the method proposed in this work, which purposely relies on surface matching and not on CT voxel intensities, can be applied interchangeably to uncalibrated and calibrated images. Finally, although the registration method is fully automatic, the segmentation of the tibias was done semimanually. This requirement for human intervention should not be seen as a limitation as automatic segmentation of the tibial bone is possible [43].

5 Conclusion

In conclusion, a registration method was presented to quantify 3D BMD distribution in the proximal tibia based on routine knee CT scans. It was shown to be reproducible and to offer promising possibilities to analyze BMD and other bone properties. In particular, it could be used to detect or monitor the progression of bone alterations and to improve the understanding and treatment of musculoskeletal pathologies.

Acknowledgment

The funding source had no involvement in the study design, collection, analysis and interpretation of data; in the writing of the paper; and in the decision to submit the paper for publication.

Funding Data

- Lausanne Orthopedic Research Foundation.

Conflict of Interest

The authors declare that there are no conflicts of interest associated with this research.

References

[1] Lo, G. H., Niu, J., McLennan, C. E., Kiel, D. P., McLean, R. R., Guermazi, A., Genant, H. K., McAlindon, T. E., and Hunter, D. J., 2008, "Meniscal Damage Associated With Increased Local Subchondral Bone Mineral Density: A Framingham Study," Osteoarthritis Cartilage, **16**(2), pp. 261–267.
[2] van der Wal, R. J., Attia, D., Waarsing, E. H., Thomassen, B. J., and van Arkel, E. R., 2018, "Two-Year Follow-Up of Bone Mineral Density Changes in the Knee After Meniscal Allograft Transplantation: Results of an Explorative Study," Knee, **25**(6), pp. 1091–1099.
[3] van Meer, B. L., Waarsing, J. H., van Eijsden, W. A., Meuffels, D. E., van Arkel, E. R. A., Verhaar, J. A. N., Bierma-Zeinstra, S. M. A., and Reijman, M., 2014, "Bone Mineral Density Changes in the Knee Following Anterior Cruciate Ligament Rupture," Osteoarthritis Cartilage, **22**(1), pp. 154–161.
[4] Bayar, A., Sarıkaya, S., Keser, S., Özdolap, Ş., Tuncay, İ., and Ege, A., 2008, "Regional Bone Density Changes in Anterior Cruciate Ligament Deficient Knees: A DEXA Study," Knee, **15**(5), pp. 373–377.
[5] Edwards, W., Schnitzer, T. J., and Troy, K., 2014, "Bone Mineral and Stiffness Loss at the Distal Femur and Proximal Tibia in Acute Spinal Cord Injury," Osteoporosis Int., **25**(3), pp. 1005–1015.
[6] Garland, D. E., Stewart, C. A., Adkins, R. H., Hu, S. S., Rosen, C., Liotta, F. J., and Weinstein, D. A., 1992, "Osteoporosis After Spinal Cord Injury," J. Orthop. Res., **10**(3), pp. 371–378.
[7] Shi, M., Chen, L., Wu, H., Wang, Y., Wang, W., Zhang, Y., and Yan, S., 2018, "Effect of Bisphosphonates on Periprosthetic Bone Loss After Total Knee Arthroplasty: A Meta-Analysis of Randomized Controlled Trials," BMC Musculoskelet. Disord., **19**(1), p. 177.
[8] Winther, N., Jensen, C., Petersen, M., Lind, T., Schrøder, H., and Petersen, M., 2016, "Changes in Bone Mineral Density of the Proximal Tibia After Uncemented Total Knee Arthroplasty. A Prospective Randomized Study," Int. Orthop., **40**(2), pp. 285–294.

[9] Hulet, C., Sabatier, J. P., Souquet, D., Locker, B., Marcelli, C., and Vielpeau, C., 2002, "Distribution of Bone Mineral Density at the Proximal Tibia in Knee Osteoarthritis," Calcif. Tissue Int., **71**(4), pp. 315–22. Oct
[10] Lo, G. H., Zhang, Y., McLennan, C., Niu, J., Kiel, D. P., McLean, R. R., Aliabadi, P., Felson, D. T., and Hunter, D. J., 2006, "The Ratio of Medial to Lateral Tibial Plateau Bone Mineral Density and Compartment-Specific Tibiofemoral Osteoarthritis," Osteoarthritis Cartilage, **14**(10), pp. 984–990.
[11] Li, W., Kezele, I., Collins, D. L., Zijdenbos, A., Keyak, J., Kornak, J., Koyama, A., Saeed, I., LeBlanc, A., Harris, T., Lu, Y., and Lang, T., 2007, "Voxel-Based Modeling and Quantification of the Proximal Femur Using Inter-Subject Registration of Quantitative CT Images," Bone, **41**(5), pp. 888–895.
[12] Carballido-Gamio, J., Harnish, R., Saeed, I., Streeper, T., Sigurdsson, S., Amin, S., Atkinson, E. J., Therneau, T. M., Siggeirsdottir, K., Cheng, X., Melton, L. J., Keyak, J., Gudnason, V., Khosla, S., Harris, T. B., and Lang, T. F., 2013, "Proximal Femoral Density Distribution and Structure in Relation to Age and Hip Fracture Risk in Women," J Bone Miner Res, **28**(3), pp. 537–46.
[13] Bredbenner, T. L., Mason, R. L., Havill, L. M., Orwoll, E. S., Nicolella, D. P., and Study, O. F. I. M., for the Osteoporotic Fractures in Men (MrOS) Study, 2014, "Fracture Risk Predictions Based on Statistical Shape and Density Modeling of the Proximal Femur," J. Bone Miner. Res., **29**(9), pp. 2090–2100.
[14] Marangalou, J. H., Ito, K., Taddei, F., and Van Rietbergen, B., 2014, "Inter-Individual Variability of Bone Density and Morphology Distribution in the Proximal Femur and T12 Vertebra," Bone, **60**, pp. 213–220.
[15] Li, W., Kornak, J., Harris, T., Keyak, J., Li, C., Lu, Y., Cheng, X., and Lang, T., 2009, "Identify Fracture-Critical Regions Inside the Proximal Femur Using Statistical Parametric Mapping," Bone, **44**(4), pp. 596–602.
[16] Engelke, K., Libanati, C., Fuerst, T., Zysset, P., and Genant, H., 2013, "Advanced CT Based In Vivo Methods for the Assessment of Bone Density, Structure, and Strength," Curr. Osteoporos. Rep., **11**(3), pp. 246–255.
[17] Zerfass, P., Lowitz, T., Museyko, O., Bousson, V., Laouisset, L., Kalender, W. A., Laredo, J.-D., and Engelke, K., 2012, "An Integrated Segmentation and Analysis Approach for QCT of the Knee to Determine Subchondral Bone Mineral Density and Texture," IEEE Trans. Biomed. Eng., **59**(9), pp. 2449–2458.
[18] Lowitz, T., Museyko, O., Bousson, V., Kalender, W. A., Laredo, J. D., and Engelke, K., 2014, "Characterization of Knee Osteoarthritis-Related Changes in Trabecular Bone Using Texture Parameters at Various Levels of Spatial Resolution—a Simulation Study," BoneKEy Rep., **3**, p. 615.
[19] Johnston, J. D., Masri, B. A., and Wilson, D. R., 2009, "Computed Tomography Topographic Mapping of Subchondral Density (CT-TOMASD) in Osteoarthritic and Normal Knees: Methodological Development and Preliminary Findings," Osteoarthritis Cartilage, **17**(10), pp. 1319–26. Oct
[20] Bennell, K. L., Creaby, M. W., Wrigley, T. V., and Hunter, D. J., 2008, "Tibial Subchondral Trabecular Volumetric Bone Density in Medial Knee Joint Osteoarthritis Using Peripheral Quantitative Computed Tomography Technology," Arthritis Rheum, **58**(9), pp. 2776–2785.
[21] Bousson, V., Lowitz, T., Laouisset, L., Engelke, K., and Laredo, J. D., 2012, "CT Imaging for the Investigation of Subchondral Bone in Knee Osteoarthritis," Osteoporos Int., **23**(S8), pp. 861–865.
[22] Omoumi, P., Babel, H., Jolles, B. M., and Favre, J., 2017, "Quantitative Regional and Sub-Regional Analysis of Femoral and Tibial Subchondral Bone Mineral Density (sBMD) Using Computed Tomography (CT): Comparison of Non-Osteoarthritic (OA) and Severe OA Knees," Osteoarthritis Cartilage, **25**(11), pp. 1850–1857. Nov
[23] Carballido-Gamio, J., and Nicolella, D. P., 2013, "Computational Anatomy in the Study of Bone Structure," Curr. Osteoporos. Rep., **11**(3), pp. 237–45.
[24] Oliveira, F. P., and Tavares, J. M., 2014, "Medical Image Registration: A Review," Comput. Methods Biomech. Biomed. Eng., **17**(2), pp. 73–93.
[25] Miyabara, Y., Holmes, D., III, Camp, J., Miller, V. M., and Kearns, A., 2012, "Comparison of Calibrated and Uncalibrated Bone Mineral Density by CT to DEXA in Menopausal Women," Climacteric, **15**(4), pp. 374–381.
[26] Boomsma, M. F., Slouwerhof, I., van Dalen, J. A., Edens, M. A., Mueller, D., Milles, J., and Maas, M., 2015, "Use of Internal References for Assessing CT Density Measurements of the Pelvis as Replacement for Use of an External Phantom," Skelet. Radiol., **44**(11), pp. 1597–1602.
[27] Wolff, J., 1892, "Das Gesetz Der Transformation Der Knochen," A Hirshwald, **1**, pp. 1–152.
[28] Johnston, J. D., Kontulainen, S. A., Masri, B. A., and Wilson, D. R., 2010, "A Comparison of Conventional Maximum Intensity Projection With a New Depth-Specific Topographic Mapping Technique in the CT Analysis of Proximal Tibial Subchondral Bone Density," Skelet. Radiol., **39**(9), pp. 867–76.
[29] Bryan, R., Nair, P. B., and Taylor, M., 2009, "Use of a Statistical Model of the Whole Femur in a Large Scale, Multi-Model Study of Femoral Neck Fracture Risk," J. Biomech., **42**(13), pp. 2171–2176.
[30] Nicolella, D. P., and Bredbenner, T. L., 2012, "Development of a Parametric Finite Element Model of the Proximal Femur Using Statistical Shape and Density Modelling," Comput. Methods Biomech. Biomed. Eng., **15**(2), pp. 101–110.
[31] Favre, J., Erhart-Hledik, J. C., Blazek, K., Fasel, B., Gold, G. E., and Andriacchi, T. P., 2017, "Anatomically Standardized Maps Reveal Distinct Patterns of Cartilage Thickness With Increasing Severity of Medial Compartment Knee Osteoarthritis," J. Orthop. Res., **35**(11), pp. 2442–2451. Nov
[32] Möller, T., 1997, "A Fast Triangle-Triangle Intersection Test," J. Graphics Tools, **2**(2), pp. 25–30.
[33] Byrd, R. H., Gilbert, J. C., and Nocedal, J., 2000, "A Trust Region Method Based on Interior Point Techniques for Nonlinear Programming," Math. Program., **89**(1), pp. 149–185.
[34] Amberg, B., Romdhani, S., and Vetter, T., 2007, "Optimal Step Nonrigid ICP Algorithms for Surface Registration," Computer Vision and Pattern Recognition, 2007, CVPR'07, IEEE Conference, Minneapolis, MN, June 17–22, pp. 1–8.
[35] Donato, G., and Belongie, S. J., 2003, "Approximation Methods for Thin Plate Spline Mappings and Principal Warps," A. Heyden, G. Sparr, M. Nielsen, and P. Johansen, eds., *Proceedings, Part III, Lecture Notes in Computer Science, Computer Vision – ECCV 2002: 7th European Conference on Computer Vision*, Copenhagen, Denmark, pp. 21–31.
[36] Botsch, M., Kobbelt, L., Pauly, M., Alliez, P., and Lévy, B., 2010, *Polygon Mesh Processing*, AK Peters/CRC Press, Natick, MA.
[37] Rockafellar, R. T., and Wets, R. J.-B., 1998, *Variational Analysis*, Springer, Berlin.
[38] Fisher, R. A., 1992, "Statistical Methods for Research Workers," *Breakthroughs in Statistics*, Springer, New York, pp. 66–70.
[39] Brock, K. K., Mutic, S., McNutt, T. R., Li, H., and Kessler, M. L., 2017, "Use of Image Registration and Fusion Algorithms and Techniques in Radiotherapy: Report of the AAPM Radiation Therapy Committee Task Group No. 132," Med. Phys., **44**(7), pp. e43–e76.
[40] Pothuaud, L., Carceller, P., and Hans, D., 2008, "Correlations Between Grey-Level Variations in 2D Projection Images (TBS) and 3D Microarchitecture: Applications in the Study of Human Trabecular Bone Microarchitecture," Bone, **42**(4), pp. 775–87. Apr
[41] Ambellan, F., Tack, A., Ehlke, M., and Zachow, S., 2019, "Automated Segmentation of Knee Bone and Cartilage Combining Statistical Shape Knowledge and Convolutional Neural Networks: Data From the Osteoarthritis Initiative," Med. Image Anal., **52**, pp. 109–118.
[42] Heimann, T., Morrison, B. J., Styner, M. A., Niethammer, M., and Warfield, S., 2010, "Segmentation of Knee Images: A Grand Challenge," Proc. MICCAI Workshop on Medical Image Analysis for the Clinic, Beijing, China, Sept. 20–24, pp. 207–214.
[43] Taddei, F., Cristofolini, L., Martelli, S., Gill, H., and Viceconti, M., 2006, "Subject-Specific Finite Element Models of Long Bones: An In Vitro Evaluation of the Overall Accuracy," J. Biomech., **39**(13), pp. 2457–2467.

Journal of
Clinical Medicine

MDPI

Article

Three-Dimensional Quantification of Bone Mineral Density in the Distal Femur and Proximal Tibia Based on Computed Tomography: In Vitro Evaluation of an Extended Standardization Method

Hugo Babel [1,*], Patrick Omoumi [2], Killian Cosendey [1], Hugues Cadas [3], Brigitte M. Jolles [1,4] and Julien Favre [1]

[1] Swiss BioMotion Lab, Department of Musculoskeletal Medicine, Lausanne University Hospital and University of Lausanne (CHUV-UNIL), CH-1011 Lausanne, Switzerland; killian.cosendey@chuv.ch (K.C.); brigitte.jolles-haeberli@chuv.ch (B.M.J.); julien.favre@chuv.ch (J.F.)
[2] Service of Diagnostic and Interventional Radiology, Lausanne University Hospital and University of Lausanne (CHUV-UNIL), CH-1011 Lausanne, Switzerland; patrick.omoumi@chuv.ch
[3] Unité Facultaire d'Anatomie et de Morphologie (UFAM), University of Lausanne (UNIL), CH-1005 Lausanne, Switzerland; hugues.cadas@unil.ch
[4] Institute of Microengineering, Ecole Polytechnique Fédérale Lausanne (EPFL), CH-1015 Lausanne, Switzerland
* Correspondence: hugo.babel@chuv.ch

Abstract: While alterations in bone mineral density (BMD) are of interest in a number of musculoskeletal conditions affecting the knee, their analysis is limited by a lack of tools able to take full advantage of modern imaging modalities. This study introduced a new method, combining computed tomography (CT) and computational anatomy algorithms, to produce standardized three-dimensional BMD quantification in the distal femur and proximal tibia. The method was evaluated on ten cadaveric knees CT-scanned twice and processed following three different experimental settings to assess the influence of different scans and operators. The median reliability (intraclass correlation coefficient (ICC)) ranged from 0.96 to 0.99 and the median reproducibility (precision error (RMSSD)) ranged from 3.97 to 10.75 mg/cc for the different experimental settings. In conclusion, this paper presented a method to standardize three-dimensional knee BMD with excellent reliability and adequate reproducibility to be used in research and clinical applications. The perspectives offered by this novel method are further reinforced by the fact it relies on conventional CT scan of the knee. The standardization method introduced in this work is not limited to BMD and could be adapted to quantify other bone parameters in three dimension based on CT images or images acquired using different modalities.

Keywords: bone mineral density; knee; registration; osteoarthritis; osteoporosis; quantitative computed tomography; computational anatomy

Citation: Babel, H.; Omoumi, P.; Cosendey, K.; Cadas, H.; Jolles, B.M.; Favre, J. Three-Dimensional Quantification of Bone Mineral Density in the Distal Femur and Proximal Tibia Based on Computed Tomography: In Vitro Evaluation of an Extended Standardization Method. *J. Clin. Med.* **2021**, *10*, 160. https://doi.org/10.3390/jcm10010160

Received: 27 November 2020
Accepted: 22 December 2020
Published: 5 January 2021

1. Introduction

Quantifying the alterations in bone mineral density (BMD) is of interest in a number of conditions affecting the knee, including fractures [1–3], arthroplasty [4–6], meniscal damage and repair [7–9], osteoporosis [10,11], and osteoarthritis [12–14]. So far, in-vivo analysis of BMD has primarily relied on dual x-ray absorptiometry (DXA). However, the two-dimensional nature of DXA limits the assessment of spatial variations and the detection of localized alterations in BMD. To improve our understanding of the pathophysiological implications of BMD alterations, a primer to wider uses of BMD measures in clinical evaluation, there is a need for noninvasive methods allowing for more comprehensive assessment of BMD in the knee.

Computed tomography (CT) is an interesting alternative for the three-dimensional quantification of BMD [1,14–17]. The assessment of knee BMD is of particular interest [14,18], as radiation dose exposure with CT is not significant at this joint, contrary to other anatomical locations [19]. However, in order to conduct interpatient comparisons, there is a need to establish an anatomical correspondence between knees, as they naturally differ in size and shape. An anatomical correspondence is also necessary for longitudinal analyses in the case of pathologies that could alter the shape of the bones, such as osteoarthritis or tumors [20–22]. So far, the question of anatomical correspondence in the analysis of CT scans has generally been eluded by relying on regions of interest (ROIs) based on anatomical landmarks or geometrical guidelines [14,16,17,23–26]. However, the use of ROIs hinders the assessment of spatial variations in bone properties and does not take full advantage of CT scans by reducing information to a limited and low-resolution set of regional values.

Recently, computational anatomy methods were proposed to study bone structures [27]. These methods, firstly developed for brain analysis [28], register individual bones to a reference bone, thus allowing standardization of bone properties such as BMD. One such method was recently proposed for the proximal tibia [18]. However, as global changes in BMD have been observed in both the tibia and the femur in various pathologies [1–9,12–14], there is an interest to extend this method to the distal femur as well.

To ensure the suitability of BMD measures for clinical and research applications, the reproducibility and reliability of the BMD measures with respect to different scans and operators should be evaluated. To the authors' knowledge, this evaluation, though essential, has seldom been undertaken in computational anatomy algorithms, particularly in those aiming to standardize BMD.

Thus, the study aimed to present a method to standardize BMD within the distal femur by extending an algorithm developed for the proximal tibia [18]. This work also aimed to evaluate the reproducibility and reliability of the proposed BMD standardization method.

2. Materials and Methods

2.1. Experimental Setup

Ten formalin-fixed cadaveric adult knees were scanned with CT and rescanned after repositioning. The acquisition was performed on a 40-row detector helical CT scanner (Discovery CT750HD; GE Medical Systems) using the following parameters: tube voltage, 120 kVp; reference tube current-time product, 200 mAs; and bone convolution kernel (U70u), voxel size of $0.5 \times 0.5 \times 0.312$ mm. A solid calcium hydroxyapatite-based bone mineral reference phantom (Mindways Software, Austin, TX, USA) was used to establish a correspondence between the CT units and volumetric BMD (mg/cc). The knees had been stored in a refrigerator for up to 48 months before being scanned for this study. The research protocol was approved by the local ethics committee, and following local regulations regarding research on deceased persons, no demographic data was available for the samples. A senior musculoskeletal radiologist with more than 10 years of experience read the CT scans and, based on the presence and severity of osteophytes [29], concluded that five of the knees had degenerative changes (three mild and two severe changes).

2.2. Segmentation and Registration

The tibial and femoral bones were segmented in the CT images using custom semi-manual segmentation tools [17,30], yielding three-dimensional triangular tibial and femoral bone meshes (Figure 1).

To describe the registration procedure, this paper uses the convention of moving and reference bones, with the moving bone being registered to the reference bone. Similar to a prior method for the proximal tibia [18], the registration involves two phases: (1) registering the surface of the moving bone to the surface of the reference bone (Section 2.2.1), followed by (2) propagating the surface-to-surface transformations to the CT voxels within the

moving tibia and femur (Section 2.2.2). Following these two phases, both the surface of the bones and the BMD information contained within the image are registered to the reference bones.

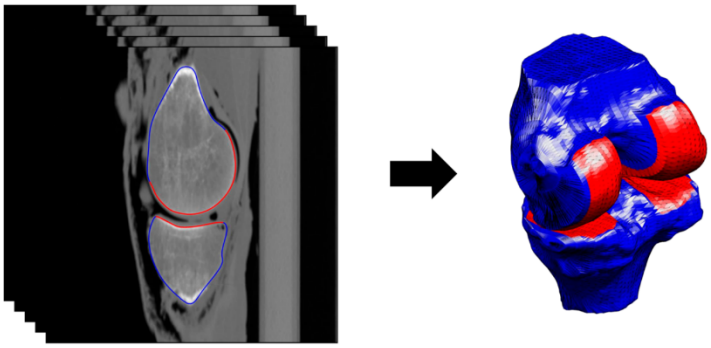

Figure 1. Segmentation of the femoral and tibial bones and identification of the subchondral bone areas (**left**), and resulting three-dimensional femoral and tibial bone meshes (**right**). In both plots, the subchondral bones are in red and the non-subchondral bones are in blue.

2.2.1. Phase 1

For the proximal tibia, the surface (mesh) of the moving bone was registered to the reference bone following a previously described method [18], involving three steps (Figure 2). First, the moving tibia is aligned to the reference tibia by combining a translation, a rotation, and an isotropic scaling based on the medial and lateral subchondral bone areas. Second, the moving tibia is scaled along its longitudinal axis to match the reference tibia. Third, the moving tibia is deformed locally using nonrigid registration to closely match the bone surface of the reference tibia.

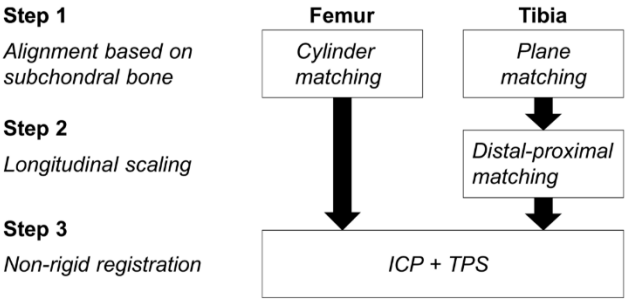

Figure 2. Flowchart of the first phase consisting of bone surface registration. ICP: Iterative Closest Point, TPS: Thin Plate Splines.

For the distal femur, the method in [18] was modified as follows. The first step of the registration procedure was adapted by fitting a cylinder to the subchondral bone area [30–32] of the moving and reference femurs (Figure 3, step 1a). After manual identification of the trochlear notch on both femurs, the moving femur was translated and rotated to align its cylinder axis and the projection of its trochlear notch on the cylinder axis to the cylinder axis and projection of the trochlear notch of the reference femur (Figure 3, step 1a). Then, the moving femur was scaled such that the radius of the two cylinders coincide and the condylar regions, from the trochlear notch to the medial and lateral epicondyles, were scaled separately along the cylinder axis to account for their individual sizes (Figure 3, step 1b). Next, the subchondral areas of the moving and reference femurs were aligned by rotating the moving femur around the cylinder axis to minimize the distance between

subchondral areas (Figure 3, step 1c). This first step was necessary to limit differences between the two femurs in terms of bone size and placement in the scanner and to account for differences in orientation within the field of view of the scanner. The second step in the tibial registration procedure, which consisted in scaling the proximal tibia along its longitudinal axis to account for the high level of symmetry in the tibia, was not necessary for the distal femur (Figure 2). Finally, in the third step, the same method as previously described for the tibia, which combines nonrigid iterative closest point (ICP) [33] and thin-plate splines (TPS) [34], was used to locally deform the moving bone such that its surface closely matched the surface of the reference bone (Figure 3, step 3).

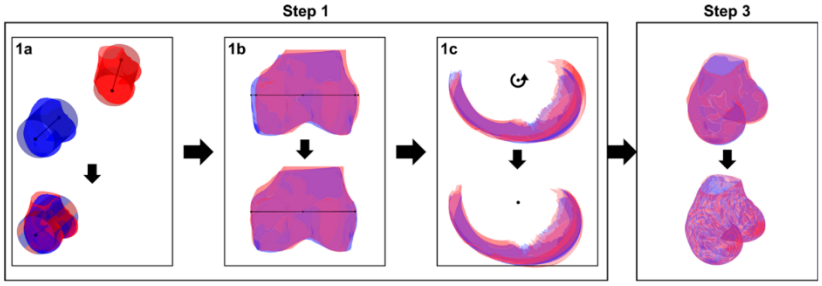

Figure 3. Illustration of the first phase of the registration procedure for the distal femur (see Figure 2 for an overall Figure 1. (**a**): the cylinder fitted to the subchondral bone area of the moving femur is aligned and scaled to coincide with the cylinder of the reference femur. Step 1. (**b**): the moving femur is scaled around and along the cylinder axis to match the size of the reference femur. Step 1. (**c**): the moving femur is rotated around the cylinder axis in order to align its subchondral bone area to the subchondral area of the reference femur. Step 2: not necessary for the femur. Step 3: a nonrigid transformation is applied to the moving femur to locally match the reference femur.

2.2.2. Phase 2

During the second phase, the surface-to-surface transformations calculated in the first phase were applied to the voxels of the moving tibia and femur, as previously described for the tibia [18]. With this operation, the CT voxels were translated, scaled, rotated, and deformed.

2.3. Evaluation of the Method

For each cadaveric knee, the images from the (first) CT scan were segmented by two operators and the images from the rescan were segmented by one of the two operators, resulting in three sets of 10 segmented knees. The tibial and femoral bones resulting from each segmentation were then registered to a reference tibia and femur [18], following the procedure described above. Standardized BMD reporting was achieved through three-dimensional maps created by filling the reference tibia and femur with 7000 and 12,000 isotropic cells of 2 mm sides, respectively, and by determining the BMD value of each cell, for each segmentation, as the average of all registered CT voxels contained within the cell's boundaries [18].

The reliability and reproducibility of the standardized BMD measures were evaluated in three settings: intra-operator/inter-scan, inter-operator/intra-scan, and inter-operator/inter-scan. The reliability was assessed for each of the 7000 tibial and 12,000 femoral cells by calculating the two-way random-effects intraclass correlation coefficient (ICC) [35] over the 10 knees for the repeated measurement. The reliability was classified as poor (ICC < 0.5), moderate ($0.5 \leq$ ICC < 0.75), good ($0.75 \leq$ ICC < 0.9), and excellent (ICC > 0.9) [36]. The reproducibility was assessed for each of the 7000 tibial and 12,000 femoral cells as the root mean square over the 10 knees for the precision error of the repeated measurement (RMSSD) [37]. The reliability and reproducibility were compared between settings using Wilcoxon signed-rank tests [38] with a Bonferroni correction for multiple comparisons,

and the effect size was reported [39]. Lastly, the reproducibility and reliability maps were visually examined to assess local effects.

All processing in this study was done with custom software using Matlab R2019 b (Mathworks, Natick, MA, USA).

3. Results

The median reliability of the 12,000 femoral cells ranged from 0.96 to 0.97 among the three experimental settings (Table 1), with more than 84% of the cells reporting an excellent ICC for each setting (Figure 4). The reliability in the inter-operator/inter-scan setting was statistically lower than in the two other settings ($z \leq -27.7$, $p \leq 0.001$), with a small effect size ($\leq$0.29), and statistically higher in the intra-operator/inter-scan compared to the inter-operator/intra-scan setting ($z = 4.0$, $p < 0.001$), with a very small effect size (0.04). Two areas of lower reliability were observed within the femur for the two inter-operator settings: at the epicondyles and around the trochlear notch (Figure 5). The median reproducibility ranged from 9.56 mg/cc (2.5% of the BMD range) in the intra-operator/inter-scan setting to 10.75 mg/cc (2.8% of the BMD range) in the inter-operator/inter-scan setting (Table 1). The reproducibility in the inter-operator/inter-scan setting was statistically higher than in the two other settings ($z \geq 21.9$, $p \leq 0.001$), with a small effect size ($\geq$0.33), and statistically higher in the inter-operator/intra-scan setting compared to the intra-operator/inter-scan setting ($z = 5.7$, $p < 0.001$), with a very small effect size (0.05).

Table 1. Reliability and reproducibility of the bone mineral density (BMD) standardization.

	Intra-Operator Inter-Scan	Inter-Operator Intra-Scan	Inter-Operator Inter-Scan
	Femur		
Reliability [#]	0.97 (0.94, 0.98)	0.97 (0.93, 0.98)	0.96 (0.93, 0.98)
Reproducibility [#]	9.56 (7.10, 13.46)	9.67 (6.61, 14.68)	10.75 (8.16, 14.96)
	Tibia		
Reliability [*,#]	0.97 (0.96, 0.98)	0.99 (0.98, 1.0)	0.97 (0.95, 0.98)
5	6.58 (5.70, 8.49)	3.97 (2.39, 7.39)	7.29 (5.92, 10.30)

Reliability (ICC) and reproducibility (RMSSD) data are presented as the median [1st quartile, 3rd quartile] over the 12,000 femoral or 7000 tibial cells. Reproducibility data are in mg/cc. Symbols indicate differences between experimental settings that achieved statistical significance (adjusted $p < 0.05$): * between the intra-operator/inter-scan and inter-operator/intra-scan settings, [#] between the intra-operator/inter-scan and inter-operator/inter-scan settings, and between the inter-operator/intra-scan and inter-operator/inter-scan settings.

In the tibia, the median reliability of the 7000 cells was excellent (ICC $\geq$ 0.97) for the three experimental settings (Table 1), with more than 92% of the cells having an ICC over 0.9 for each setting (Figure 4). The reliability was statistically higher in the inter-operator/intra-scan setting than in the two other settings ($z \geq 46.5$, $p < 0.001$), with a medium effect size ($\geq$0.56), and higher in the intra-operator/inter-scan setting than in the inter-operator/inter-scan setting ($z = 32.8$, $p < 0.001$), with a small effect size (0.39). The lower ICC were heterogeneously distributed among the cells. The median reproducibility ranged from 3.97 mg/cc (1.0% of the BMD range) in the inter-operator/intra-scan setting to 7.29 mg/cc (1.9% of the BMD range) in the inter-operator/inter-scan setting (Table 1). The reproducibility was statistically lower in the inter-operator/intra-scan setting than in the other two settings ($z \leq 41.2$, $p < 0.001$), with a small to medium effect size ($\geq$0.49), and lower in the intra-operator/inter-scan setting than in the inter-operator/inter-scan setting ($z = -36.8$, $p < 0.001$), with a small effect size ($\geq$0.44).

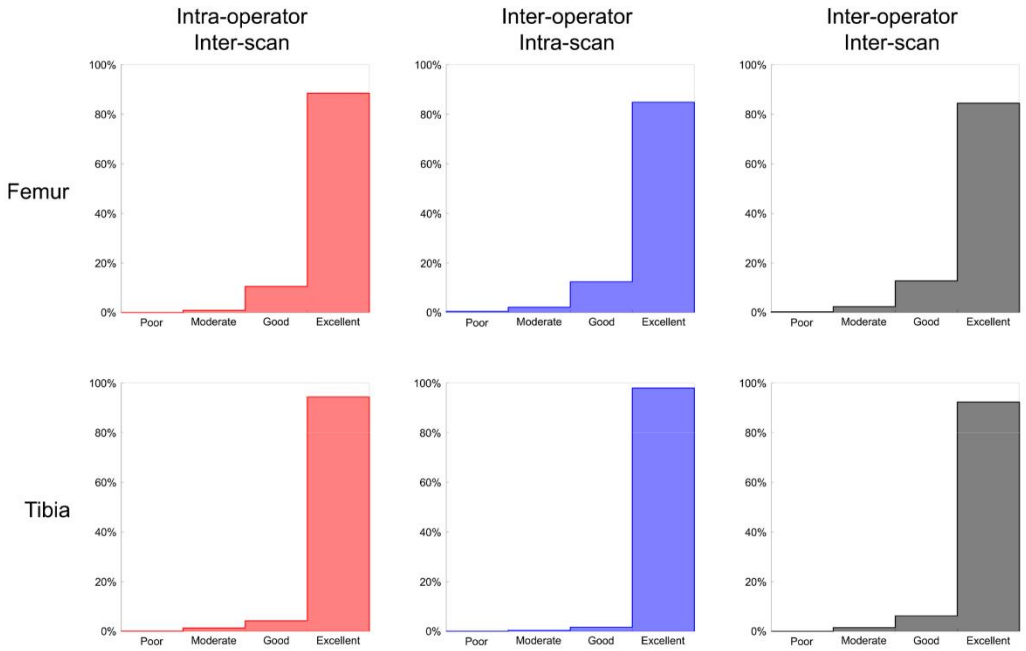

Figure 4. Histogram of the reliability for the 12,000 femoral (**top**) and 7000 tibial (**bottom**) cells in the three settings.

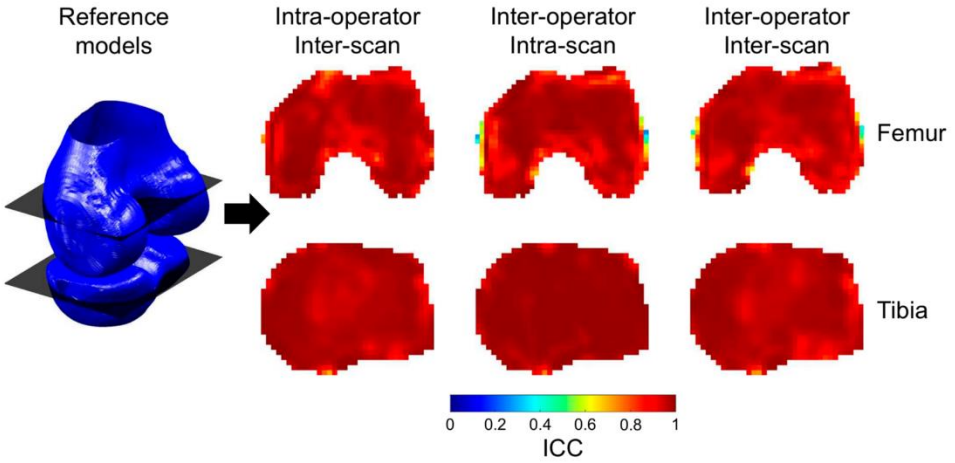

Figure 5. Illustration of the spatial variations in reliability: (**left**) reference distal femur and proximal tibia bone models with two representative coronal slices and (**right**) intraclass correlation (ICC) maps for the three settings at the coronal slices for the tibia (**top**) and the femur (**bottom**).

4. Discussion

A method was presented to standardize BMD in the distal femur and proximal tibia with excellent reliability and adequate reproducibility to be used in clinical and research applications. This new possibility of comprehensive quantification of knee BMD in three dimension offers promising perspectives to improve our understanding of the role of BMD in the initiation and progression of musculoskeletal pathologies as well as to introduce novel BMD measures in clinics. In this regard, it is important to mention that the method reported in this work can be combined with existent techniques to automatically segment

CT images [40,41], thus allowing standardized high-resolution reporting of knee BMD with minimal operator intervention.

While the reliability of the BMD standardization was excellent in all three settings, both for the femur and the tibia, there were local areas of lower reliability within the femur. Interestingly, lower reliability was observed in regions where segmenting the CT images was more delicate, such as peripheral regions around the epicondyles. Therefore, the lower reliability in these regions is most likely due to segmentation and not the registration procedure. Although differences in reliability among experimental settings achieved statistical significance, the reliability remained excellent for all three settings, suggesting that the standardization method can be used independently of the experimental conditions. No comparison with previous BMD standardization methods could be performed, as the reliability of femoral or tibial BMD has seldom been assessed in computational anatomy studies.

The reproducibility of the BMD standardization ranged from 4.0 to 10.7 mg/cc, which appears adequate with respect to the BMD differences, ranging from 33 to 150 mg/cc, previously reported with knee osteoarthritis or bone fractures [42–46]. Furthermore, the reproducibility reported in this study was consistent with data in the literature for proximal femoral BMD. Indeed, the reproducibility reported in Carballido-Gamio et al. [47] and Li et al. [48] for relatively large regions of interest (ROIs) ranges between 1.1 and 28 mg/cc. When attempting such a comparison across studies, it is important to note that the cells used in the present work are much smaller than the ROIs in Carballido-Gamio et al. and Li et al. and that, by definition, the reproducibility tends to be higher for larger volumes of interest [49,50]. Similar to the reliability results, reproducibility differences were observed among settings but were 3.1 to 37.5 times smaller than BMD differences reported in prior studies comparing control and pathological knees [42–46]. This further suggests that the standardization method is suitable independently of the experimental settings.

The present study has several strengths. First, the reliability and reproducibility were quantified on knees representative of the general population, suggesting that the results are applicable to a wide range of clinical presentations. Second, to the authors' knowledge, this study is the first to assess comprehensively the reliability and reproducibility of a computational anatomy method to standardize BMD. The reliability and reproducibility data in the present work provide valuable information for future applications of the proposed method and for the field in general. Third, the method introduced in this work could be used to standardize other bone parameters, such as texture [51], or to assess the spatial distribution of bone defects, such as osteophytes, bone cysts, or bone marrow lesions, which are currently only assessed semi-quantitatively [52]. Fourth, the registration procedure establishes an anatomical correspondence based solely on bone surfaces. As such, it does not depend on the acquisition parameters or bone size. In addition, the registration procedure could be applied across imaging modalities.

This study also has limitations which should be discussed. First, the evaluation relied on cadaveric knees because subjecting individuals to repeated CT scans would have represented unnecessary and unethical risks [53]. An in vivo assessment of the method would be expected to yield similar results, as BMD differences between fresh and formalin-fixed cadavers have been reported to remain negligible, even after several months [54,55]. However, assessing the method with undocumented cadaveric specimens prevented evaluating the sensitivity of the method. Future applications of the method to longitudinal data or to knees of different conditions should therefore evaluate its capacity to detect changes or differences in BMD [37]. Further studies will also be necessary to compare BMD data obtained using the present method to data obtained using DXA. Additionally, although the evaluation relied on a small sample size, the number of knees was sufficient with respect to the study objectives and in the range of previous studies evaluating methods to quantify BMD at the hip joint [47,48].

5. Conclusions

In conclusion, this paper presented a method to standardize BMD in the distal femur and proximal tibia with excellent reliability and reproducibility. This method could find applications in both research and clinics. Specifically, it could contribute to novel BMD measures or be used to visualize and analyze location-specific three-dimensional BMD patterns.

Author Contributions: Conceptualization, H.B., P.O., B.M.J. and J.F.; methodology, H.B., P.O. and J.F.; software, H.B. and J.F.; validation, H.B., K.C. and J.F.; formal analysis, H.B.; investigation, H.B., K.C. and J.F.; resources, H.B., P.O., K.C., H.C., B.M.J., and J.F.; data curation, H.B.; writing—original draft preparation, H.B. and J.F.; writing—review and editing, H.B., P.O., K.C., H.C., B.M.J. and J.F.; visualization, H.B.; supervision, P.O., B.M.J. and J.F.; project administration, H.B., P.O., K.C., H.C., B.M.J. and J.F.; funding acquisition, P.O., B.M.J. and J.F.; P.O., B.M.J. and J.F. supervised this study and should be considered as last authors. All authors have read and agreed to the published version of the manuscript.

Funding: This research was funded by the Swiss National Science Foundation (SNSF), Switzerland (Grant: CRSII5_177155) and the Lausanne Orthopedic Research Foundation (LORF), Switzerland.

Institutional Review Board Statement: The study was approved by the local ethics committee (CER-VD 2019-01102).

Data Availability Statement: The data are not publicly available due to regulatory provisions.

Acknowledgments: The authors would like to thank Isabelle Raymond and Patrice Rüegg for their assistance with the in vitro experiment and Christel Elandoy for her assistance in CT scanning.

Conflicts of Interest: The authors declare no conflict of interest.

References

1. Edwards, W.B.; Schnitzer, T.J.; Troy, K.L. Bone mineral and stiffness loss at the distal femur and proximal tibia in acute spinal cord injury. *Osteoporos. Int.* **2014**, *25*, 1005–1015. [CrossRef]
2. Garland, D.E.; Stewart, C.A.; Adkins, R.H.; Hu, S.S.; Rosen, C.; Liotta, F.J.; Weinstein, D.A. Osteoporosis after spinal cord injury. *J. Orthop. Res.* **1992**, *10*, 371–378. [CrossRef]
3. Henderson, R.C.; Berglund, L.M.; May, R.; Zemel, B.S.; Grossberg, R.I.; Johnson, J.; Plotkin, H.; Stevenson, R.D.; Szalay, E.; Wong, B.; et al. The Relationship Between Fractures and DXA Measures of BMD in the Distal Femur of Children and Adolescents with Cerebral Palsy or Muscular Dystrophy. *J. Bone Miner. Res.* **2010**, *25*, 520–526. [CrossRef]
4. Shi, M.; Chen, L.; Wu, H.; Wang, Y.; Wang, W.; Zhang, Y.; Yan, S. Effect of bisphosphonates on periprosthetic bone loss after total knee arthroplasty: A meta-analysis of randomized controlled trials. *BMC Musculoskelet. Disord.* **2018**, *19*, 177. [CrossRef]
5. Winther, N.; Jensen, C.; Petersen, M.; Lind, T.; Schroder, H.; Petersen, M. Changes in bone mineral density of the proximal tibia after uncemented total knee arthroplasty. A prospective randomized study. *Int. Orthop.* **2016**, *40*, 285–294. [CrossRef]
6. Petersen, M.M.; Olsen, C.; Lauritzen, J.B.; Lund, B. Changes in bone mineral density of the distal femur following uncemented total knee arthroplasty. *J. Arthroplasty* **1995**, *10*, 7–11. [CrossRef]
7. Petersen, M.M.; Olsen, C.; Lauritzen, J.B.; Lund, B.; Hede, A. Late changes in bone mineral density of the proximal tibia following total or partial medial meniscectomy. A randomized study. *J. Orthop. Res.* **1996**, *14*, 16–21. [CrossRef]
8. Lo, G.H.; Niu, J.; McLennan, C.E.; Kiel, D.P.; McLean, R.R.; Guermazi, A.; Genant, H.K.; McAlindon, T.E.; Hunter, D.J. Meniscal damage associated with increased local subchondral bone mineral density: A Framingham study. *Osteoarthr. Cartil.* **2008**, *16*, 261–267. [CrossRef] [PubMed]
9. Van der Wal, R.J.P.; Attia, D.; Waarsing, E.H.; Thomassen, B.J.W.; van Arkel, E.R.A. Two-year follow-up of bone mineral density changes in the knee after meniscal allograft transplantation: Results of an explorative study. *Knee* **2018**, *25*, 1091–1099. [CrossRef] [PubMed]
10. Bayar, A.; Sarikaya, S.; Keser, S.; Ozdolap, S.; Tuncay, I.; Ege, A. Regional bone density changes in anterior cruciate ligament deficient knees: A DEXA study. *Knee* **2008**, *15*, 373–377. [CrossRef] [PubMed]
11. Parker, R.K.; Ross, G.J.; Urso, J.A. Transient osteoporosis of the knee. *Skeletal Radiol.* **1997**, *26*, 306–309. [CrossRef] [PubMed]
12. Hulet, C.; Sabatier, J.P.; Souquet, D.; Locker, B.; Marcelli, C.; Vielpeau, C. Distribution of bone mineral density at the proximal tibia in knee osteoarthritis. *Calcif. Tissue Int.* **2002**, *71*, 315–322. [CrossRef] [PubMed]
13. Lo, G.H.; Zhang, Y.; McLennan, C.; Niu, J.; Kiel, D.P.; McLean, R.R.; Aliabadi, P.; Felson, D.T.; Hunter, D.J. The ratio of medial to lateral tibial plateau bone mineral density and compartment-specific tibiofemoral osteoarthritis. *Osteoarthr. Cartil.* **2006**, *14*, 984–990. [CrossRef] [PubMed]

14. Johnston, J.D.; Masri, B.A.; Wilson, D.R. Computed tomography topographic mapping of subchondral density (CT-TOMASD) in osteoarthritic and normal knees: Methodological development and preliminary findings. *Osteoarthr. Cartil.* **2009**, *17*, 1319–1326. [CrossRef]
15. Bousson, V.; Lowitz, T.; Laouisset, L.; Engelke, K.; Laredo, J.D. CT imaging for the investigation of subchondral bone in knee osteoarthritis. *Osteoporos. Int.* **2012**, *23*, 861–865. [CrossRef]
16. Bennell, K.L.; Creaby, M.W.; Wrigley, T.V.; Hunter, D.J. Tibial subchondral trabecular volumetric bone density in medial knee joint osteoarthritis using peripheral quantitative computed tomography technology. *Arthr. Rheum.* **2008**, *58*, 2776–2785. [CrossRef]
17. Omoumi, P.; Babel, H.; Jolles, B.M.; Favre, J. Quantitative regional and sub-regional analysis of femoral and tibial subchondral bone mineral density (sBMD) using computed tomography (CT): Comparison of non-osteoarthritic (OA) and severe OA knees. *Osteoarthr. Cartil.* **2017**, *25*, 1850–1857. [CrossRef]
18. Babel, H.; Wageli, L.; Sonmez, B.; Thiran, J.-P.; Omoumi, P.; Jolles, B.; Favre, J. A Registration Method for Three-Dimensional Analysis of Bone Mineral Density in the Proximal Tibia. *J. Biomech. Eng.* **2020**. [CrossRef]
19. Biswas, D.; Bible, J.E.; Bohan, M.; Simpson, A.K.; Whang, P.G.; Grauer, J.N. Radiation exposure from musculoskeletal computerized tomographic scans. *J. Bone Joint Surg. Am.* **2009**, *91*, 1882–1889. [CrossRef]
20. Bowes, M.; Lohmander, L.; Wolstenholme, C.; Vincent, G.; Conaghan, P.; Frobell, R. Marked and rapid change of bone shape in acutely ACL injured knees–An exploratory analysis of the Kanon trial. *Osteoarthr. Cartilage* **2019**, *27*, 638–645. [CrossRef]
21. Hunter, D.; Nevitt, M.; Lynch, J.; Kraus, V.B.; Katz, J.N.; Collins, J.E.; Bowes, M.; Guermazi, A.; Roemer, F.W.; Losina, E. Longitudinal validation of periarticular bone area and 3D shape as biomarkers for knee OA progression? Data from the FNIH OA Biomarkers Consortium. *Annal. Rheum. Dis.* **2016**, *75*, 1607–1614. [CrossRef]
22. Campanacci, M. *Bone and Soft Tissue Tumors*; Springer: New York, NY, USA, 2013.
23. Koo, S.; Gold, G.E.; Andriacchi, T.P. Considerations in measuring cartilage thickness using MRI: Factors influencing reproducibility and accuracy. *Osteoarthr. Cartil.* **2005**, *13*, 782–789. [CrossRef] [PubMed]
24. Wirth, W.; Eckstein, F. A technique for regional analysis of femorotibial cartilage thickness based on quantitative magnetic resonance imaging. *IEEE Trans. Med. Imaging* **2008**, *27*, 737–744. [CrossRef] [PubMed]
25. Hurwitz, D.E.; Sumner, D.R.; Andriacchi, T.P.; Sugar, D.A. Dynamic knee loads during gait predict proximal tibial bone distribution. *J. Biomech.* **1998**, *31*, 423–430. [CrossRef]
26. Wada, M.; Maezawa, Y.; Baba, H.; Shimada, S.; Sasaki, S.; Nose, Y. Relationships among bone mineral densities, static alignment and dynamic load in patients with medial compartment knee osteoarthritis. *Rheumatology* **2001**, *40*, 499–505. [CrossRef] [PubMed]
27. Carballido-Gamio, J.; Nicolella, D.P. Computational anatomy in the study of bone structure. *Curr. Osteoporos. Rep.* **2013**, *11*, 237–245. [CrossRef]
28. Grenander, U.; Miller, M.I. Computational anatomy: An emerging discipline. *Q. Appl. Math.* **1998**, *56*, 617–694. [CrossRef]
29. Peterfy, C.G.; Guermazi, A.; Zaim, S.; Tirman, P.F.; Miaux, Y.; White, D.; Kothari, M.; Lu, Y.; Fye, K.; Zhao, S.; et al. Whole-Organ Magnetic Resonance Imaging Score (WORMS) of the knee in osteoarthritis. *Osteoarthr. Cartil.* **2004**, *12*, 177–190. [CrossRef]
30. Favre, J.; Erhart-Hledik, J.C.; Blazek, K.; Fasel, B.; Gold, G.E.; Andriacchi, T.P. Anatomically Standardized Maps Reveal Distinct Patterns of Cartilage Thickness With Increasing Severity of Medial Compartment Knee Osteoarthritis. *J. Orthop. Res.* **2017**, *35*, 2442–2451. [CrossRef]
31. Scanlan, S.F.; Favre, J.; Andriacchi, T.P. The relationship between peak knee extension at heel-strike of walking and the location of thickest femoral cartilage in ACL reconstructed and healthy contralateral knees. *J. Biomech.* **2013**, *46*, 849–854. [CrossRef]
32. Favre, J.; Scanlan, S.F.; Erhart-Hledik, J.C.; Blazek, K.; Andriacchi, T.P. Patterns of femoral cartilage thickness are different in asymptomatic and osteoarthritic knees and can be used to detect disease-related differences between samples. *J. Biomech. Eng.* **2013**, *135*, 101002–101010. [CrossRef]
33. Amberg, B.; Romdhani, S.; Vetter, T. Optimal step nonrigid ICP algorithms for surface registration. In Proceedings of the Computer Vision and Pattern Recognition Conference, CVPR'07, Minneapolis, MN, USA, 17–22 June 2007; pp. 1–8.
34. Donato, G.; Belongie, S.J. *Approximation Methods for Thin Plate Spline Mappings and Principal Warps*; Citeseer; Department of Computer Science and Engineering, University of California: San Diego, CA, USA, 2003.
35. McGraw, K.O.; Wong, S.P. Forming inferences about some intraclass correlation coefficients. *J. Psychol. Methods* **1996**, *1*, 30. [CrossRef]
36. Koo, T.K.; Li, M.Y. A Guideline of Selecting and Reporting Intraclass Correlation Coefficients for Reliability Research. *J. Chiropr. Med.* **2016**, *15*, 155–163. [CrossRef]
37. Gluer, C.C.; Blake, G.; Lu, Y.; Blunt, B.A.; Jergas, M.; Genant, H.K. Accurate Assessment of Precision Errors–How to Measure the Reproducibility of Bone Densitometry Techniques. *Osteoporos. Int.* **1995**, *5*, 262–270. [CrossRef] [PubMed]
38. Wilcoxon, F. Individual comparisons by ranking methods. In *Breakthroughs in Statistics*; Springer: New York, NY, USA, 1992; pp. 196–202.
39. Cohen, J. *Statistical Power Analysis for the Behavioral Sciences*; Routledge: New York, NY, USA, 2013.
40. Ramme, A.J.; Criswell, A.J.; Wolf, B.R.; Magnotta, V.A.; Grosland, N.M. EM segmentation of the distal femur and proximal tibia: A high-throughput approach to anatomic surface generation. *Ann. Biomed. Eng.* **2011**, *39*, 1555–1562. [CrossRef] [PubMed]
41. Wang, L.I.; Greenspan, M.; Ellis, R. Validation of bone segmentation and improved 3-D registration using contour coherency in CT data. *IEEE Trans. Med. Imaging* **2006**, *25*, 324–334. [CrossRef]

42. Burnett, W.D.; Kontulainen, S.A.; McLennan, C.E.; Hazel, D.; Talmo, C.; Hunter, D.J.; Wilson, D.R.; Johnston, J.D. Knee osteoarthritis patients with severe nocturnal pain have altered proximal tibial subchondral bone mineral density. *Osteoarthr. Cartilage* **2015**, *23*, 1483–1490. [CrossRef]
43. Johannesdottir, F.; Poole, K.E.; Reeve, J.; Siggeirsdottir, K.; Aspelund, T.; Mogensen, B.; Jonsson, B.Y.; Sigurdsson, S.; Harris, T.B.; Gudnason, V.G.; et al. Distribution of cortical bone in the femoral neck and hip fracture: A prospective case-control analysis of 143 incident hip fractures; the AGES-REYKJAVIK Study. *Bone* **2011**, *48*, 1268–1276. [CrossRef]
44. Veitch, S.W.; Findlay, S.C.; Hamer, A.J.; Blumsohn, A.; Eastell, R.; Ingle, B.M. Changes in bone mass and bone turnover following tibial shaft fracture. *Osteoporos. Int.* **2006**, *17*, 364–372. [CrossRef]
45. Li, W.J.; Kornak, J.; Harris, T.; Keyak, J.; Li, C.X.; Lu, Y.; Cheng, X.G.; Lang, T. Identify fracture-critical regions inside the proximal femur using statistical parametric mapping. *Bone* **2009**, *44*, 596–602. [CrossRef]
46. Carballido-Gamio, J.; Harnish, R.; Saeed, I.; Streeper, T.; Sigurdsson, S.; Amin, S.; Atkinson, E.J.; Therneau, T.M.; Siggeirsdottir, K.; Cheng, X.; et al. Proximal femoral density distribution and structure in relation to age and hip fracture risk in women. *J. Bone Miner. Res.* **2013**, *28*, 537–546. [CrossRef]
47. Carballido-Gamio, J.; Bonaretti, S.; Saeed, I.; Harnish, R.; Recker, R.; Burghardt, A.J.; Keyak, J.H.; Harris, T.; Khosla, S.; Lang, T.F. Automatic multi-parametric quantification of the proximal femur with quantitative computed tomography. *Quant. Imaging Med. Surg.* **2015**, *5*, 552–568. [CrossRef] [PubMed]
48. Li, W.J.; Kezele, I.; Collins, D.L.; Zijdenbos, A.; Keyak, J.; Kornak, J.; Koyama, A.; Saeed, I.; LeBlanc, A.; Harris, T.; et al. Voxel-based modeling and quantification of the proximal femur using inter-subject registration of quantitative CT images. *Bone* **2007**, *41*, 888–895. [CrossRef] [PubMed]
49. Poole, K.E.S.; Skingle, L.; Gee, A.H.; Turmezei, T.D.; Johannesdottir, F.; Blesic, K.; Rose, C.; Vindlacheruvu, M.; Donell, S.; Vaculik, J.; et al. Focal osteoporosis defects play a key role in hip fracture. *Bone* **2017**, *94*, 124–134. [CrossRef] [PubMed]
50. Treece, G.; Gee, A. Cortical Bone Mapping: Measurement and Statistical Analysis of Localised Skeletal Changes. *Curr. Osteoporos. Rep.* **2018**, *16*, 617–625. [CrossRef] [PubMed]
51. Haralick, R.M. Statistical and Structural Approaches to Texture. *Proc. IEEE* **1979**, *67*, 786–804. [CrossRef]
52. Lowitz, T.; Museyko, O.; Bousson, V.; Laouisset, L.; Kalender, W.A.; Laredo, J.D.; Engelke, K. Bone marrow lesions identified by MRI in knee osteoarthritis are associated with locally increased bone mineral density measured by QCT. *Osteoarthr. Cartil.* **2013**, *21*, 957–964. [CrossRef]
53. Brenner, D.J.; Hall, E.J. Computed tomography—An increasing source of radiation exposure. *N. Engl. J. Med.* **2007**, *357*, 2277–2284. [CrossRef]
54. Topp, T.; Müller, T.; Huss, S.; Kann, P.H.; Weihe, E.; Ruchholtz, S.; Zettl, R.P. Embalmed and fresh frozen human bones in orthopedic cadaveric studies: Which bone is authentic and feasible? A mechanical study. *Acta Orthopaedica* **2012**, *83*, 543–547. [CrossRef]
55. Stefan, U.; Michael, B.; Werner, S. Effects of three different preservation methods on the mechanical properties of human and bovine cortical bone. *Bone* **2010**, *47*, 1048–1053. [CrossRef]

An Expert-Supervised Registration Method for Multi-Parameter Description of the Knee Joint Using Complementary Imaging Protocols

Abstract: Knee osteoarthritis being a disease of the entire joint, our pathophysiological understanding could improve with the characterization of the relationships among knee components. Diverse acquisition protocols for magnetic resonance imaging (MRI) and computed tomography (CT) allow capturing numerous parameters of the knee. However, a lack of methods for coordinated measurement of multiple parameters hinders global analyses. This study aimed to design an expert-supervised registration method to facilitate multi-parameter description using complementary acquisition protocols. The method is based on three-dimensional tissue models positioned in the images sets of interest using manually placed attraction points. Two datasets, with ten knees CT-scanned twice and ten knees imaged by CT and MRI, were used to assess the method when registering the distal femur and proximal tibia. The median inter-operator registration errors, quantified using the mean absolute distance and Dice index, were lower than 0.44 mm and higher than 0.97 units, respectively. These values differed by less than 0.1 mm and 0.1 units compared to the errors obtained with gold standard methods. In conclusion, an expert-supervised registration method was introduced. Its capacity to register the distal femur and proximal tibia supports further developments for multi-parameter description of healthy and osteoarthritic knee joints, among other applications.

1. Introduction

Knee osteoarthritis (OA) is a painful, incapacitating joint disease affecting the quality of life of hundreds of millions of persons worldwide [1-3]. Reducing this major socio-economic burden will notably require improving our pathophysiological understanding, as a basis to earlier disease detection and more effective treatments. While knee OA is recognized as a complex disease involving multiple tissues and parameters, most research so far performed isolated analyses and there is scant knowledge regarding the relationships among knee parameters, although this could lead to more representative disease models [4,5]. As the paucity of global analyses is heavily related to the deficiency of methods for coordinated measurement of multiple parameters, there is a need for new developments facilitating multi-parameter description of knee tissues.

Advances in medical imaging during the last decades resulted in a vast panel of acquisition protocols for magnetic resonance imaging (MRI) and computed tomography (CT) able to capture numerous parameters of the knee joint in three-dimension [6,7]. For example, particular MRI protocols allow quantifying cartilage morphology

[8] or composition [9], and bone mineral density can be measured using CT [10]. Furthermore, it is possible to image the joint successively using diverse devices and/or protocols, a procedure known as multi-modal imaging, in order to supplement the description of the tissues. Surprisingly, multi-modal imaging has seldom been performed to characterize the relationships among parameters in knee OA [11-13]. Additionally, to the authors' knowledge, none of the relationship studies registered the acquisition. In fact, the parameters were extracted independently from each set of images using regions of interest determined separately. While achieving multi-parameter description, this methodology suffers from some limitations. Specifically, a consistency among regions of interest is not guaranteed, the benefit of having complementary acquisition protocols allowing the identification of different tissues is underused, and processing time might be squandered by the replication of some operations with each images set [14-18]. Furthermore, although this methodology works for analyses based on large regions of interest [11,19-21], it prevents applications requiring higher resolution, for example to analyze the spatial variation of the parameters [10,22-24]. Consequently, relationship analyses would benefit from a registration among images sets.

A few authors have already registered knee images acquired with different protocols, mainly to help identifying regions of interest that could not be (accurately) identified in some sets of images [25-28]. In these cases, the images were registered globally based on mutual information, such as voxel intensities [29,30]. Although common in medical imaging, this fully-automatic approach is not always possible. Indeed, some acquisition protocols have been designed to capture local properties of the knee and it would be risky to base the registration on the entire images without considering the specificities of the acquisition protocols. Therefore, there is a need for an alternative approach where the registrations would be guided by an expert. Advanced knee OA analyses usually involve image segmentations in order to build three-dimensional mesh models of the tissues of interest. Thus, the registration could be done by positioning the three-dimensional models in the various images sets using features specific to the acquisition protocols identified by an operator. Recently, a method in this sense was proposed where femoral bone and cartilage models were built using an images set and then visually positioned in another images set where the tissue contours were only partially identifiable [31]. The method was shown to be reliable, supporting an expert-based approach to multi-modal registration. However, this method, where the operator has to manually update translation and rotation values until the models are positioned correctly, could be improved by limiting the action of the operator to the placement of "attraction points" and having an algorithm automatically positioning the models according to the attraction points.

This study aimed to develop an expert-supervised multi-modal registration method based on three-dimensional tissue models and attraction points. While such a generic method could reveal useful for a variety of applications, in agreement with the need to improve our understanding of knee OA and the availability of acquisition protocols that can be crosschecked, it was evaluated in the cases of distal femoral and proximal tibial bone registrations [4,5,7,32]. Specifically, the influence of the number of attraction points, as well as the intra- and inter-modality registration error were characterized.

2. Materials and Methods

2.1. Expert-Supervized Registration Method

The method proposed in this study requires at least one set of images allowing segmenting the tissue of interest to create a three-dimensional mesh model and one or more other sets of images where the three-dimensional model will be imported based on attraction points placed manually. The method works equivalently with entire or partial tissues. In addition to single tissues, it is possible working with an agglomeration of full and/or partial tissues. In the present study, there were two distinct (partial) tissues of interest: the distal femoral bone and the proximal tibial bone. These structures correspond to the portion of the bones that are imaged in routine clinical evaluation of the knee joint [33]. To account for possible movements of the femur with respect to the tibia between images sets, the femoral and tibial bones were registered separately.

The procedure, which is similar for both bones, is illustrated for the femur in Figure 1. Specifically, previously described methods were used to segment and build three-dimensional mesh model of the bones (Fig. 1a and 1b) [33-35]. The segmentation followed a sub-pixel approach consisting in contouring the tissues in the sagittal plane with B-spline curves. A graphical interface was designed to load a set of images and let an operator navigate through the images in order to manually place attraction points on the edge of the bones (Fig. 1c and 1d). To facilitate future uses, the method was implemented to work with attraction points distributed more or less homogeneously in space. Concretely, with this methodology, the operator is simply asked to distribute the points, without having to localize particular features or follow more specific guidelines. After placement of the points for a bone model in an images set, the three-dimensional model was automatically positioned following its attraction points using the Coherent Point Drift (CPD) algorithm (Fig. 1e) [36]. At this stage, the procedure is completed, with the bone model from one images set registered to another images set. The registration can be used to identify the bone voxels in the second images set (Fig. 1f) or to establish an anatomical correspondence for more advanced analyses [27].

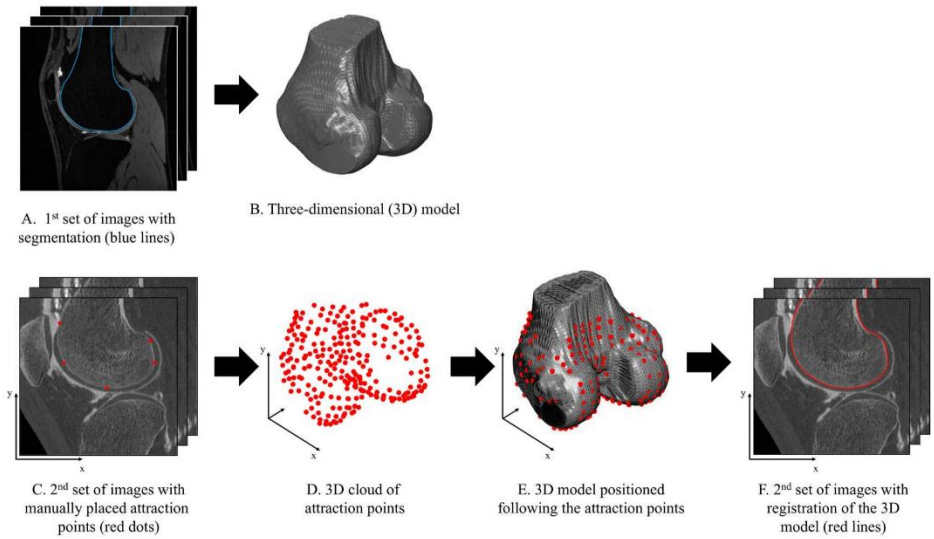

Figure 1. Illustration of the expert-supervised registration method for the distal femur. The method can accommodate other tissues, such as the proximal tibia, and a higher number of images sets.

2.2. Imaging Datasets

Two datasets were used for this research project approved by the relevant ethics committees.

The first dataset corresponded to 10 formalin-fixed cadaveric adults knees scanned (*DATA1_CT1*) and rescanned (*DATA1_CT2*) after repositioning using a 40 row detector helical CT machine (Discovery CT750HD; GE Medical Systems). To have a gold standard to which comparing the proposed expert-supervised registration method, five fiducial markers were embedded in each distal femur and proximal tibia before scanning. The acquisition protocol was as follows: tube voltage, 120 kVp; reference tube current-time product, 200 mAs; bone convolution kernel (U70u); voxel size of 0.5 × 0.5 × 0.312 mm. Following local regulations regarding research on deceased persons, no demographic data was available for the samples. A senior musculoskeletal radiologist read the CT scans and, based on the presence and severity of osteophytes [37], concluded that five of the knees had degenerative changes (three mild and two severe changes).

The second dataset was composed of 10 knees imaged by CT (*DATA2_CT*) and MRI (*DATA2_MRI*) on the same day. The CT scans in this dataset were obtained using a 40-detecor row CT scanner (Somatom Definition AS; Siemens Healthcare, Forchheim, Germany). The acquisition protocol was: tube voltage, 120 kVp; reference tube current–time product, 350 mAs with application of a dose modulation protocol (Care Dose 4D; Siemens Healthcare); bone convolution kernel, U70u; voxel size of 0.3 × 0.3 × 0.3 mm. The MR images were acquired on a 3-Tesla device (Magnetom Verio, Siemens Healthcare, Erlangen, Germany), using a double echo steady state (DESS) sequence (repetition time (TR), 14.25 ms; echo time (TE), 5.09 ms; matrix size of 320 × 320; voxel size

of 0.5 × 0.5 × 0.5 mm). The knees were from 5 males and 5 females with a median age of 62 years old (1st – 3rd quartiles: 59 – 67). A radiographic grading [38] performed by a senior musculoskeletal radiologist indicated that five of the knees were osteoarthritic (three moderately and two severely).

The femoral and tibial bones were segmented in each acquisition and three-dimensional bone models were reconstructed, as explained above (see 2.1). One operator (H.B.) processed the knees in DATA1_CT1 and DATA2_MRI, whereas a second operator (K.C.) handled the knees in DATA1_CT2 and DATA2_CT. The segmentation was shared between two persons to allow inter-operator assessment, which is more relevant than intra-operator characterization [35].

2.3. Number of Attraction Points

The attraction points are a key element of the proposed expert-supervised registration method. Consequently, before anything else, their influence should be determined to ensure that the method is used properly. As explained above (see 2.1), the method was designed to work with attraction points distributed more or less evenly in space. Therefore, the influence of the attraction points reduces to the question of the number of points. To characterize this aspect, one operator (H.B.) placed 4,000 points on the edges of both the femoral and tibial bones for each images set in DATA1_CT2. Then, the three-dimensional models obtained from the segmentation of DATA1_CT1 by the same operator were positioned in the DATA1_CT2 acquisitions using the proposed method. For each bone, the positioning was computed 10 times, with 32, 64, 128, 256, 512 and 1024 randomly selected attractions points, respectively. The 600 (10 knees x 6 numbers of points x 10 repeats) femoral and tibial models obtained this way in the images sets of DATA1_CT2 were compared to the models from the segmentation of DATA1_CT2 by the second operator (K.C.), considered as references. Two common metrics were used to compare the registered and reference models: the mean absolute distance (MAD) and the Dice index [39]. Finally, Wilcoxon rank-sum tests [40], with a Bonferroni correction for multiple comparisons, were performed to compare the MAD and Dice index between consecutive numbers of points. This analysis allowed defining an ideal number of attraction points that was used in the rest of the study.

2.4. Intra-Modality Registration Error

While the proposed expert-supervised method will fully reveal its usefulness in inter-modality registrations, an intra-modality assessment is instructive because it provides a basis evaluation independently of the differences among acquisition protocols. To assess the registration error intra-modality, the three-dimensional bone models from the segmentation of DATA1_CT1 by one operator (H.B.) were imported in the DATA1_CT2 images sets and compared to the bone models from the segmentation of DATA1_CT2 by the second operator (K.C.) that served

as reference models. To allow a pertinent interpretation of the results, three registration methods were tested. First, the bone models were positioned using the proposed expert-supervised method based on an ideal number of attraction points (see 2.3) placed by the operator who segmented the acquisitions in DATA1_CT1 (H.B.). Second, the bone models were positioned by overlapping the fiducial markers that were embedded in the bones before CT scanning [41]. This method represents the gold standard, but it is rarely possible in vivo and inter-modality. Therefore, to allow the assessment of the method in an inter-modality setting (see 2.5), a substitution gold standard was also considered, where the bone models were positioned by registration of the entire bone models using a standard algorithm [36]. This third method corresponds to an ultimate version of the proposed method, where the operator would place an excessive number of attraction points. In practice, the third method is obviously suboptimal as it would require unnecessary segmentation work and would not be applicable to acquisition protocols allowing only partial segmentation of the tissues. For the three methods, the registered bone models of the 10 femurs and tibias in DATA1 were compared to the reference bone models using the MAD and Dice index. Lastly, to evaluate the proposed expert-supervised method and the substitution gold standard method, the MAD and Dice index values obtained with these methods were compared to the results of the gold standard method using Wilcoxon signed rank tests [40].

2.5. Inter-Modality Registration Error

The inter-modality registration error was evaluated similarly to the intra-modality error by having one operator (H.B.) segmenting one dataset (DATA2_MRI) and importing the bone models obtained that way into another dataset (DATA2_CT). The other dataset was processed by a second operator (K.C.), leading to reference bone models that could be compared to the registered models using the MAD and Dice index. Differently from the intra-modality assessment, this time, MRI-based models were positioned in CT images. Moreover, since it was impossible using fiducial markers, only two registration methods were considered, and the MAD and Dice index values of the proposed expert-supervised method were compared to the values obtained with the substitution gold standard method using Wilcoxon signed rank tests [40].

All processing and statistical analyses were performed using Matlab R2019b (Mathworks, Natick, MA, USA). An alpha-level set a priori at 5% was used to determine statistical significance.

3. Results

3.1. Number of Attraction Points

The median MAD between the registered and reference models decreased from 0.53 mm with 32 points to 0.39 mm with 1024 points in the femur, and from 0.54 mm with 32 points to 0.35 mm with 1024 points in the tibia (Figure 2, Table 1). Differences in MAD achieved statistical significance between 32 and 64 points, as well as between 64 and 128 points, both in the femur and the tibia ($Z \geq 2.8$, adjusted $p \leq 0.03$). Dice indices differed significantly between 32 and 64 points in the femur ($Z = 2.8$, adjusted $p = 0.03$), and between 32 and 64 points as well as between 64 and 128 points in the tibia ($Z \geq 2.6$, adjusted $p \leq 0.04$).

Based on the statistically significant differences and the magnitude of the differences, the ideal number of attraction points was defined as 256. In fact, the errors obtained with 256 points were not significantly different from the errors obtained with 512 points and the median errors varied by less than 5% between these two numbers of points.

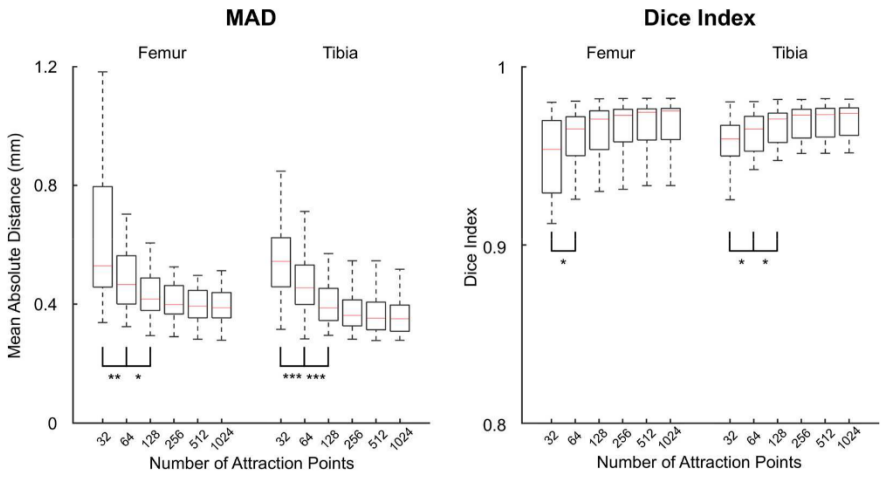

Figure 2. Boxplots of the mean absolute distances (MAD, left) and Dice indices (right) between the registered and reference bone models for varying number of attraction points. Asterisks indicate statistically significant differences between successive numbers of points (*: adjusted $p < 0.05$, **: adjusted $p < 0.01$, ***: adjusted $p < 0.001$).

Table 1. Mean absolute distances (MAD) and Dice indices between the registered and reference bone models for varying number of attraction points.

	Number of Attraction Points					
	32	64	128	256	512	1024
Femur						
MAD	0.53^{A} [0.46, 0.80]	$0.47^{A,b}$ [0.40, 0.56]	0.42^{b} [0.38, 0.49]	0.40 [0.37, 0.46]	0.39 [0.35, 0.45]	0.39 [0.35, 0.44]
Dice Index	0.95^{a} [0.93, 0.97]	0.97^{a} [0.95, 0.97]	0.97 [0.95, 0.98]	0.97 [0.96, 0.98]	0.97 [0.96, 0.98]	0.98 [0.96, 0.98]
Tibia						
MAD	$0.54^{\mathbf{A}}$ [0.46, 0.62]	$0.45^{\mathbf{A,B}}$ [0.40, 0.53]	$0.39^{\mathbf{B}}$ [0.34, 0.45]	0.36 [0.33, 0.41]	0.35 [0.31, 0.41]	0.35 [0.31, 0.40]
Dice Index	0.96^{a} [0.95, 0.97]	$0.97^{a,b}$ [0.95, 0.97]	0.97^{b} [0.96, 0.97]	0.97 [0.96, 0.98]	0.97 [0.96, 0.98]	0.97 [0.96, 0.98]

MAD and Dice indices are presented as the median [1st quartile, 3rd quartile] of 100 registrations (10 knees x 10 repeats). MAD are reported in mm and Dice indices are unitless. Superscript letters indicate statistically significant differences between successive numbers of points (lowercase: adjusted $p < 0.05$, uppercase: adjusted $p < 0.01$, bold uppercase: adjusted $p < 0.001$). Letters $^{a, A \text{ and } \mathbf{A}}$ correspond to differences between 32 and 64 points, whereas letters $^{b, B \text{ and } \mathbf{B}}$ correspond to differences between 64 and 128 points.

3.2. Intra-Modality Registration Error

The intra-modality results are presented in Figure 3 and Table 2. Before describing them in details, it is useful recalling that this study assessed the methods using an inter-operator setting. With this setting, the MAD and Dice indices are sensitive to the different segmentations produced by the two operators. These segmentation differences explain why the MAD and Dice indices obtained with the gold standard do not indicate perfect matching. This being said, the results in Figure 3 and Table 2 are twofold.

First, the proposed expert-supervised method resulted in larger MAD than the gold standard method, in median by 0.02 mm, and in lower Dice indices, in median by 0.01 unit. Only in the femur, did the methods achieved statistically significantly different MAD ($W = 55$, $p = 0.002$) and Dice indices ($W = 0$, $p = 0.002$).

Second, the MAD and Dice indices differed, in median, by less than 0.01 mm and less than 0.001 unit between the gold standard and its substitution, respectively. There was no statistically significant difference between these two methods.

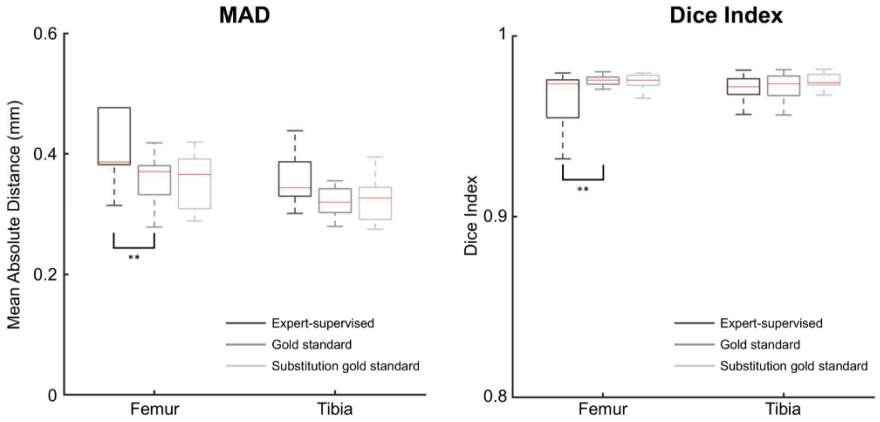

Figure 1. Boxplot of the mean absolute distances (MAD, left) and Dice indices (right) between the registered and reference bone models for three registration methods. The expert-supervised method was run with 256 attraction points. Asterisks indicate statistically significant differences between methods (**: $p < 0.01$).

Table 2. Mean absolute distances (MAD) and Dice indices between the registered and reference bone models for three registration methods used intra-modality.

	Expert-supervised	Gold standard	Substitution gold standard
Femur			
MAD	0.39** [0.38, 0.48]	0.37 [0.33, 0.38]	0.37 [0.31, 0.39]
Dice Index	0.97** [0.95, 0.98]	0.98 [0.97, 0.98]	0.98 [0.97, 0.98]
Tibia			
MAD	0.34 [0.33, 0.39]	0.32 [0.30, 0.34]	0.33 [0.29, 0.34]
Dice Index	0.97 [0.97, 0.98]	0.97 [0.97, 0.98]	0.97 [0.97, 0.98]

Data are presented as median [1st quartile, 3rd quartile] over 10 knees. MAD are reported in mm and Dice indices are unitless. Asterisks indicate statistically significant differences with respect to the gold standard (**: $p < 0.01$).

3.3. Inter-Modality Registration Error

When used to register MRI-based bone models in CT images sets, in an inter-operator setting, the proposed expert-supervised method reported larger MAD than the substitution gold standard method, in median by 0.08 mm for the femur and 0.03 mm for the tibia, and lower Dice indices, in median by 0.01 unit (Figure 4, Table 3). The only statistically significant difference between the two methods was with the femoral MAD ($W = 143$, $p = 0.005$).

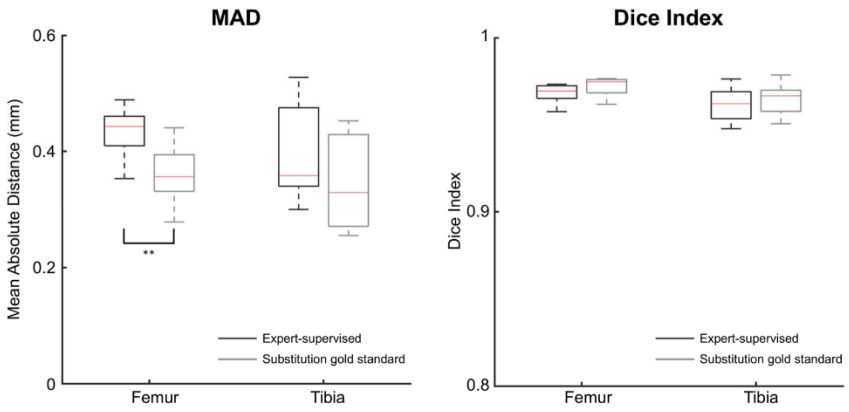

Figure 4. Boxplot of the mean absolute distances (MAD, left) and Dice indices (right) between the registered and reference bone models for two registration methods. The expert-supervised method was run with 256 attraction points. Asterisks indicate statistically significant differences between methods (**: $p < 0.01$).

Table 3. Mean absolute distances (MAD) and Dice indices between the registered and reference bone models for two registration methods used inter-modality.

	Expert-supervised	Substitution gold standard
Femur		
MAD**	0.44 [0.41, 0.46]	0.36 [0.33, 0.39]
Dice Index	0.97 [0.97, 0.97]	0.97 [0.97, 0.98]
Tibia		
MAD	0.36 [0.34, 0.48]	0.33 [0.27, 0.43]
Dice Index	0.96 [0.95, 0.97]	0.97 [0.96, 0.97]

Data are presented as median [1st quartile, 3rd quartile] over 10 knees. MAD are reported in mm and Dice indices are unitless. Asterisks indicate statistically significant differences between the two methods (**: $p < 0.01$).

4. Discussion

This study presented an expert-supervised registration method and showed its capacity to register the distal femur and proximal tibia. The method has the potential to contribute to the advancement of knee OA research, by facilitating multi-parameter description of the joint and stimulating the use of multi-modal imaging [42]. While it was designed with the aim to improve our understanding of the relationships among knee parameters in the

framework of OA [4,5], it could certainly reveal useful for a variety of pathologies that would benefit from a more comprehensive characterization of the tissues using multi-modal imaging, such as osteoporosis and cancer [43-45].

Establishing a spatial correspondence among images sets acquired with different devices and/or protocols, as proposed in this study, offers several advantages. First, it could enhance the quality of the three-dimensional tissue models by limiting the segmentation to the images sets offering the most distinct contours. Working with images sets easier to segment could also prove beneficial for the use of automatic segmentation [46,47]. Second, placing attraction points in some images sets rather than segmenting all the images sets could save a significant amount of time. The gain could become even more appreciable when some images sets display poor contours. Third, registering the models could enhance the analysis by a better spatial consistency among images sets and the possibility to perform analyses at higher resolution, for example in term of spatial variations [10,22-24]. On top of that, the method introduced in this study is interesting because it uses the expertise of an operator. This characteristic confers a control to the operator who could specify the features to consider in the images. This adaptability could reveal extremely useful with acquisition protocols optimized to measure specific parameters and not trustable over the entire images [6,7].

As expected, the registration errors decreased with larger number of attraction points. However, there was a plateau starting at about 256 points, confirming the practicability of the method. Indeed, less than five minutes were required to place 256 points. Statistically significant differences were observed between the proposed method and the gold standard / substitution gold standard, but they were small, with differences below 0.1 mm in median MAD and 0.1 unit in median Dice indices. Speaking about gold standard, it is worth noting that although the substitution gold standard is frequently used in literature [48], to the authors' knowledge, it was never assessed for distal femur and proximal tibia registrations. In this regard, the present study confirmed its validity, at least with acquisition protocols providing clear bone contours. The registration of knee tissues being a relatively new consideration, there is only few prior data for comparison. Nevertheless, the median MAD ($\leq$ 0.44 mm) and Dice indices ($\geq$ 0.97) obtained with the proposed method both intra- and inter-modality were in line with previous studies reporting inter-modality precision errors between 0.48 and 0.81 mm [49] and Dice indices between 0.96 and 0.98 [27,50] for the distal femur and proximal tibia. While this comparison should be interpreted with caution due to numerous experimental differences among studies, such as the number and condition of the study knees, the acquisition protocols and the intra/inter-operator settings, it suggests that the proposed method based on attraction points could perform at least equivalently to other methods requiring fully segmentation of the bones.

Basing the registration on attraction points is interesting because it does not require preprocessing the images sets to have specific field of view or resolution. In addition to improving the accuracy of the data extracted from the images after registration and speeding up computation time [29], directly working with the original data makes the method compatible with a larger panel of acquisition protocols. This could prove particularly relevant for a democratization of analyses based on registration in clinics, as routine acquisition protocols can include anisotropic resolutions or partial imaging of the joint.

It should be noted that, beyond a specific method, the present study introduced a registration concept for multimodal imaging. In fact, the idea of positioning a three-dimensional model using attraction points could be implemented using other segmentation, model building and distance minimizing algorithms [29]. In order to assess the registration error, this study focused on the distal femoral and proximal tibial bones. The method is obviously also applicable to other tissues and images sets where only a portion of the tissue contour is identifiable. Once the position of a tissue model is known in two or more images sets, a spatial correspondence exists among the images sets. This correspondence could be used to register other tissues, or more generally to register voxels [51,52]. For example, a bone & cartilage model could be created with one image set and then, by positioning the model based on the bone contour, it could be possible identifying the cartilage in another images set where cartilage edges are hardly identifiable [31].

Following the study objectives, this work assessed the influence of the number of attraction points and the registration error. While this was done appropriately, with an adequate number of knees representative of the general population [53-56] and by having the knees processed by two operators with typical levels of experience, further research will be necessary to characterize the proposed method in situation. Indeed, the convincing practicability and error results obtained so far call for the method to be used for multi-parameter description of the knee joint, among others. Doing so will notably involve different acquisition protocols, measures, and clinical presentations, and specific validations will be needed according to these future applications.

5. Conclusions

In conclusion, this study presented an expert-supervised registration method and showed its capacity to register the distal femur and proximal tibia. This promising initial step supports further developments using this method for multi-parameter description of healthy and OA knee joints, among other applications. By facilitating the characterization of the relationship among knee parameters using multi-modal imaging, over time, this study could contribute to a better understanding and management of OA.

References

1. Conaghan, P.G.; Kloppenburg, M.; Schett, G.; Bijlsma, J.W.J. Osteoarthritis research priorities: a report from a EULAR ad hoc expert committee. **2014**, *73*, 1442-1445, doi:10.1136/annrheumdis-2013-204660 %J Annals of the Rheumatic Diseases.
2. Safiri, S.; Kolahi, A.A.; Smith, E.; Hill, C.; Bettampadi, D.; Mansournia, M.A.; Hoy, D.; Ashrafi-Asgarabad, A.; Sepidarkish, M.; Almasi-Hashiani, A., et al. Global, regional and national burden of osteoarthritis 1990-2017: a systematic analysis of the Global Burden of Disease Study 2017. *Ann Rheum Dis* **2020**, *79*, 819-828, doi:10.1136/annrheumdis-2019-216515.
3. Vos, T.; Flaxman, A.D.; Naghavi, M.; Lozano, R.; Michaud, C.; Ezzati, M.; Shibuya, K.; Salomon, J.A.; Abdalla, S.; Aboyans, V., et al. Years lived with disability (YLDs) for 1160 sequelae of 289 diseases and injuries 1990–2010: a systematic analysis for the Global Burden of Disease Study 2010. *The Lancet* **2012**, *380*, 2163-2196, doi:10.1016/s0140-6736(12)61729-2.
4. Edd, S.N.; Omoumi, P.; Andriacchi, T.P.; Jolles, B.M.; Favre, J. Modeling knee osteoarthritis pathophysiology using an integrated joint system (IJS): a systematic review of relationships among cartilage thickness, gait mechanics, and subchondral bone mineral density. *Osteoarthritis Cartilage* **2018**, *26*, 1425-1437, doi:10.1016/j.joca.2018.06.017.
5. Andriacchi, T.P.; Favre, J.; Erhart-Hledik, J.C.; Chu, C.R. A Systems View of Risk Factors for Knee Osteoarthritis Reveals Insights into the Pathogenesis of the Disease. *Annals of Biomedical Engineering* **2015**, *43*, 376-387, doi:10.1007/s10439-014-1117-2.
6. Peterfy, C.; Gold, G.; Eckstein, F.; Cicuttini, F.; Dardzinski, B.; Stevens, R. MRI protocols for whole-organ assessment of the knee in osteoarthritis. *Osteoarthr Cartilage* **2006**, *14*, 95-111.
7. Hayashi, D.; Roemer, F.W.; Guermazi, A. Imaging for osteoarthritis. *Ann. Phys. Rehabil. Med.* **2016**, *59*, 161-169, doi:10.1016/j.rehab.2015.12.003.
8. Eckstein, F.; Wirth, W.; Nevitt, M.C. Recent advances in osteoarthritis imaging—the Osteoarthritis Initiative. *Nature Reviews Rheumatology* **2012**, *8*, 622.
9. Burstein, D.; Gray, M.; Mosher, T.; Dardzinski, B. Measures of molecular composition and structure in osteoarthritis. *Radiol. Clin. North Am.* **2009**, *47*, 675-686, doi:10.1016/j.rcl.2009.04.003.
10. Babel, H.; Omoumi, P.; Cosendey, K.; Cadas, H.; Jolles, B.M.; Favre, J. Three-Dimensional Quantification of Bone Mineral Density in the Distal Femur and Proximal Tibia Based on Computed Tomography: In Vitro Evaluation of an Extended Standardization Method. *J Clin Med* **2021**, *10*, 160, doi:10.3390/jcm10010160.
11. Cao, Y.; Stannus, O.P.; Aitken, D.; Cicuttini, F.; Antony, B.; Jones, G.; Ding, C. Cross-sectional and longitudinal associations between systemic, subchondral bone mineral density and knee cartilage thickness in older adults with or without radiographic osteoarthritis. *Ann Rheum Dis* **2014**, *73*, 2003-2009, doi:10.1136/annrheumdis-2013-203691.
12. Lo, G.H.; Tassinari, A.M.; Driban, J.B.; Price, L.L.; Schneider, E.; Majumdar, S.; McAlindon, T.E. Cross-sectional DXA and MR measures of tibial periarticular bone associate with radiographic knee osteoarthritis severity. *Osteoarthr Cartilage* **2012**, *20*, 686-693.
13. Multanen, J.; Heinonen, A.; Häkkinen, A.; Kautiainen, H.; Kujala, U.M.; Lammentausta, E.; Jämsä, T.; Kiviranta, I.; Nieminen, M.T. Bone and cartilage characteristics in postmenopausal women with mild knee radiographic osteoarthritis and those without radiographic osteoarthritis. *J. Musculoskelet. Neuronal Interact.* **2015**, *15*, 69.
14. Ahn, C.; Bui, T.D.; Lee, Y.W.; Shin, J.; Park, H. Fully automated, level set-based segmentation for knee MRIs using an adaptive force function and template: data from the osteoarthritis initiative. *Biomed. Eng. Online* **2016**, *15*, 99, doi:10.1186/s12938-016-0225-7.

15. Tack, A.; Mukhopadhyay, A.; Zachow, S. Knee menisci segmentation using convolutional neural networks: data from the Osteoarthritis Initiative. *Osteoarthr Cartilage* **2018**, *26*, 680-688, doi:10.1016/j.joca.2018.02.907.
16. Kapur, T.; Beardsley, P.; Gibson, S.; Grimson, W.; Wells, W. Model-based segmentation of clinical knee MRI. In Proceedings of Proc. IEEE Int'l Workshop on Model-Based 3D Image Analysis; pp. 97-106.
17. Dam, E.B.; Lillholm, M.; Marques, J.; Nielsen, M. Automatic segmentation of high- and low-field knee MRIs using knee image quantification with data from the osteoarthritis initiative. *J Med Imaging (Bellingham)* **2015**, *2*, 024001, doi:10.1117/1.JMI.2.2.024001.
18. Shim, H.; Chang, S.; Tao, C.; Wang, J.H.; Kwoh, C.K.; Bae, K.T. Knee cartilage: efficient and reproducible segmentation on high-spatial-resolution MR images with the semiautomated graph-cut algorithm method. *Radiology* **2009**, *251*, 548-556, doi:10.1148/radiol.2512081332.
19. Lo, G.H.; Hunter, D.J.; Zhang, Y.; McLennan, C.E.; LaValley, M.P.; Kiel, D.P.; McLean, R.R.; Genant, H.K.; Guermazi, A.; Felson, D.T.J.A., et al. Bone marrow lesions in the knee are associated with increased local bone density. **2005**, *52*, 2814-2821.
20. Lo, G.H.; Niu, J.; McLennan, C.E.; Kiel, D.P.; McLean, R.R.; Guermazi, A.; Genant, H.K.; McAlindon, T.E.; Hunter, D.J. Meniscal damage associated with increased local subchondral bone mineral density: a Framingham study. *Osteoarthritis Cartilage* **2008**, *16*, 261-267, doi:10.1016/j.joca.2007.07.007.
21. Williams, A.; Winalski, C.S.; Chu, C.R. Early articular cartilage MRI T2 changes after anterior cruciate ligament reconstruction correlate with later changes in T2 and cartilage thickness. *J Orthop Res* **2017**, *35*, 699-706, doi:10.1002/jor.23358.
22. Babel, H.; Omoumi, P.; Andriacchi, T.P.; Jolles, B.M.; Favre, J. New insight on the subchondral bone and cartilage functional unit: bone mineral density and cartilage thickness are spatially correlated in non-osteoarthritic femoral condyles. *Osteoarthritis Cartilage Open* **2020**, 100079.
23. Favre, J.; Erhart-Hledik, J.C.; Blazek, K.; Fasel, B.; Gold, G.E.; Andriacchi, T.P. Anatomically Standardized Maps Reveal Distinct Patterns of Cartilage Thickness With Increasing Severity of Medial Compartment Knee Osteoarthritis. *J Orthop Res* **2017**, *35*, 2442-2451, doi:10.1002/jor.23548.
24. Favre, J.; Scanlan, S.F.; Erhart-Hledik, J.C.; Blazek, K.; Andriacchi, T.P. Patterns of femoral cartilage thickness are different in asymptomatic and osteoarthritic knees and can be used to detect disease-related differences between samples. *J Biomech Eng* **2013**, *135*, 101002-101010, doi:10.1115/1.4024629.
25. Li, X.; Benjamin Ma, C.; Link, T.M.; Castillo, D.D.; Blumenkrantz, G.; Lozano, J.; Carballido-Gamio, J.; Ries, M.; Majumdar, S. In vivo T(1rho) and T(2) mapping of articular cartilage in osteoarthritis of the knee using 3 T MRI. *Osteoarthritis Cartilage* **2007**, *15*, 789-797, doi:10.1016/j.joca.2007.01.011.
26. Carballido-Gamio, J.; Stahl, R.; Blumenkrantz, G.; Romero, A.; Majumdar, S.; Link, T.M. Spatial analysis of magnetic resonance T1rho and T2 relaxation times improves classification between subjects with and without osteoarthritis. *Med. Phys.* **2009**, *36*, 4059-4067, doi:10.1118/1.3187228.
27. Lowitz, T.; Museyko, O.; Bousson, V.; Laouisset, L.; Kalender, W.A.; Laredo, J.D.; Engelke, K. Bone marrow lesions identified by MRI in knee osteoarthritis are associated with locally increased bone mineral density measured by QCT. *Osteoarthritis Cartilage* **2013**, *21*, 957-964, doi:10.1016/j.joca.2013.04.006.
28. Li, X.; Pai, A.; Blumenkrantz, G.; Carballido-Gamio, J.; Link, T.; Ma, B.; Ries, M.; Majumdar, S. Spatial distribution and relationship of T1ρ and T2 relaxation times in knee cartilage with osteoarthritis. *Magnetic Resonance in Medicine: An Official Journal of the International Society for Magnetic Resonance in Medicine* **2009**, *61*, 1310-1318.
29. Oliveira, F.P.; Tavares, J.M. Medical image registration: a review. *Comput Methods Biomech Biomed Engin* **2014**, *17*, 73-93, doi:10.1080/10255842.2012.670855.

30. Pluim, J.P.W.; Maintz, J.B.A.; Viergever, M.A. Mutual-information-based registration of medical images: a survey. *IEEE transactions on medical imaging* **2003**, *22*, 986-1004.
31. Edd, S.N.; Babel, H.; Kerkour, N.; Jolles, B.M.; Omoumi, P.; Favre, J.J.T.K. Comprehensive description of T2 value spatial variations in non-osteoarthritic femoral cartilage using three-dimensional registration of morphological and relaxometry data. **2019**, *26*, 555-563.
32. Peterfy, C.G.; Gold, G.; Eckstein, F.; Cicuttini, F.; Dardzinski, B.; Stevens, R. MRI protocols for whole-organ assessment of the knee in osteoarthritis. *Osteoarthritis Cartilage* **2006**, *14 Suppl A*, A95-111, doi:10.1016/j.joca.2006.02.029.
33. Omoumi, P.; Babel, H.; Jolles, B.M.; Favre, J. Quantitative regional and sub-regional analysis of femoral and tibial subchondral bone mineral density (sBMD) using computed tomography (CT): comparison of non-osteoarthritic (OA) and severe OA knees. *Osteoarthritis Cartilage* **2017**, *25*, 1850-1857, doi:10.1016/j.joca.2017.07.014.
34. Koo, S.; Gold, G.E.; Andriacchi, T.P. Considerations in measuring cartilage thickness using MRI: factors influencing reproducibility and accuracy. *Osteoarthritis Cartilage* **2005**, *13*, 782-789, doi:10.1016/j.joca.2005.04.013.
35. Favre, J.; Babel, H.; Cavinato, A.; Blazek, K.; Jolles, B.M.; Andriacchi, T.P. Analyzing Femorotibial Cartilage Thickness Using Anatomically Standardized Maps: Reproducibility and Reference Data. *Journal of Clinical Medicine* **2021**, *10*, 461.
36. Myronenko, A.; Song, X.J.I.t.o.p.a.; intelligence, m. Point set registration: Coherent point drift. **2010**, *32*, 2262-2275.
37. Peterfy, C.G.; Guermazi, A.; Zaim, S.; Tirman, P.F.; Miaux, Y.; White, D.; Kothari, M.; Lu, Y.; Fye, K.; Zhao, S., et al. Whole-Organ Magnetic Resonance Imaging Score (WORMS) of the knee in osteoarthritis. *Osteoarthritis Cartilage* **2004**, *12*, 177-190, doi:10.1016/j.joca.2003.11.003.
38. Felson, D.T.; McAlindon, T.E.; Anderson, J.J.; Weissman, B.W.; Aliabadi, P.; Evans, S.; Levy, D.; LaValley, M.P. Defining radiographic osteoarthritis for the whole knee. *Osteoarthr Cartilage* **1997**, *5*, 241-250.
39. Dice, L.R. Measures of the amount of ecologic association between species. *Ecology* **1945**, *26*, 297-302.
40. Wilcoxon, F. Individual comparisons by ranking methods. In *Breakthroughs in statistics*, Springer: 1992; pp. 196-202.
41. Veldpaus, F.; Woltring, H.; Dortmans, L.J.J.o.b. A least-squares algorithm for the equiform transformation from spatial marker co-ordinates. **1988**, *21*, 45-54.
42. Hayashi, D.; Roemer, F.W.; Guermazi, A. Recent advances in research imaging of osteoarthritis with focus on MRI, ultrasound and hybrid imaging. *Clin. Exp. Rheumatol.* **2018**, *36*, 43-52.
43. Bayar, A.; Sarikaya, S.; Keser, S.; Ozdolap, S.; Tuncay, I.; Ege, A. Regional bone density changes in anterior cruciate ligament deficient knees: a DEXA study. *Knee* **2008**, *15*, 373-377, doi:10.1016/j.knee.2008.05.005.
44. Parker, R.K.; Ross, G.J.; Urso, J.A. Transient osteoporosis of the knee. *Skeletal Radiol* **1997**, *26*, 306-309, doi:10.1007/s002560050241.
45. Campanacci, M. *Bone and soft tissue tumors*; Springer: 2013.
46. Taddei, F.; Cristofolini, L.; Martelli, S.; Gill, H.; Viceconti, M. Subject-specific finite element models of long bones: an in vitro evaluation of the overall accuracy. *J. Biomech.* **2006**, *39*, 2457-2467.
47. Bowes, M.A.; McLure, S.W.; Wolstenholme, C.B.; Vincent, G.R.; Williams, S.; Grainger, A.; Conaghan, P.G. Osteoarthritic bone marrow lesions almost exclusively colocate with denuded cartilage: a 3D study using data from the Osteoarthritis Initiative. *Ann Rheum Dis* **2016**, *75*, 1852-1857, doi:10.1136/annrheumdis-2015-208407.
48. Williams, T.G.; Holmes, A.P.; Bowes, M.; Vincent, G.; Hutchinson, C.E.; Waterton, J.C.; Maciewicz, R.A.; Taylor, C.J. Measurement and visualisation of focal cartilage thickness change by MRI in a study of knee osteoarthritis using a novel image analysis tool. *The British journal of radiology* **2010**, *83*, 940-948.

49. Moro-oka, T.a.; Hamai, S.; Miura, H.; Shimoto, T.; Higaki, H.; Fregly, B.J.; Iwamoto, Y.; Banks, S. Can magnetic resonance imaging–derived bone models be used for accurate motion measurement with single-plane three-dimensional shape registration? *Journal of orthopaedic research* **2007**, *25*, 867-872.
50. Lowitz, T.; Museyko, O.; Bousson, V.; Chappard, C.; Laouisset, L.; Laredo, J.D.; Engelke, K. Advanced Knee Structure Analysis (AKSA): a comparison of bone mineral density and trabecular texture measurements using computed tomography and high-resolution peripheral quantitative computed tomography of human knee cadavers. *Arthritis Res Ther* **2017**, *19*, 1, doi:10.1186/s13075-016-1210-z.
51. Batiste, D.L.; Kirkley, A.; Laverty, S.; Thain, L.M.F.; Spouge, A.R.; Gati, J.S.; Foster, P.J.; Holdsworth, D.W. High-resolution MRI and micro-CT in an ex vivo rabbit anterior cruciate ligament transection model of osteoarthritis. *Osteoarthr Cartilage* **2004**, *12*, 614-626, doi:https://doi.org/10.1016/j.joca.2004.03.002.
52. MacKay, J.W.; Kaggie, J.D.; Treece, G.M.; McDonnell, S.M.; Khan, W.; Roberts, A.R.; Janiczek, R.L.; Graves, M.J.; Turmezei, T.D.; McCaskie, A.W. Three-dimensional surface-based analysis of cartilage MRI data in knee osteoarthritis: Validation and initial clinical application. *Journal of Magnetic Resonance Imaging* **2020**, *52*, 1139-1151.
53. Xue, N.; Doellinger, M.; Fripp, J.; Ho, C.P.; Surowiec, R.K.; Schwarz, R. Automatic model-based semantic registration of multimodal MRI knee data. *J. Magn. Reson. Imaging* **2015**, *41*, 633-644, doi:10.1002/jmri.24609.
54. Stammberger, T.; Hohe, J.; Englmeier, K.H.; Reiser, M.; Eckstein, F. Elastic registration of 3D cartilage surfaces from MR image data for detecting local changes in cartilage thickness. *Magn Reson Med* **2000**, *44*, 592-601, doi:10.1002/1522-2594(200010)44:4<592::aid-mrm13>3.0.co;2-j.
55. Carballido-Gamio, J.; Bauer, J.S.; Stahl, R.; Lee, K.Y.; Krause, S.; Link, T.M.; Majumdar, S. Inter-subject comparison of MRI knee cartilage thickness. *Med Image Anal* **2008**, *12*, 120-135, doi:10.1016/j.media.2007.08.002.
56. Borotikar, B.S.; Sipprell III, W.H.; Wible, E.E.; Sheehan, F.T.J.J.o.b. A methodology to accurately quantify patellofemoral cartilage contact kinematics by combining 3D image shape registration and cine-PC MRI velocity data. **2012**, *45*, 1117-1122.

Osteoarthritis and Cartilage Open 2 (2020) 100079

Contents lists available at ScienceDirect

Osteoarthritis and Cartilage Open

journal homepage: www.elsevier.com/journals/osteoarthritis-and-cartilage-open/2665-9131

New insight on the subchondral bone and cartilage functional unit: Bone mineral density and cartilage thickness are spatially correlated in non-osteoarthritic femoral condyles

Hugo Babel [a,*], Patrick Omoumi [b], Thomas P. Andriacchi [c,d,e], Brigitte M. Jolles [a,f], Julien Favre [a]

[a] Lausanne University Hospital and University of Lausanne (CHUV-UNIL), Department of Musculoskeletal Medicine, Swiss BioMotion Lab, Lausanne, Switzerland
[b] Lausanne University Hospital and University of Lausanne (CHUV-UNIL), Department of Diagnostic and Interventional Radiology, Lausanne, Switzerland
[c] Stanford University, Department of Mechanical Engineering, Stanford, CA, USA
[d] Palo Alto Veterans Affairs, Palo Alto, CA, USA
[e] Stanford University Medical Center, Department of Orthopaedic Surgery, Stanford, CA, USA
[f] Ecole Polytechnique Fédérale de Lausanne (EPFL), Institute of Microengineering, Lausanne, Switzerland

ARTICLE INFO

Keywords:
CT arthrography
Knee joint
Loading
Osteochondral unit

ABSTRACT

Objective: This study aimed to improve our understanding of the relationship between bone and cartilage by characterizing the morphological coupling between these mechanosensitive tissues exposed to the same mechanical environment within each knee. Specifically, it reanalyzed a prior dataset to test the hypothesis that the locations of thickest cartilage and densest subchondral bone are correlated in non-osteoarthritic femoral condyles.
Method: Anatomically standardized maps of cartilage thickness (CTh) and subchondral bone mineral density (sBMD) were calculated for 50 non-osteoarthritic distal femurs based on computed tomography arthrography examinations. The locations of thickest CTh and densest sBMD were identified in the load-bearing region of the medial and lateral compartments, and correlation analyses were performed to quantify the associations between these locations, with inclusion of age, gender, femoral bone size and femorotibial angle as cofounding variables. Paired Student's t-tests were also performed to compare CTh and sBMD locations.
Results: Locations of thickest CTh and densest sBMD were positively correlated along the anteroposterior direction in both compartments ($r \geq 0.45$, $p \leq 0.001$). Furthermore, thickest CTh was more posterior than densest sBMD in the medial ($p = 0.014$) and lateral ($p < 0.001$) compartments, and more lateral than densest sBMD in the lateral compartment ($p < 0.001$). On average, these location differences were of 1.3, 5.3 and 2.1% of the subchondral bone size.
Conclusion: The positive spatial relationship between the locations of thickest CTh and densest sBMD supports the idea of a functional cartilage/subchondral bone unit with morphological coupling conditioned by the individual loading pattern.

1. Introduction

While it is now established that knee osteoarthritis (OA) is a complex disease affecting the whole joint [1,2], there remains a lack of understanding of the interactions between the diverse elements of the disease. Indeed, while numerous knee properties have been described at various stages of the disease [1,2], little is known about their relationships. Characterizing the relationships seems however necessary at this moment because recent disease models have suggested that the relationships could be more meaningful than isolated properties to understand OA pathophysiology [3].

One relationship of particular interest is between cartilage thickness (CTh) and subchondral bone mineral density (sBMD) [4], two hallmarks of the disease. Focusing on these two properties is particularly motivated

Abbreviations: CT, computerized tomography; OA, osteoarthritis; CTh, cartilage thickness; sBMD, subchondral bone mineral density.

* Corresponding author. Department of Musculoskeletal Medicine, Lausanne University Hospital and University of Lausanne, Av. Pierre Decker 4, CH-1011 Lausanne, Switzerland.
E-mail addresses: hugo.babel@chuv.ch (H. Babel), patrick.omoumi@chuv.ch (P. Omoumi), tandriac@stanford.edu (T.P. Andriacchi), brigitte.jolles-haeberli@chuv.ch (B.M. Jolles), julien.favre@chuv.ch (J. Favre).

https://doi.org/10.1016/j.ocarto.2020.100079
Received 4 December 2019; Accepted 27 May 2020

by the fact that cartilages and subchondral bones are mechanosensitive tissues thought to interact as functional units. There is growing evidence of a biomechanical coupling between these tissues conditioned by gait mechanics [2,5,6]. For example, in non-OA knees the ratio of bone mineral density in the medial and lateral compartments was shown to be positively correlated with loading during gait (knee adduction moment) [7], and a similar positive correlation was described for CTh and the knee adduction moment [6]. Nevertheless, there is a paucity of studies analysing both CTh and sBMD in the same knees [8,9], and therefore few data on the relationship between these two properties.

Interestingly, a recent study measuring CTh and sBMD simultaneously using computed tomography arthrography (CT arthrogram) reported an association between the magnitudes of CTh and sBMD in non-OA femoral condyles [8]. Specifically, thicker CTh was positively correlated with denser sBMD. Although this later study brought new insights to the relationship between CTh and sBMD and thus to the understanding of the osteochondral unit, it only analysed CTh and sBMD magnitudes. Since CTh and sBMD have been shown to vary spatially [10–20], our understanding of non-OA femurs could be enhanced by determining if thicker CTh and denser sBMD are also correlated spatially. Establishing such correlations for non-OA knees could be an important step towards characterizing knee homeostasis. It could also contribute to the development of new methods for assessing early changes leading to knee OA, as some relationships between CTh, sBMD and gait mechanics have been reported to differ with the disease [3].

Thus, the purpose of this study was to reanalyse the dataset in Ref. [8], using novel methods, to test the hypothesis that the locations of thickest CTh and densest sBMD are positively correlated along the anteroposterior and mediolateral directions in the medial and lateral load-bearing regions of non-OA femoral condyles. A secondary objective was to compare the locations of thickest CTh and densest sBMD.

2. Methods

2.1. Population and image acquisition

The dataset reanalyzed in this study consisted of 50 CT arthrograms of non-OA knees from 32 females and 18 males (median age: 58.7 [IQR 6.6] years; biepicondylar femoral diameter: 7.9 [0.9] cm; femorotibial angle: 4.4 [2.6] degrees). The dataset and the acquisition procedure were described previously in details [8]. Briefly, it was composed of consecutive patients aged over 50 years referred to a single imaging center over a 24-month period who had a CT arthrogram and weight-bearing radiographs of their knees the same day. The exclusion criteria were: a Kellgren-Lawrence grade > 1 in any of the medial, lateral or trochlear compartments [21], any imaging sign of previous knee surgery (including knee replacement surgery, ligamentoplasty, cartilage or meniscal repair procedures), post-traumatic or rheumatological disorders (including the presence of intra-articular calcifications), and poor image quality. This pre-existing dataset was of sufficient size to test the hypothesis in this study, as a sample size calculation estimated that a minimum of 47 knees was necessary to test for two-tailed correlation of $r \geq 0.4$ with α of 0.05 and power of 0.80. Expected correlations for the sample size calculation were based on a recent systematic review of relationships between CTh, sBMD and gait mechanics [3]. The study was approved by the institutional ethics committee without requirement for informed consent of the participants due to the retrospective study design.

2.2. Image acquisition and processing

CT examinations were performed after intraarticular injection of 10 mL of ionic contrast material [10]. Patients were lying supine, with the knees extended. Acquisitions were made using a 40-detector row CT scanner (Somatom Definition AS; Siemens Healthcare, Forchheim, Germany) with the following parameters: tube voltage of 120 kVp; reference tube current-time product of 350 mAs with the application of a dose modulation protocol (Care Dose 4D; Siemens Healthcare); bone convolution kernel (U70u), voxel size of $0.3 \times 0.3 \times 0.3$ mm.

Two-dimensional (2D) anatomically standardized maps of CTh and sBMD were obtained using previously published methods, summarized as follows and illustrated in Fig. 1. Each CT arthrogram was segmented semi-manually to build three-dimensional (3D) models of distal femoral bone and cartilage [10,22]. CTh and sBMD values were then calculated for each subchondral vertex of the bone model by, respectively, measuring the distance between the bone and cartilage models [22] and averaging the CT intensity of the bone voxels within a distance of 3 mm [10]. The inter-observer reliability of these magnitude measurement methods was shown to be adequate in prior studies [8,23]. Since CTh and sBMD measurements were paired (i.e., performed at the same positions in the CT frame of each knee), the 3D CTh and sBMD maps were automatically registered for each femur. Lastly, a registration technique was applied to standardize the individual 3D CTh and sBMD maps and allow comparing the 50 femurs [22]. This resulted in 2D anatomically standardized maps of CTh and sBMD for each knee.

2.3. Locations of thickest CTh and densest sBMD

For each femur, the locations of thickest CTh and densest sBMD were identified in medial and lateral load-bearing regions of interest common to both properties using a weighted average method (Fig. 1) [24]. The regions of interest were defined as squares with sides' length equal to half the mediolateral size of the standardized maps. Mediolaterally, they were positioned in each half of the map to avoid any overlap. Their anteroposterior positions were determined independently for the medial and lateral compartments using an automatized iterative method [11]. Each iteration of this method consisted in determining the locations of thickest CTh and densest sBMD of the 50 femurs in the current regions of interest and then in updating the position of the regions of interest by centering them on the average location of the 50 thickest CTh and densest sBMD locations. Iterations were repeated until the convergence of both regions of interest to a constant position. The regions used in this study to locate the thickest CTh and densest sBMD in 2D anatomically standardized maps agreed with regions described in literature [11]. In addition, five knees randomly selected were processed twice by different observers (segmentation and location of thickest CTh and densest sBMD) to assess the inter-observer reliability. This evaluation reported excellent reliability, with an intraclass correlation coefficient (ICC) of 0.99. The locations of thickest CTh and densest sBMD were expressed in percent of the anteroposterior and mediolateral sizes of the standardized maps.

2.4. Statistical analysis

First, four separate Pearson correlations were used to assess the relationships between the locations of thickest CTh and densest sBMD along the anteroposterior and mediolateral directions in the medial and lateral compartments. Second, since gender, age, biepicondylar diameter and femorotibial angle have been shown to be associated with CTh and sBMD [25,26], partial correlations were calculated to describe the relationship between the locations of thickest CTh and densest sBMD while controlling for these four confounding variables [22]. Additionally, paired Student's t-tests were performed to compare the locations of thickest CTh and densest sBMD along both directions in both compartments. Parametric statistics was used after confirmation of the normal distribution of the data using Kolmogorov-Smirnov tests. All statistical calculations were done with R version 3.4.2 (R Core Team, 2017), and an α-level of 5% was considered statistically significant for all tests.

3. Results

The Pearson correlations indicated that, along the anteroposterior direction, the locations of thickest CTh was statistically significantly

positively correlated to the location of densest sBMD in both the medial ($r = 0.45$, 95% confidence interval (CI) [0.20, 0.65], $p = 0.001$) and the lateral ($r = 0.46$, 95% CI [0.21, 0.65], $p < 0.001$) compartments (Table 1, Fig. 2). No relationship along the mediolateral direction achieved statistical significance ($p \geq 0.124$). The partial correlation analyses resulted in the same statistically significant relationships between the locations of thickest CTh and densest sBMD (Table 1).

The location of thickest CTh was more posterior than the location of densest sBMD in both the medial (43.6 ± 3.5 vs. 44.9 ± 3.6% of the anteroposterior standardized map size; $p = 0.014$) and lateral (59.5 ± 4.5 vs. 64.8 ± 3.8%; $p < 0.001$) compartments (Table 2, Fig. 3). In addition, the location of the densest sBMD along the mediolateral direction was more medial than the location of thickest CTh in the lateral compartment (23.0 ± 3.3 vs. 20.9 ± 2.2% of the mediolateral standardized map size; $p < 0.001$). To help the interpretation, for an average knee with an anteroposterior and mediolateral subchondral bone size of 96 mm and 64 mm [22], respectively, these differences would correspond on average to 1.2 mm along the anteroposterior direction in the medial compartment, to 5.1 mm along the anteroposterior direction in the lateral compartment, and to 1.3 mm along the mediolateral direction in the lateral compartment.

4. Discussion

In this paper, we showed that the locations of thickest CTh and densest sBMD are positively correlated along the anteroposterior direction of non-OA femoral condyles, suggesting that spatial morphological variations are coupled between subchondral bones and cartilages consistently with the main motion of the joint. These results are consistent with the current understanding of the knee function. Indeed, cartilage growth and bone densification are both stimulated by mechanical loading [24,27]; load experienced by both tissues should occur in neighboring locations within each femur [2,5]; ambulatory mechanics differ among individuals, leading to variations in the areas of the joint exposed to larger loads [28,29].

The positive relationships in non-OA knees between CTh and sBMD along the anterior-posterior direction are in line with previous reports showing that the spatial variations in thickest CTh location were associated with variations in sagittal plane kinematics during walking [24,30]. Thus, the current results taken together with prior gait studies provide additional support for the idea of a local coupling between articular cartilage and subchondral bone related to each tissue adapting to gait mechanics. In particular, this observation suggests that mechanical signals can transcend scales from whole-body mechanics to a response detectable at the scale of the tissue. The coupling observed in the present study reveals a clinical importance when considered together with prior descriptions of spatial shifts in femorotibial loading during walking with pathological conditions associated to knee OA, such as rupture of the anterior cruciate ligament [24]. In fact, changes in loading pattern without adaptation of cartilage and/or bone to the new loading condition can lead to a degenerative pathway [6].

The results in this study bring additional support to OA pathophysiology models such as the "Integrated Joint System (IJS) [3]", which postulate that knee health depends on homeostatic relationships where

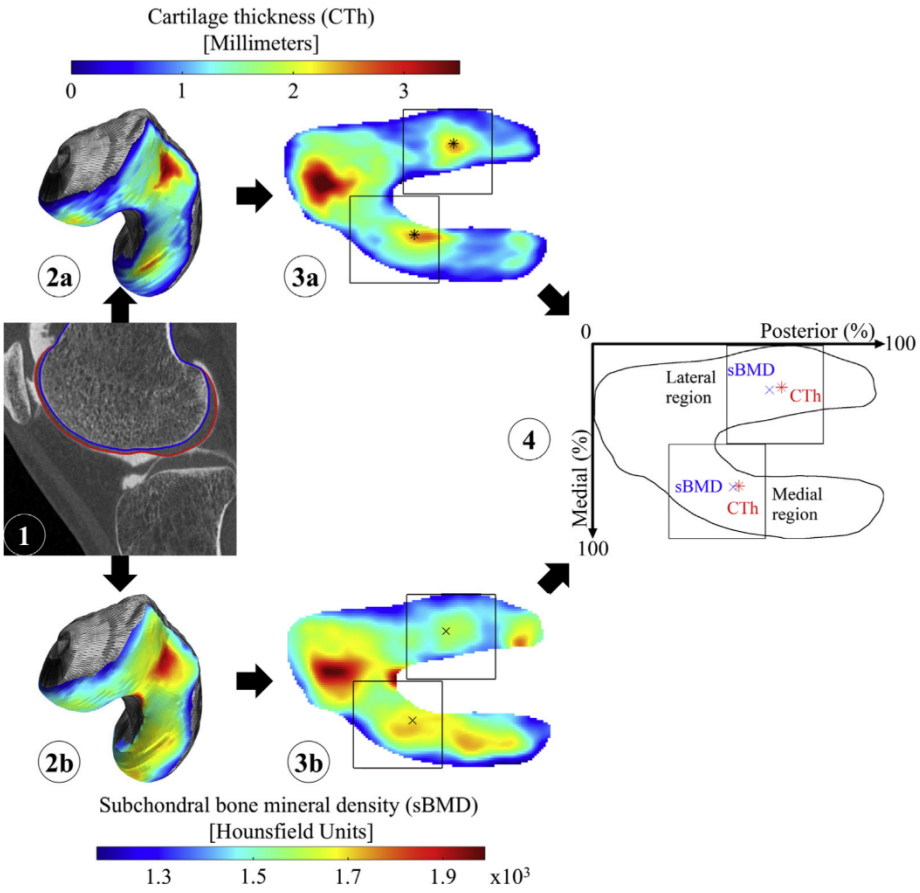

Fig. 1. Illustration of the method used to measure the location of the thickest CTh and densest sBMD in an individual femur. First, the femoral bone and cartilage are segmented on the CT arthrogram (1), yielding three-dimensional maps of CTh (2a) and sBMD (2b). Each map is then anatomically standardized (3) and the locations of thickest CTh (star in 3a) and densest sBMD (cross in 3b) are identified in the medial (top) and lateral (bottom) load-bearing regions of interest, yielding a pair of locations for each region of interest (4).

Table 1
Relationships between the locations of thickest cartilage thickness (CTh) and densest subchondral bone mineral density (sBMD) in the medial and lateral femoral compartments.

	Pearson correlation		Partial correlation[a]	
	R [95% CI]	P–value	R [95% CI]	P–value
Medial compartment				
Anteroposterior direction	0.45 [0.20, 0.65]	**0.001**	0.46 [0.19, 0.66]	**0.001**
Mediolateral direction	0.22 [-0.06, 0.47]	0.124	0.22 [-0.07, 0.48]	0.133
Lateral compartment				
Anteroposterior direction	0.46 [0.21, 0.65]	**<0.001**	0.38 [0.10, 0.61]	**0.009**
Mediolateral direction	0.07 [-0.21, 0.34]	0.636	0.09 [-0.21, 0.37]	0.553

P-values in bold indicate statistically significant relationships between thickest CTh and densest sBMD locations ($p < 0.05$). Statistically significant relationships are illustrated in Fig. 2.

[a] Partial correlation between CTh and sBMD locations while controlling for age, gender, biepicondylar femoral diameter and femorotibial angle confounding variables.

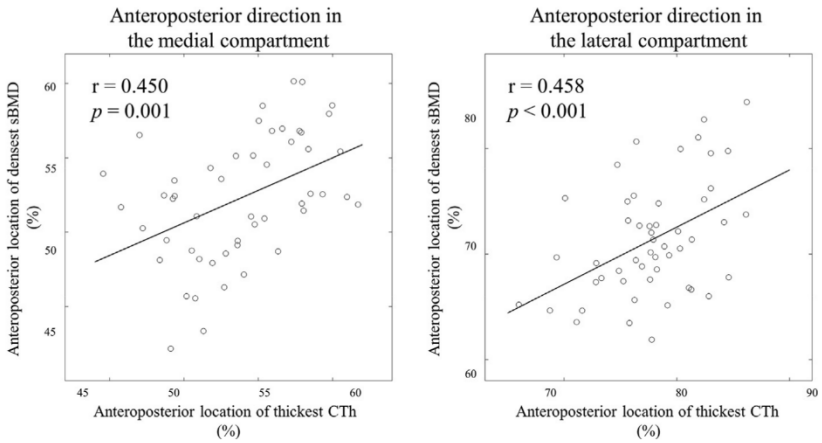

Fig. 2. Scatter plots of the location of densest sBMD with respect to the location of thickest CTh along the anteroposterior direction in the medial (left) and lateral (right) compartments.

tissue properties are mutually adapted. Although only a few studies so far focused on the relationships between knee properties, some relationships have been shown to differ with knee OA [3]. Specifically, a previous work reported a positive relationship between CTh and sBMD magnitudes in non-OA femurs and a negative relationship in OA femurs [8]. The transition from positive to negative relationships with OA could provide a basis for early disease detection as it might reflect metabolic changes that occur early in the disease [31]. For example, the greater metabolic activity of bone relative to cartilage would suggest different morphological adaptations to loading changes in cartilage compared to bone as OA develops. Thus, the detection sensitivity could be enhanced by using a metric based on the coupling of CTh and sBMD rather than by analysing these properties in isolation. Altogether, these observations warrant further research on the relationship between CTh and sBMD as well as the extension to other properties. The interest of extending to other properties in the future is particularly well supported by a recent study reporting positive correlations between thicker CTh and thicker subchondral bone plate in normal sheep knees and changes in the relationships between these properties after partial meniscectomy [15].

Table 2
Locations and magnitudes of thickest cartilage thickness (CTh) and densest subchondral bone mineral density (sBMD) in the medial and lateral femoral compartments.

	Thickest CTh	Densest sBMD	P-values
Medial compartment			
Anteroposterior location	44.9 ± 3.6%	43.6 ± 3.5%	**0.014**
Mediolateral location	69.3 ± 4.2%	70.0 ± 4.2%	0.357
Magnitude	2.1 ± 0.4 mm	1697.5 ± 70.1 HU	n/a
Lateral compartment			
Anteroposterior location	64.8 ± 3.8%	59.5 ± 4.5%	**<0.001**
Mediolateral location	20.9 ± 2.2%	23.0 ± 3.3%	**<0.001**
Magnitude	2.1 ± 0.5 mm	1577.3 ± 71.8 HU	n/a

Location and magnitude data are presented as mean ± standard deviation of the 50 knees. Location data are in percent of the anteroposterior or mediolateral sizes of the standardized maps (see Fig. 3), whereas magnitude data are in mm for CTh and in Hounsfield units (HU) for sBMD.

P-values in bold indicate statistically significant differences between CTh and sBMD locations ($p < 0.05$).

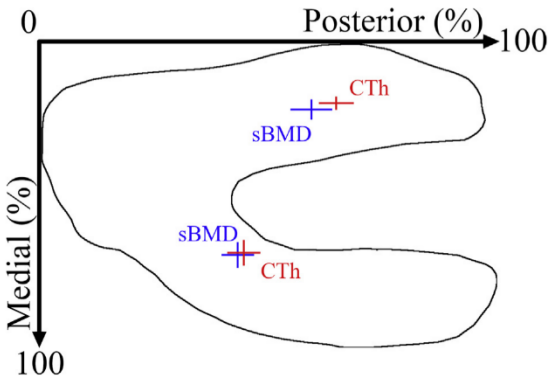

Fig. 3. Average (± standard deviation) location of thickest CTh (red) and densest sBMD (blue) for the 50 knees.

This study presents some limitations, including its retrospective design that limited the confounding variables that could be included in the analyses. Further studies should consider other confounding variables such as participants' size and body mass index. Similarly, taking into account the inter-individual differences in local knee morphology could help explain the absence of correlation along the mediolateral direction [32,33]. Another limitation is the absence of mechanical loading data. Although the locations of thickest CTh and densest sBMD agree with prior works reporting the areas of the femur in contact with the tibia during daily activities [16,29,34,35] and although the location of thickest CTh has been related to the knee flexion angle during walking [24,30], future studies should consider knee dynamics and loading patterns in addition to bone and cartilage properties for a global understanding of the osteochondral unit. In addition, the methodology is only applicable to non-OA knees, as measuring the location of thickest CTh is irrelevant in knees with substantial cartilage loss. A previous work on CTh and sBMD magnitudes has shown different relationships in non-OA and severe OA knees [8]. It is therefore of particular interest to develop new methods allowing the characterization of the spatial relationship between CTh and sBMD in both OA and non-OA knees. Lastly, BMD quantified by clinical CT is a measure of apparent density. As such, it includes calcified cartilage, whose thickness varies topographically, and non-mineralized tissues in the attenuation calculation [4]. In particular, BMD should not be mistaken for true tissue mineral density (TMD) which requires a segmentation of the bone to distinguish calcified bone tissue from surrounding tissue [36].

In conclusion, this study showed a positive *in vivo* relationship between locations of thickest CTh and densest sBMD. These results support the idea of a functional unit with morphological coupling between articular cartilage and subchondral bone, and more generally support OA pathophysiology models based on relationships between joint properties. Future research characterizing the spatial relationship in intermediate and severe OA stages could further improve our understanding of knee OA.

Contributions

Hugo Babel made substantial contributions to: analysis and interpretation of the data; drafting of the article; critical revision of the article for important intellectual content; final approval of the article.

Patrick Omoumi made substantial contributions to: conception and design; acquisition of data; analysis and interpretation of data; drafting of the article; critical revision of the article for important intellectual content; final approval of the article; obtaining of funding. PO made equal contributions to this work than BMJ and JF.

Thomas P. Andriacchi made substantial contributions to: analysis and interpretation of data; drafting of the article; critical revision of the article for important intellectual content; final approval of the article.

Brigitte M. Jolles made substantial contributions to: analysis and interpretation of data; critical revision of the article for important intellectual content; final approval of the article; obtaining of funding. BMJ made equal contributions to this work than PO and JF.

Julien Favre made substantial contributions to: conception and design; analysis and interpretation of data; drafting of the article; critical revision of the article for important intellectual content; final approval of the article; obtaining of funding.

Funding source

This work was funded by the "Swiss National Science Foundation, Switzerland (SNSF Grant #CRSII5_177155)" and the “Lausanne Orthopedic Research Foundation, Switzerland”. The funding sources had no involvement in the study design, collection, analysis and interpretation of data; in the writing of the manuscript; and in the decision to submit the manuscript for publication.

Declaration of Competing Interest

None.

Acknowledgements

None.

References

[1] H.A. Wieland, M. Michaelis, B.J. Kirschbaum, K.A. Rudolphi, Osteoarthritis—an untreatable disease? Nat. Rev. Drug Discov. 4 (4) (2005) 331–345.
[2] S.R. Goldring, M.B. Goldring, Changes in the osteochondral unit during osteoarthritis: structure, function and cartilage-bone crosstalk, Nat. Rev. Rheumatol. 12 (11) (2016) 632–644, https://doi.org/10.1038/nrrheum.2016.148. Epub 2016/10/21 PubMed PMID: 27652499.
[3] S.N. Edd, P. Omoumi, T.P. Andriacchi, B.M. Jolles, J. Favre, Modeling knee osteoarthritis pathophysiology using an integrated joint system (IJS): a systematic review of relationships among cartilage thickness, gait mechanics, and subchondral bone mineral density, Osteoarthritis Cartilage 26 (11) (2018) 1425–1437, https://doi.org/10.1016/j.joca.2018.06.017. Epub 2018/07/30 PubMed PMID: 30056214.
[4] V. Bousson, T. Lowitz, L. Laouisset, K. Engelke, J.D. Laredo, CT imaging for the investigation of subchondral bone in knee osteoarthritis, Osteoporos. Int. 23 (Suppl 8) (2012) S861–S865, https://doi.org/10.1007/s00198-012-2169-5. Epub 2012/11/28 PubMed PMID: 23179574.
[5] H. Imhof, I. Sulzbacher, S. Grampp, C. Czerny, S. Youssefzadeh, F. Kainberger, Subchondral bone and cartilage disease: a rediscovered functional unit, Invest. Radiol. 35 (10) (2000) 581–588.
[6] T.P. Andriacchi, S. Koo, S.F. Scanlan, Gait mechanics influence healthy cartilage morphology and osteoarthritis of the knee, J. Bone Jt. Surg. Am. Vol. 91 (Suppl 1) (2009) 95–101, https://doi.org/10.2106/JBJS.H.01408. Epub 2009/02/21 PubMed PMID: 19182033; PubMed Central PMCID: PMCPMC2663350.
[7] D.E. Hurwitz, D.R. Sumner, T.P. Andriacchi, D.A. Sugar, Dynamic knee loads during gait predict proximal tibial bone distribution, J. Biomech. 31 (5) (1998) 423–430.
[8] P. Omoumi, H. Babel, B.M. Jolles, J. Favre, Relationships between cartilage thickness and subchondral bone mineral density in non-osteoarthritic and severely osteoarthritic knees: in vivo concomitant 3D analysis using CT arthrography, Osteoarthritis Cartilage 27 (4) (2019) 621–629, https://doi.org/10.1016/j.joca.2018.12.014. PubMed PMID: WOS:000461674500010.
[9] Y. Cao, O.P. Stannus, D. Aitken, F. Cicuttini, B. Antony, G. Jones, et al., Cross-sectional and longitudinal associations between systemic, subchondral bone mineral density and knee cartilage thickness in older adults with or without radiographic osteoarthritis, Ann. Rheum. Dis. 73 (11) (2014) 2003–2009, https://doi.org/10.1136/annrheumdis-2013-203691. Epub 2013/08/02 PubMed PMID: 23904471.
[10] P. Omoumi, H. Babel, B.M. Jolles, J. Favre, Quantitative regional and sub-regional analysis of femoral and tibial subchondral bone mineral density (sBMD) using computed tomography (CT): comparison of non-osteoarthritic (OA) and severe OA knees, Osteoarthritis Cartilage 25 (11) (2017) 1850–1857, https://doi.org/10.1016/j.joca.2017.07.014. Epub 2017/07/27. PubMed PMID: 28743608.
[11] J. Favre, S.F. Scanlan, J.C. Erhart-Hledik, K. Blazek, T.P. Andriacchi, Patterns of femoral cartilage thickness are different in asymptomatic and osteoarthritic knees and can be used to detect disease-related differences between samples, J. Biomech. Eng. 135 (10) (2013) 101002–101010, https://doi.org/10.1115/1.4024629. Epub 2013/06/01 PubMed PMID: 23722563; PubMed Central PMCID: PMCPMC3792405.
[12] M. Terukina, H. Fujioka, S. Yoshiya, M. Kurosaka, T. Makino, N. Matsui, et al., Analysis of the thickness and curvature of articular cartilage of the femoral condyle, Arthrosc. J. Arthrosc. Relat. Surg. 19 (9) (2003) 969–973.
[13] Z.A. Cohen, D.M. Mccarthy, S.D. Kwak, P. Legrand, F. Fogarasi, E.J. Ciaccio, et al., Knee cartilage topography, thickness, and contact areas from MRI: in-vitro calibration and in-vivo measurements, Osteoarthritis Cartilage 7 (1) (1999) 95–109.
[14] Z.A. Cohen, V.C. Mow, J.H. Henry, W.N. Levine, G.A. Ateshian, Templates of the cartilage layers of the patellofemoral joint and their use in the assessment of osteoarthritic cartilage damage, Osteoarthritis Cartilage 11 (8) (2003) 569–579, https://doi.org/10.1016/s1063-4584(03)00091-8.
[15] T. Oláh, J. Reinhard, L. Gao, S. Haberkamp, L.K. Goebel, M. Cucchiarini, et al., Topographic modeling of early human osteoarthritis in sheep, Sci. Transl. Med. 11 (508) (2019), eaax6775.
[16] G. Li, S.E. Park, L.E. DeFrate, M.E. Schutzer, L. Ji, T.J. Gill, et al., The cartilage thickness distribution in the tibiofemoral joint and its correlation with cartilage-to-cartilage contact, Clin. Biomech. 20 (7) (2005) 736–744.
[17] S.J. Armstrong, R.A. Read, R. Price, Topographical variation within the articular cartilage and subchondral bone of the normal ovine knee joint: a histological approach, Osteoarthritis Cartilage 3 (1) (1995) 25–33.
[18] J.D. Johnston, B.A. Masri, D.R. Wilson, Computed tomography topographic mapping of subchondral density (CT-TOMASD) in osteoarthritic and normal knees: methodological development and preliminary findings, Osteoarthritis Cartilage 17 (10) (2009) 1319–1326, https://doi.org/10.1016/j.joca.2009.04.013. Epub 2009/05/12 PubMed PMID: 19427927.
[19] K.L. Bennell, M.W. Creaby, T.V. Wrigley, D.J. Hunter, Tibial subchondral trabecular volumetric bone density in medial knee joint osteoarthritis using peripheral

quantitative computed tomography technology, Arthritis Rheum. 58 (9) (2008) 2776–2785, https://doi.org/10.1002/art.23795. Epub 2008/09/02 PubMed PMID: 18759296.

[20] A. Phillips, N.J. Burton, C.M.R. Warren-Smith, E.R. Kulendra, K.J. Parsons, Topographic bone density of the radius and ulna in Greyhounds and Labrador Retrievers with and without medial coronoid process disease, Vet. Surg. 44 (2) (2015) 180–190.

[21] D.T. Felson, T.E. McAlindon, J.J. Anderson, B.W. Weissman, P. Aliabadi, S. Evans, et al., Defining radiographic osteoarthritis for the whole knee, Osteoarthritis Cartilage 5 (4) (1997) 241–250.

[22] J. Favre, J.C. Erhart-Hledik, K. Blazek, B. Fasel, G.E. Gold, T.P. Andriacchi, Anatomically standardized maps reveal distinct patterns of cartilage thickness with increasing severity of medial compartment knee osteoarthritis, J. Orthop. Res. 35 (11) (2017) 2442–2451, https://doi.org/10.1002/jor.23548. Epub 2017/02/25 PubMed PMID: 28233332.

[23] S. Koo, G.E. Gold, T.P. Andriacchi, Considerations in measuring cartilage thickness using MRI: factors influencing reproducibility and accuracy, Osteoarthritis Cartilage 13 (9) (2005) 782–789, https://doi.org/10.1016/j.joca.2005.04.013. Epub 2005/06/18 PubMed PMID: 15961328.

[24] S.F. Scanlan, J. Favre, T.P. Andriacchi, The relationship between peak knee extension at heel-strike of walking and the location of thickest femoral cartilage in ACL reconstructed and healthy contralateral knees, J. Biomech. 46 (5) (2013) 849–854, https://doi.org/10.1016/j.jbiomech.2012.12.026. Epub 2013/02/05 PubMed PMID: 23375789.

[25] R.B. Frobell, M.C. Nevitt, M. Hudelmaier, W. Wirth, B.T. Wyman, O. Benichou, et al., Femorotibial subchondral bone area and regional cartilage thickness: a cross-sectional description in healthy reference cases and various radiographic stages of osteoarthritis in 1,003 knees from the Osteoarthritis Initiative, Arthritis Care Res (Hoboken). 62 (11) (2010) 1612–1623, https://doi.org/10.1002/acr.20262. Epub 2010/05/25 PubMed PMID: 20496431.

[26] T. Baum, M. Sauerschnig, J. Penzel, P.M. Jungmann, S. Waldt, E.J. Rummeny, et al., Early changes of trabecular bone structure in asymptomatic subjects with knee malalignment 38 (1) (2014) 137–141.

[27] C. Turner, Three rules for bone adaptation to mechanical stimuli, Bone 23 (5) (1998) 399–407.

[28] E. Chehab, T. Andriacchi, Favre JJJob, Speed, age, sex, and body mass index provide a rigorous basis for comparing the kinematic and kinetic profiles of the lower extremity during walking 58 (2017) 11–20.

[29] B. Akpinar, E. Thorhauer, S. Tashman, J.J. Irrgang, F.H. Fu, Anderst WJJOjosm, Tibiofemoral cartilage contact differences between level walking and downhill running 7 (4) (2019), 2325967119836164.

[30] S. Koo, J.H. Rylander, T.P. Andriacchi, Knee joint kinematics during walking influences the spatial cartilage thickness distribution in the knee, J. Biomech. 44 (7) (2011) 1405–1409, https://doi.org/10.1016/j.jbiomech.2010.11.020. Epub 2011/03/05 PubMed PMID: 21371712; PubMed Central PMCID: PMCPMC3078989.

[31] L.S. Lohmander, M. Ionescu, H. Jugessur, A.R. Poole, Changes in joint cartilage aggrecan after knee injury and in osteoarthritis, Arthritis Rheum.: Off. J. Am. coll. Rheumatol. 42 (3) (1999) 534–544.

[32] S. Koo, T.P. Andriacchi, A comparison of the influence of global functional loads vs. local contact anatomy on articular cartilage thickness at the knee, J. Biomech. 40 (13) (2007) 2961–2966, https://doi.org/10.1016/j.jbiomech.2007.02.005. Epub 2007/04/10 PubMed PMID: 17418219; PubMed Central PMCID: PMCPMC2358971.

[33] A.L. Clouthier, C.R. Smith, M.F. Vignos, D.G. Thelen, K.J. Deluzio, Rainbow MJJMe, et al., The effect of articular geometry features identified using statistical shape modelling on knee biomechanics 66 (2019) 47–55.

[34] J.-S. Li, A. Hosseini, L. Cancre, N. Ryan, H.E. Rubash, G.J.G. Li, et al., Kinematic characteristics of the tibiofemoral joint during a step-up activity 38 (4) (2013) 712–716.

[35] P. Yin, J.-S. Li, W.A. Kernkamp, T.-Y. Tsai, S.-H. Baek, A. Hosseini, et al., Analysis of in-vivo articular cartilage contact surface of the knee during a step-up motion 49 (2017) 101–106.

[36] M.L. Bouxsein, S.K. Boyd, B.A. Christiansen, R.E. Guldberg, K.J. Jepsen, Müller RJJob, et al., Guidelines for assessment of bone microstructure in rodents using micro–computed tomography 25 (7) (2010) 1468–1486.

Decreased adaptation of cartilage thickness (CTh) and bone mineral density (sBMD) spatial variations in osteoarthritic versus non-osteoarthritic knees

Abstract

Objective: This study aimed to characterize the spatial relationship between cartilage thickness (CTh) and subchondral bone mineral density (sBMD) for non-osteoarthritic (OA) knees and knees spanning all medial OA severities.

Methods: Anatomically standardized maps of CTh and sBMD were calculated for 51 non-OA (Kellgren and Lawrence (K/L) scores 0-1) and 60 knees of varying severities (K/L 2-4). In addition to the spatial association quantified using Lee's L, average CTh and sBMD values were calculated within the load-bearing regions of the femorotibial compartment. Pairwise differences between consecutive groups of increasing OA severity were assessed using Wilcoxon rank-sum tests.

Results: The spatial association between medial CTh and sBMD progressively decreased from positive ($L \geq 0.70$) in non-OA knees, to negative in K/L 4 knees ($L \leq -0.42$), with all differences between groups of sequential severity achieving statistical significance (adjusted $p \leq 0.04$). Average CTh and sBMD measurements exhibited an inconsistent trend of decreasing CTh and increasing sBMD with increasing OA severity which seldom achieved statistical significance.

Conclusion: The study showed a strong positive CTh-sBMD relationship in non-OA knees, and a progressive reversal of the relationship with increasing OA severity in the medial femorotibial compartment. In addition, assessing the relationship instead of isolated components presented more consistent patterns. The *in vivo* data bring support to pathophysiological models of OA based on the disruption of homoeostasis, and highlight the promising potential of assessing spatial variations and relationships to evaluate the osteochondral health and differentiate between disease states.

1. Introduction

Although knee osteoarthritis (OA) affects the whole joint [1], the articular structures have primarily been studied in isolation, limiting the global understanding of the disease. More recent models of OA pathophysiology point to the value of studying the relationships between joint components [2]. According to these models, in the homeostatic state,

articular structures are mutually adapted in what could be described "healthy" relationships among joint components. With OA, these relationships progressively deteriorate, to the point of being reversed in severe OA compared to non-OA knees. This relationship-based approach to the disease could significantly improve our understanding of knee OA.

The relationship between cartilage and subchondral bone is of particular interest. These tissues are thought to form a functional unit, the osteochondral unit, specialized in the transfer of load [3]. Numerous histological, biochemical and genetic data point to the interaction and crosstalk between cartilage and subchondral bone, and their role in the pathogenesis of OA [3-5]. While imaging could play a key role in further characterizing the relationships between cartilage and subchondral bone, imaging-based studies in this area are still scarce [3,4]. Using the capability of CT arthrography to concomitantly provide information on cartilage thickness (CTh) and subchondral bone mineral density (sBMD) at high resolution, two recent studies have brought in vivo evidence on the relationships that exist between these tissues in human knees [6,7]. First, non-OA knees with thicker CTh were shown to have denser sBMD, whereas in severe OA, knees with thinner CTh had denser sBMD [6]. Second, in non-OA knees, an association was shown between the locations of thickest CTh and densest sBMD [7]. While these results have improved our understanding of the relationships between cartilage and subchondral bone, there remain some knowledge gaps. In particular, there is a need to characterize the relationships between cartilage and subchondral bone in terms of spatial variations of the tissue characteristics along the articular surfaces [8], and to compare these relationships among varying OA severity. Indeed, so far the relationships between CTh and sBMD have been assessed between knees and only for some disease stages.

This study aimed to characterize the spatial relationship between CTh and sBMD within non-OA knees, as well as in knees spanning all medial OA severities. Based on previous data reviewed above [6,7], the hypotheses of this study were: 1) there is a positive relationship in non-OA compartments, with denser sBMD spatially associated with thicker CTh, and 2) there is a progressive reversal in the relationship with increasing OA severity, to the point of having denser sBMD spatially associated with thinner CTh in compartments with severe OA.

2. Methodology

2.1. Population sample

This retrospective cross-sectional study analyzed consecutive knee CT arthrograms performed in the work-up of meniscochondral injuries. The inclusion criteria were CT arthrograms and posteroanterior weight-bearing (Lyon-

Schuss) and lateral radiographic views of the knee obtained the same day for patients aged over 50 years old. A musculoskeletal with 10 years of experience graded the knee radiographs using a modified Kellgren-Lawrence (K/L) system (medial and lateral compartment graded separately) [29]. Knees with lateral compartment OA were excluded (lateral compartment K/L≥2), as well as knees presenting imaging signs of osteoligamentous injury, previous knee surgery (including cartilage repair procedures, ligamentoplasty and knee replacement procedures), crystal arthropathy, inflammatory joint disease, or poor image quality. In total, 111 knees from 111 patients were included. They were divided in four groups based on the K/L grade in the medial femorotibial compartment: non-OA (K/L≤1)(*n*=51, 18 men, 58.6 [1st quartile 55.9, 3rd quartile 62.7] years old), K/L2 (*n*=26, 11 men, 61.7 [56.0, 69.5] years old), K/L3 (*n*=25, 11 men, 62.3 [56.4, 76.3] years old) and K/L4 knees (*n*=9, 5 men, 64.5 [59.8, 68.9] years old). Chi-square and Kruskall-Wallis tests were used to assess group differences in categorical (sex) and continuous variables (age, femoral and tibial bone sizes). Age differences between the subgroups achieved statistical significance ($H(3) = 8.46$, $p = 0.037$) but post-hoc Wilcoxon rank-sum tests with Bonferroni corrections for multiple comparisons indicated that no differences achieved statistical significance (adjusted $p \geq 0.095$). There were no significant differences between KL groups for patient sex ($X^2(3, 111)=1.67$, $p=0.637$), femoral bone size ($H(3)=1.51$, $p=0.679$), represented by the bicondylar femoral diameters, or tibial bone size ($H(3)=1.57$, $p=0.667$), represented by the tibial diameter, measured on axial CT images following previously reported methodology [9]. The study was approved by the institutional ethical committee without requirement for informed consent of participants due to the retrospective study design.

Table 1. Demographics and bone morphometric parameters of the groups.

	non-OA	K/L 2	K/L 3	K/L 4
Subjects (n)	51	26	25	9
Sex (male/female)	18 / 33	11 / 15	11 / 14	5 / 4
Age (years)	58.6 [55.9, 62.7]	61.7 [56.0, 69.5]	62.3 [56.4, 76.3]	64.5 [59.8, 68.9]
Femoral bone size: biepicondylar femoral diameter (cm)	7.9 [7.5, 8.4]	7.8 [7.5, 8.9]	8.1 [7.9, 8.7]	8.3 [7.5, 8.4]
Tibia bone size: tibial diameter (cm)	7.1 [6.9, 7.8]	7.2 [6.8, 8.0]	7.5 [7.1, 7.9]	7.6 [6.9, 7.8]

Data are presented as either number or median [1st quartile, 3rd quartile]. Group comparison statistics were performed using a chi-square test (sex) and Kruskal-Wallis test followed by post-hoc Wilcoxon rank-sum tests with a Bonferroni correction for pairwise differences between columns(age, femoral bone size, tibial bone size) and no difference achieved statistical significance (adjusted $p \geq 0.095$)

2.2 Image acquisition and processing

Intraarticular injection of 10mL of ionic contrast material was performed in each knee following the same fluoroscopy-guided procedure. CT examinations were then acquired with the patient supine, with extension of the knee, on a 40-row detector helical CT scanner (Somatom Definition AS; Siemens Healthcare, Forchheim, Germany), using the following acquisition parameters: tube voltage, 120 kVp; reference tube current-time product, 350 mAs with the application of a dose modulation protocol (Care Dose 4D; Siemens Healthcare); bone convolution kernel (U70u), voxel size of 0.3x0.3x0.3mm. In order to avoid significant penetration of contrast material into surrounding structures such as bone and cartilage, the acquisition of CT was done within 15 min after the intraarticular injection [6,10].

2.3 sBMD, CTh and their association

Anatomically standardized maps of CTh and sBMD were calculated using previously described and validated methods [11,12]. Briefly, each CT arthrogram was segmented semi-manually using in-house software to build three-dimensional models of femoral and tibial bones and cartilages (Fig. 1a). Three-dimensional CTh and sBMD maps were then calculated based on the distance between the bone and cartilage models [13] and the CT intensity of the bone voxels [10], respectively (Fig. 1b). Next, two-dimensional anatomically standardized CTh and sBMD maps were derived from the three-dimensional maps using the method described by Favre et al. [11,12] (Fig. 1c). Finally, the spatial relationship between CTh and sBMD was assessed in the load-bearing regions of the medial and lateral femoral condyles and tibial compartments (Fig. 1d), based on 556 to 1060 pixels. Specifically, Lee's *L* [14], a measure of bivariate spatial association extending bivariate association measures by accounting for the spatial distribution of the

maps, was used to quantify the relationship between the CTh and sBMD maps. The statistic ranges from -1≤*L*≤1, where positive values indicate that sBMD is denser where CTh is thicker, and negative values indicate that sBMD is denser where CTh is thinner. Additionally, the average CTh and sBMD values in the load-bearing region of the medial and lateral femoral condyles and tibial compartments were computed [15].

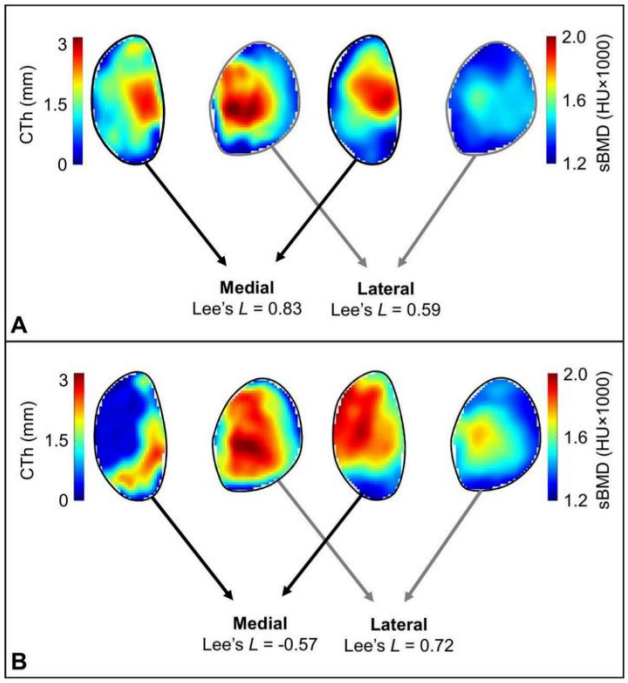

Figure 1. Measurement of Lee's L in a non-OA knee (A) and a K/L 4 knees (B).

2.4 Statistical analyses

Pairwise differences in Lee's L, CTh and sBMD were assessed between consecutive groups of increasing OA severity using Wilcoxon rank-sum tests. All processing and statistical analyses were performed using Matlab (Release 2019b, Natick, MA). An alpha-level of 5% was considered for all tests. Furthermore, the reported *p*-values were adjusted for multiple comparisons using a Bonferroni correction.

3. Results

In the medial compartment, for the femur, differences in Lee's *L* achieved statistical significance between all groups of consecutive OA severities ($z \geq 2.46$, adjusted $p \leq 0.04$), progressively decreasing from positive values in the

non-OA group (median L=0.79) to negative values in the K/L4 group (median L=-0.52) (Figure 2 and Table). Similarly, in the medial tibia, differences in Lee's L achieved statistical significance between all groups of consecutive OA severity ($z \geq 3.47$, $p < 0.01$), progressively decreasing from positive values in non-OA knees (median L=0.70) to negative values in K/L4 knees (median L=-0.42).

In the lateral compartment, the spatial variations in CTh and sBMD remained positively associated for both the femur (median $L \geq 0.55$) and the tibia (median $L \geq 0.69$) and did not vary significantly from one severity group to the next ($p \geq 0.82$).

While there was a trend for increasing sBMD and decreasing CTh with increasing OA severity in the medial compartment, statistically significant differences from one severity group to the next were rare. In the lateral compartment, no statistical difference was found for sBMD and CTh between consecutive severity grades.

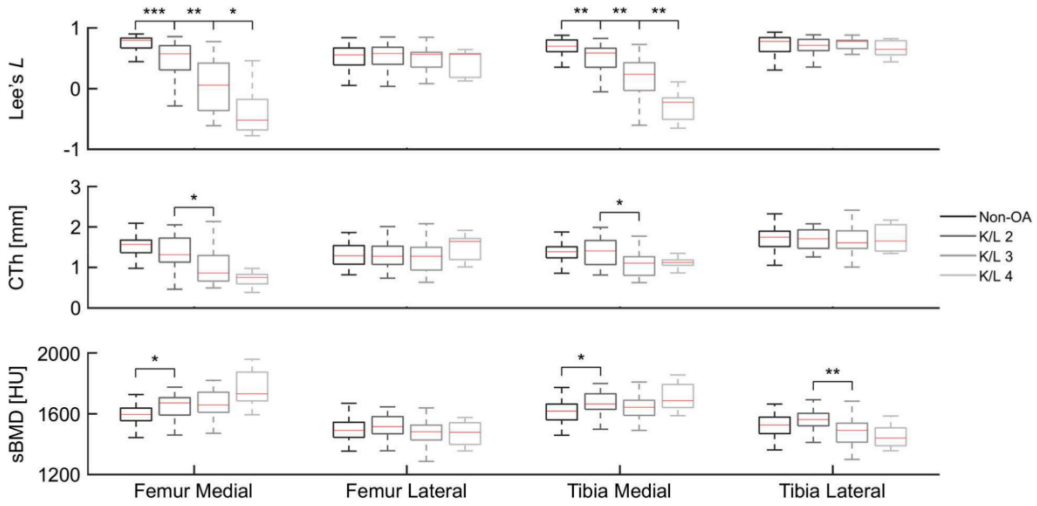

Figure 2. Distribution of Lee's L, mean CTh and sBMD values per OA severity group in the femur and the tibia. The stars indicate differences between groups of sequential OA severity that achieved statistical significance (*: adjusted $p<0.05$; **: adjusted $p<0.01$; ***: adjusted $p<0.001$).

Table 2. Lee's L, CTh and sBMD in the femoral condyle and tibial compartments

	non-OA (n = 51)	K/L 2 (n = 26)	K/L 3 (n = 25)	K/L 4 (n = 9)
Femur				
Lee's *L*				
Medial condyle	0.79 [0.67, 0.83] [2]	0.57 [0.31, 0.71] [01,3]	0.05 [-0.36, 0.42] [2,4]	-0.52 [-0.68, -0.18] [3]
Lateral condyle	0.55 [0.39, 0.67]	0.58 [0.40, 0.68]	0.56 [0.35, 0.60]	0.56 [0.18, 0.58]
CTh				
Medial condyle	1.57 [1.36, 1.67]	1.31 [1.13, 1.72] [3]	0.86 [0.66, 1.29] [2]	0.75 [0.60, 0.83]
Lateral condyle	1.29 [1.08, 1.54]	1.27 [1.07, 1.52]	1.28 [0.93, 1.50]	1.64 [1.19, 1.71]
sBMD				
Medial condyle	1594.4 [1554.4, 1637.1] [2]	1670.7 [1591.3, 1705.3] [01]	1657.1 [1609.5, 1741.1]	1730.6 [1684.0, 1872.2]
Lateral condyle	1490.5 [1445.1, 1544.0]	1514.5 [1468.4, 1581.1]	1481.7 [1427.4, 1525.3]	1477.9 [1398.5, 1540.9]
Tibia				
Lee's *L*				
Medial compartment	0.70 [0.61, 0.80] [2]	0.56 [0.35, 0.66] [01,3]	0.15 [-0.15, 0.40] [2,4]	-0.42 [-0.59, -0.23]
Lateral compartment	0.78 [0.61, 0.84]	0.69 [0.46, 0.80]	0.75 [0.56, 0.79]	0.75 [0.56, 0.79]
CTh				
Medial compartment	1.39 [1.24, 1.51]	1.41 [1.07, 1.66] [3]	1.10 [0.81, 1.26] [2]	1.12 [1.05, 1.19]
Lateral compartment	1.75 [1.51, 1.89]	1.71 [1.47, 1.93]	1.61 [1.47, 1.90]	1.65 [1.40, 2.05]
sBMD				
Medial compartment	1616.8 [1559.4, 1663.1] [2]	1663.8 [1629.0, 1731.0] [01]	1641.9 [1589.0, 1687.9]	1685.6 [1640.2, 1791.9]
Lateral compartment	1525.9 [1469.6, 1577.4]	1561.5 [1520.5, 1602.6] [3]	1490.8 [1431.4, 1538.0] [2]	1440.8 [1390.0, 1507.1]

Data are presented as median [1st quartile, 3rd quartile]. Lee's L is dimensionless, CTh measures are in mm, and sBMD measures in Hounsfield units. The [01], [2], [3] and [4] superscripts indicate differences between groups of sequential OA (adjusted $p < 0.05$).

4. Discussion

In this paper, we showed that there is 1) a strong (L>0.5) positive relationship between sBMD and CTh in non-OA medial and lateral compartments, with denser sBMD spatially associated with thicker CTh, and 2) a progressive

reversal of CTh-sBMD relationships with increasing OA severity in the compartment, from strongly positive to strongly negative associations.

Interestingly, the monotonic differences between consecutive OA grades observed by studying the spatial association between CTh and sBMD were found less consistently and in much lower number when assessing sBMD or CTh in isolation. Indeed, CTh and sBMD vary greatly among individuals, as well as within individuals between locations along the articular surfaces [8,11]. These inter- and intra-individual differences have always made it difficult to use CTh and sBMD to define the normality of the tissues, or to compare knees between individuals. While the spatial variations have been relatively overlooked so far, our results suggest that they could be highly informative. In fact, spatial variations allow the assessment of bone and cartilage with respect to each other, which could be used as a marker of the functioning of the osteochondral unit. This measure is furthermore interesting because it is "standardized" against the natural variations that exists among individuals: it is sensitive to the spatial variations but not to the magnitudes of CTh and sBMD. Consequently, it could become a powerful tool to evaluate the osteochondral health and differentiate between disease states.

Our results extend the few previous studies investigating the relationships between CTh and sBMD, as reviewed above in the Introduction [6,7]. First, they showed a reversal of CTh-sBMD relationships within knees, between non-OA and severe OA, therefore adding an intra-knee characterization to prior inter-knee observations. Second, the present study reported monotonic differences with increasing grades of OA, providing a picture of the transition from one relationship to its reverse.

This study also provides in vivo data, in the human knee, to improve our understanding of the functioning of the osteochondral unit. Specifically, our results support the ideas that, in a healthy knee, cartilage growth and bone densification are stimulated by the same mechanical patterns [3], leading to a superposition of thicker CTh and denser sBMD in areas of greater loading. With the development of the disease, this healthy positive spatial association is progressively lost in K/L2 knees, before almost disappearing in K/L3 knees. In K/L4 knees, the relationship is inverted, with thinner CTh likely contributing to denser sBMD by an increasing the mechanical load on the latter. More generally, our results bring support to the pathophysiological models of OA based on a disequilibrium in the relationships between articular structural components [2].

This study presents several limitations, including its cross-sectional, retrospective design.

While the CTh-sBMD relationship seems promising as a diagnostic tool to assess the health of the osteochondral unit, future work should focus on determining normal values and reference intervals for the spatial associations, intra-individual responsiveness to use this tool to define the health of the osteochondral unit. The assessment of relationships could be extended to other parameters such as bone texture or cartilage compositional data.

In conclusion, this study assessed the spatial relationships between CTh and sBMD within knees, showing strong positive correlations in non-OA compartments, and decreased associations in sequential groups of increasing OA severity, becoming negative in severe OA knees. The spatial association between CTh and sBMD may be used as a marker of the health of the osteochondral unit.

References

1. Wieland, H.A.; Michaelis, M.; Kirschbaum, B.J.; Rudolphi, K.A. Osteoarthritis—an untreatable disease? *Nature reviews Drug discovery* **2005**, *4*, 331-345.
2. Edd, S.N.; Omoumi, P.; Andriacchi, T.P.; Jolles, B.M.; Favre, J. Modeling knee osteoarthritis pathophysiology using an integrated joint system (IJS): a systematic review of relationships among cartilage thickness, gait mechanics, and subchondral bone mineral density. *Osteoarthritis Cartilage* **2018**, *26*, 1425-1437, doi:10.1016/j.joca.2018.06.017.
3. Goldring, S.R.; Goldring, M.B. Changes in the osteochondral unit during osteoarthritis: structure, function and cartilage-bone crosstalk. *Nat Rev Rheumatol* **2016**, *12*, 632-644, doi:10.1038/nrrheum.2016.148.
4. Findlay, D.M.; Kuliwaba, J.S. Bone–cartilage crosstalk: a conversation for understanding osteoarthritis. *Bone research* **2016**, *4*, 16028.
5. Zhou, X.; Cao, H.; Yuan, Y.; Wu, W. Biochemical Signals Mediate the Crosstalk between Cartilage and Bone in Osteoarthritis. *BioMed research international* **2020**, *2020*.
6. Omoumi, P.; Babel, H.; Jolles, B.M.; Favre, J. Relationships between cartilage thickness and subchondral bone mineral density in non-osteoarthritic and severely osteoarthritic knees: In vivo concomitant 3D analysis using CT arthrography. *Osteoarthritis Cartilage* **2019**, *27*, 621-629, doi:10.1016/j.joca.2018.12.014.
7. Babel, H.; Omoumi, P.; Andriacchi, T.P.; Jolles, B.M.; Favre, J. New insight on the subchondral bone and cartilage functional unit: bone mineral density and cartilage thickness are spatially correlated in non-osteoarthritic femoral condyles. *Osteoarthritis Cartilage Open* **2020**, 100079.
8. Favre, J.; Scanlan, S.F.; Erhart-Hledik, J.C.; Blazek, K.; Andriacchi, T.P. Patterns of femoral cartilage thickness are different in asymptomatic and osteoarthritic knees and can be used to detect disease-related differences between samples. *J Biomech Eng* **2013**, *135*, 101002-101010, doi:10.1115/1.4024629.
9. Omoumi, P.; Michoux, N.; Roemer, F.W.; Thienpont, E.; Berg, B.V. Cartilage thickness at the posterior medial femoral condyle is increased in femorotibial knee osteoarthritis: a cross-sectional CT arthrography study (Part 2). *Osteoarthr Cartilage* **2015**, *23*, 224-231.
10. Omoumi, P.; Babel, H.; Jolles, B.M.; Favre, J. Quantitative regional and sub-regional analysis of femoral and tibial subchondral bone mineral density (sBMD) using computed tomography (CT): comparison of non-osteoarthritic (OA) and severe OA knees. *Osteoarthritis Cartilage* **2017**, *25*, 1850-1857, doi:10.1016/j.joca.2017.07.014.
11. Favre, J.; Erhart-Hledik, J.C.; Blazek, K.; Fasel, B.; Gold, G.E.; Andriacchi, T.P. Anatomically Standardized Maps Reveal Distinct Patterns of Cartilage Thickness With Increasing Severity of Medial Compartment Knee Osteoarthritis. *J Orthop Res* **2017**, *35*, 2442-2451, doi:10.1002/jor.23548.
12. Favre, J.; Babel, H.; Cavinato, A.; Blazek, K.; Jolles, B.M.; Andriacchi, T.P. Analyzing Femorotibial Cartilage Thickness Using Anatomically Standardized Maps: Reproducibility and Reference Data. *Journal of Clinical Medicine* **2021**, *10*, 461.
13. Koo, S.; Gold, G.E.; Andriacchi, T.P. Considerations in measuring cartilage thickness using MRI: factors influencing reproducibility and accuracy. *Osteoarthritis Cartilage* **2005**, *13*, 782-789, doi:10.1016/j.joca.2005.04.013.

14. Lee, S.-I. Developing a bivariate spatial association measure: an integration of Pearson's r and Moran's I. *Journal of geographical systems* **2001**, *3*, 369-385.
15. Wirth, W.; Eckstein, F. A technique for regional analysis of femorotibial cartilage thickness based on quantitative magnetic resonance imaging. *IEEE Trans. Med. Imaging* **2008**, *27*, 737-744, doi:10.1109/TMI.2007.907323.

Comprehensive description of CTh, sBMD and their association using 3D anatomically standardized maps

Abstract

Purpose: The objective of this study was to characterize spatial variations in cartilage thickness (CTh) and subchondral bone mineral density (sBMD) in knee spanning all osteoarthritis (OA) severities.

Methods: Computed tomography arthrography examinations for 49 non-OA (Kellgren and Lawrence (K/L) scores 0-1) and 77 knees of varying medial OA severity (K/L 2 to 4) were segmented to create three-dimensional bone and cartilage models. Every point of the subchondral bone surface was given a CTh and sBMD value, as well as a measure of the local spatial adaptation (Lee's L_i between CTh and sBMD). The bone models were then anatomically standardized to a reference knee using computational anatomy algorithms. Differences maps and statistical parametric mapping were used to compare the non-OA and the three OA subgroups.

Results: The analysis showed distinct patterns of CTh, sBMD and L_i forming a coherent succession from the non-OA to the K/L 4 subgroups. The femorotibial patterns included thinner medial cartilage, thicker medial and lateral cartilage, higher medial sBMD, and lower L_i medially and laterally. Notably, the adaptation between CTh and sBMD progressively decreased from globally positive in non-OA knees to locally negative in K/L 2-4 knees.

Conclusions: This study used computational anatomy algorithms to simultaneously assess spatial patterns in CTh, sBMD, and the relationship between these properties. The methods were shown to be reproducible, and offer promising possibilities to improve our understanding of bone alterations in the context of integrated OA research.

1. Introduction

Knee osteoarthritis, a major public health burden [1,2], is considered as a disease of the whole joint. In particular, while cartilage has been the focus of early OA research, knee OA is now considered as a disease of the entire organ, including multiple pathogenetic mechanisms [3,4]. Furthermore, recent models in integrated OA research have suggested that joint components involved in OA should be considered in the context of the whole joint rather than in isolation [5,6], recognizing the interplay between these components.

The osteochondral unit, which is thought to play a key role in the initiation and progression of the disease [7,8], is particularly interesting in the perspective of integrated OA research. Indeed, there is evidence of physiological interactions [9] and biomechanical coupling [10-12] between these two mechanosensitive tissues, and the integrity of

both tissues is required for adequate function of the knee joint [13]. However, while cartilage has been widely studied [4], there is a paucity of in vivo data simultaneously assessing cartilage and bone properties, in particular at intermediate stages of disease severity [14-17]. Furthermore, the assessment of cartilage and bone properties, as well as of their relationship, has mostly relied on limited sets of values acquired by averaging tissue properties within regions of interest [16-21]. In contrast, there is evidence that the assessment of spatial variations in tissue properties is more sensitive to OA [21-23]. More recently, computational anatomy methods have been proposed to provide an anatomical standardization for the distal femur and proximal tibia, allowing a comprehensive comparison of knees [19,24-28]. In particular, such algorithms have been applied to create anatomically standardized maps of cartilage thickness (CTh) [19,26] and subchondral bone mineral density (sBMD) [16,29]. While providing novel *in vivo* data related to the osteochondral unit, the potential of these maps to simultaneously assess spatial variations in multiple tissue properties or relationships has not been achieved yet. Indeed, their use has focused on comprehensively assessing isolated components [19], or quantifying the spatial relationship between CTh and sBMD within ROIs [16,29].

As such, this study aimed to characterize spatial patterns related to knee OA in femorotibial CTh, sBMD and in their relationship using anatomically standardized maps. This study also aimed to provide an in vivo evaluation of the reproducibility of these maps for future research and clinical applications.

2. Materials and Methods

2.1. Population sample

For this study, 136 patients were retrospectively included (one knee per patient) from the institution's database. Patients above the age of 50 years and for whom a CT arthrograms of the knees as well as weight-bearing radiographs were available on the same day were eligible. Exclusion criteria included previous bone fracture, any imaging sign of previous knee surgery, post-traumatic or rheumatological disorders, as well as poor image quality. In addition, knees for which the field of view did not include a sufficient depth below the articular surface of the tibia were excluded. The medial, lateral and patellofemoral compartments were graded using a modified Kellgren-Lawrence (K/L) grade [30] and four groups were created based on the K/L grade in the medial femorotibial compartment: non-OA (K/L $\leq$ 1), K/L 2, K/L 3 and K/L 4.

Patient demographic data are reported in Table 1. There were no significant differences in patient sex (p = 0.40), age (p = 0.09), femoral bone size (p = 0.61), represented by the bicondylar femoral diameter, or tibial bone size (p =

0.30), represented by the tibial diameter, measured following previously reported methodology [31,32]. The study was approved by the institutional ethical committee without requirement for informed consent of participants due to the retrospective study design.

Table 1. Demographic data for the non-OA and K/L 2, 3 and 4 subgroups.

	non-OA (n = 49)	K/L 2 (n = 33)	K/L 3 (n = 32)	K/L 4 (n = 22)
Gender (female/male)	31 / 18	22 / 11	18 / 14	10 / 12
Age (years)	58.6 [55.7, 62.8]	58.9 [54.1, 67.7]	61.8 [55.3, 75.9]	62.6 [57.4, 69.0]
Tibial bone size (cm)	7.2 [6.9, 7.8]	7.2 [6.9, 7.8]	7.4 [6.9, 7.8]	7.6 [7.2, 7.8]
Femoral bone size (cm)	7.9 [7.5, 8.4]	7.8 [7.6, 8.7]	8.1 [7.8, 8.6]	8.3 [7.6, 8.5]

Data are presented as either number or median [1st quartile, 3rd quartile]. MFT: medial femorotibial compartment, K/L: Kellgren and Lawrence.

2.2 Image acquisition and processing

CT examinations were performed after intraarticular injection of 10 mL of ionic contrast material [17,18], and acquired with the patient supine, with extension of the knee, on a 40-detector row CT scanner (Somatom Definition AS; Siemens Healthcare, Forchheim, Germany). The following acquisition parameters were used: tube voltage, 120 kVp; reference tube current-time product, 350 mAs with the application of a dose modulation protocol (Care Dose 3D; Siemens Healthcare); bone convolution kernel (U70u), voxel size of 0.3 × 0.3 × 0.3 mm.

2.3 sBMD, CTh and their association

The femorotibial bone and cartilage were segmented semi-manually on each CT arthrogram [17,19,33]. 3D mesh models of the tissues were reconstructed using previously published methods, and a CTh and sBMD value was assigned to each vertex identified as subchondral bone [17]. In addition, the similarity between CTh and sBMD at each subchondral bone vertex was assessed by calculating Lee's $L_{i[34]}$, a measure of bivariate spatial association extending bivariate association measures by accounting for the spatial distribution of the two maps in the neighborhood of the vertex. Positive (resp. negative) values indicate a positive (resp. negative) spatial association between CTh and sBMD.

The femoral and tibial bones resulting from each segmentation were then registered to a reference tibia and femur, using previously published methods [24,25], and the CTh, sBMD and similarity values embedded in the vertices were projected on the reference femur and tibia.

3

2.4 Inter-operator reproducibility

The inter-operator reproducibility was assessed using 10 knees from 10 subjects (4 non-OA, 2 K/L 2, 2 K/L 3, 2 K/L 4) that were segmented by two operators and anatomically standardized as described previously, resulting in two sets of ten knees. The accuracy and precision of the pipeline was calculated as the mean (μ) and standard deviation (σ) of the error [35]. Similarly, the agreement was evaluated using a two-way random-effects intraclass correlation coefficient (ICC) [35,36]. The agreement was classified as poor (ICC < 0.5), moderate (0.5 ≤ ICC < 0.75), good (0.75 ≤ ICC < 0.9) and excellent (ICC > 0.9) [37].

2.5 Statistical analyses

For each vertex of the reference models identified as subchondral bone, independent sample t-tests were used to assess differences between the non-OA subgroup and the K/L 2, 3 and 4 subgroups. *P* values were corrected for multiple comparisons using the false discovery rate correction algorithm (FDR), with $q = 0.05$ [38].

3. Results

3.1 Evaluation of the inter-operator reproducibility

The median inter-operator accuracy was lower, in absolute value, than 0.06 mm for CTh, 16.01 HU for sBMD and BMD, and 0.06 unit for the similarity. The median inter-operator precision was lower than 0.31 mm for CTh, 38.36 HU for sBMD and BMD, and 0.41 unit for the similarity, representing 1.6 to 8.4% of the range of values found within the test knees. Lastly, the median inter-operator agreement was excellent for sBMD, BMD and tibial CTh (≥ 0.90) and good for similarity and femoral CTh (≥ 0.82).

Table 2. Accuracy, precision and agreement for CTh, sBMD and Lee's Li

	CTh	sBMD	L_i
Accuracy (μ)			
Femur	0.06 [-0.06, 0.21]	-7.89 [-22.61, 5.84]	-0.01 [-0.09, 0.03]
Tibia	0.01 [-0.09, 0.18]	-16.01 [-33.32, -5.73]	-0,06 [-0.12, 0.00]
Precision (σ)			
Femur	0.31 [0.24, 0.34]	33.54 [31.26, 38.84]	0.41 [0.35, 0.44]
Tibia	0.30 [0.25, 0.33]	34.21 [20.76, 33.35]	0.36 [0.35, 0.38]
Agreement (ICC)			
Femur	0.87 [0.83, 0.89]	0.97 [0.97, 0.97]	0.82 [0.75, 0.87]
Tibia	0.90 [0.87, 0.92]	0.99 [0.97, 0.99]	0.84 [0.71, 0.91]

Data are CTh in millimeters; sBMD in Hounsfield units; Lee's Li is unitless; presented as median [1st quartile, 3rd quartile].

The simultaneous analysis of femorotibial CTh, sBMD and similarity showed distinct patterns of each subgroup, forming a clear succession from the non-OA knees to K/L 4 knees.

Qualitative analyses of the medial tibial compartment indicated patterns of thinner cartilage medially and centrally, as well as thicker cartilage posteriorly (Figure 1.A); increased sBMD medially (Figure 1.B); lower similarity medially and centrally (Figure 1.C). The statistical analysis of tibial maps indicated that CTh, sBMD and similarity differences medially and centrally achieved statistical significance between the K/L 3, 4 and non-OA subgroups, while CTh differences posteriorly achieved statistical significance only between the K/L 4 and non-OA subgroup. Thicker cartilage, decreased sBMD and lower similarity were also observed in the lateral tibial compartment (Figure 1). Lateral differences achieved statistical significance only between the K/L 4 and K/L 0 subgroups.

Qualitative analyses of the load-bearing region of the femoral condyles (Figure 2) indicated thinner cartilage (Figure 2.A), increased sBMD (Figure 2.B) and decreased similarity (Figure 2.C) in most of the medial compartment. Furthermore, patterns of thicker cartilage (Figure 2.A) and decreased sBMD (Figure 2.B) were observed in the posterior aspect of the medial condyle, as well as in the lateral condyle.

5

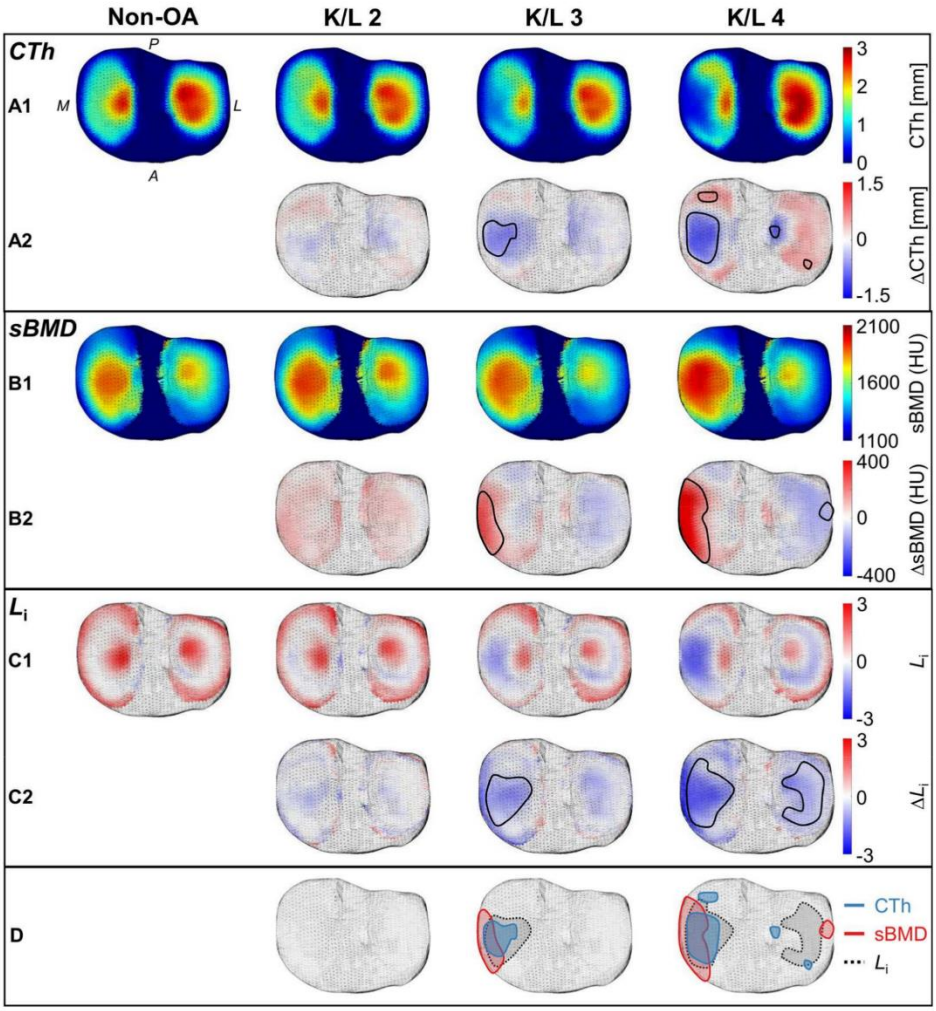

Figure 1. Transverse view of the average tibial maps of CTh (A), sBMD (B) and similarity (C) for each severity group (A1, B1, C1); average tibial difference map between K/L 2, 3, 4 and the non-OA group (A2, B2, C2); summary of the differences achieving statistical significance (D). The black line in the average difference maps (A2, B2, C2) indicates tibial vertices for which differences achieved statistical significance (adjusted $p < 0.05$).

6

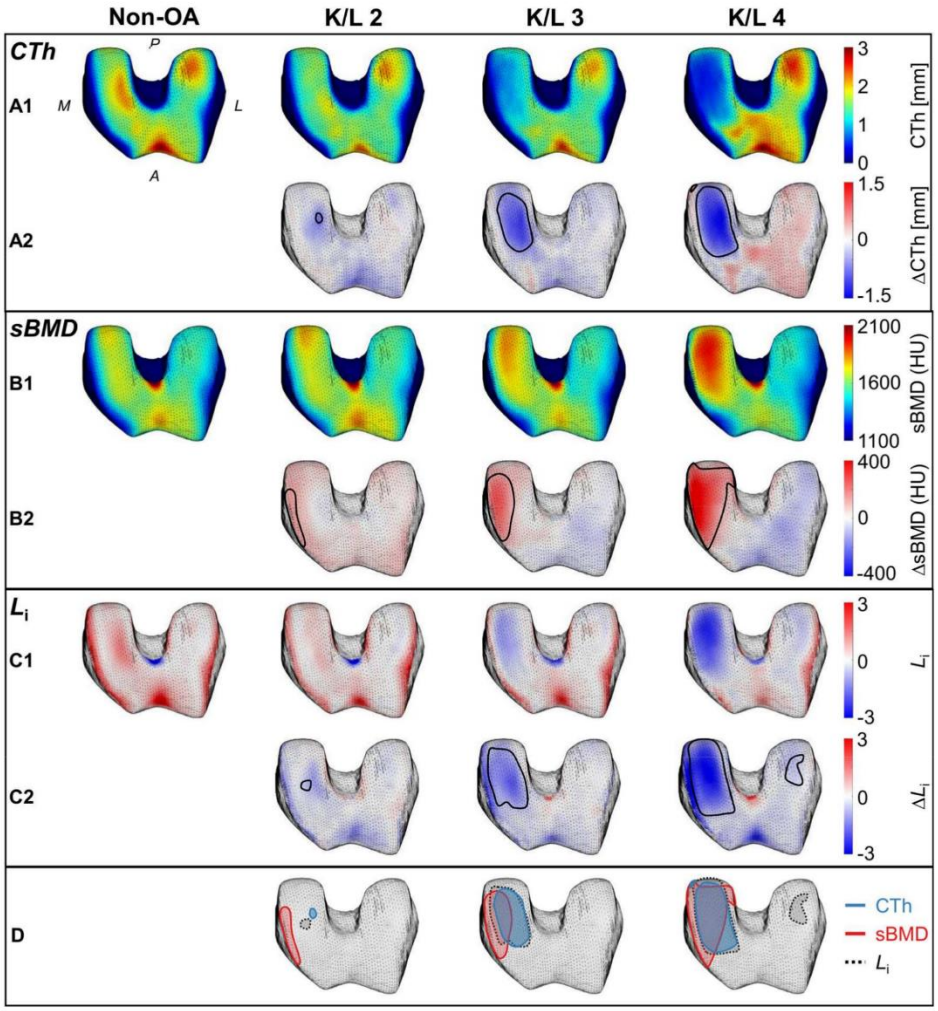

Figure 2. Transverse view of the average femoral maps of CTh (A), sBMD (B) and similarity (C) for each severity group (A1, B1, C1); average femoral difference map between K/L 2, 3, 4 and the non-OA group (A2, B2, C2); summary of the differences achieving statistical significance (D). The black line in the average difference maps (A2, B2, C2) indicates femoral vertices for which differences achieved statistical significance (adjusted $p < 0.05$).

4. Discussion

In this study, we characterized patterns related to the radiographic severity of OA knees within tissue parameters of interest in the pathophysiology of OA. The femorotibial maps showed characteristic patterns for each subgroup, forming a coherent succession from non-OA to severe OA knees. In addition, the results of the evaluation supported

the promising possibilities offered by computational anatomy algorithms in the comprehensive assessment of tissues properties.

The analysis of CTh and sBMD indicated clears patterns associated with disease severity, with thinner cartilage and increased sBMD in most of the medial femorotibial compartment. In addition, thicker cartilage in the posterior region of the medial condyle and medial compartment, as well as decreased sBMD in the lateral femorotibial compartment were also reported. The observed CTh patterns were consistent with previous studies reporting thinner cartilage in the medial compartment [17,19], and thicker cartilage in the posterior aspect of the condyles with OA[19,39]. In addition, the areas of lowest CTh in severe OA knees is also consistent cartilage denudation observed in two previous studies [26]. Similarly, the sBMD patterns observed were consistent with previous studies reporting increased sBMD in the medial condyle and the external region of the medial compartment and decreased sBMD in the lateral compartment with OA [17,18]. Furthermore, the combination of the medial and lateral sBMD patterns is consistent with increased medial-to-lateral sBMD ratios observed in non-OA compared to severe OA knees [18]. The increased sBMD in the external medial femorotibial compartment could be explained by biomechanical alterations observed with medial knee OA, leading to denser bone in the most external aspect of the medial compartment [40-42]. Interestingly, the simultaneous assessment of CTh and sBMD alterations suggests that theses alterations do not occur in the same areas (Figure 3). Indeed, increased bone density was first observed in the external region of K/L 2 and 3 knees, while cartilage thinning was more central within the femoral condyle in K/L 2 and 3 femurs. The partial overlap between CTh and sBMD alterations highlights the limitations of assessing tissue properties using ROIs, as well as the potential of assessing spatial variations in tissue properties.

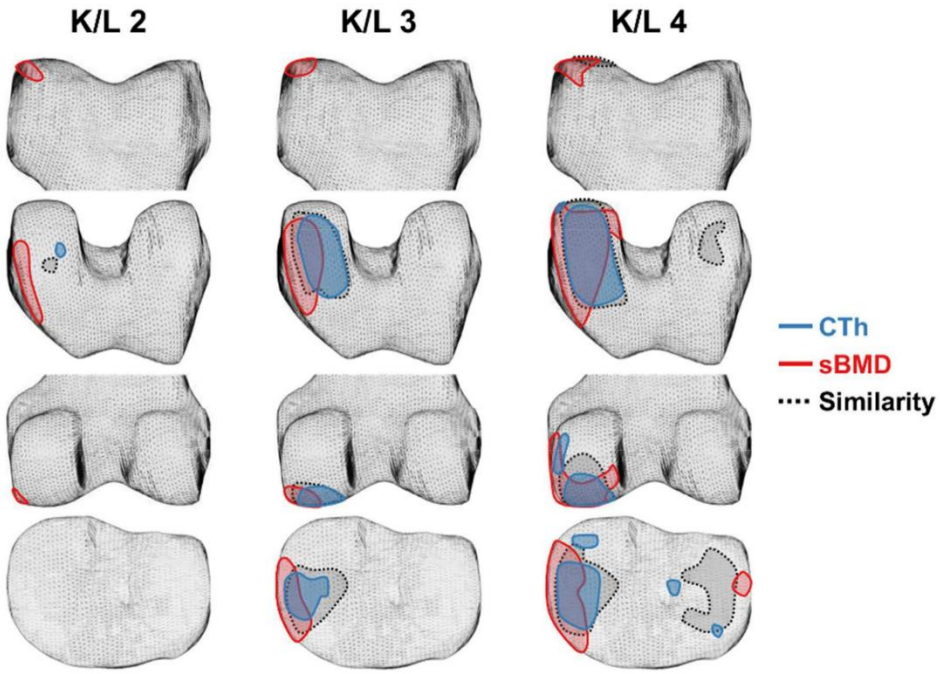

Figure 3. Summary of the CTh, sBMD and similarity differences between the non-OA and the K/L2, 3 and 4 subgroups. The blue, red and black lines indicate femorotibial vertices for which differences in CTh, sBMD and similarity achieved statistical significance (adjusted $p < 0.05$).

Similarity patterns in the knee indicated a positive spatial relationship between CTh and sBMD within the femorotibial compartments that decreases globally with the course of the disease. In particular, while femorotibial CTh and sBMD remain spatially associated in K/L 2, this relationship was negative in K/L 3 knees, suggesting that thinner cartilage is associated with denser bone. Point of inversion. The results agree with previous literature showing a positive spatial relationship between CTh and sBMD within non-OA knees[16,29], and a decrease with increasing OA severity[29]. In contrast to a previous study by the authors assessing the spatial relationship within femoral and tibial regions of interest, the assessment of spatial variations in similarity allowed the detection of specific patterns within the joint. Indeed, while the point of inversion within the medial femorotibial compartment occurred between K/L 3 and K/L 4 knees, the results of the present study indicate that, within parts of the medial condyle and of the tibial compartments, a local inversion occurs earlier. Lastly, assessing the relationship between CTh and sBMD revealed patterns of decreased adaptation within the lateral femorotibial compartment that were not seen by either of the individual components (Figure 5), stressing the potential of considering the relationship between tissue properties

rather than assessing them in isolation [5]. More broadly, the results of the similarity analysis support integrated OA model, by providing evidence of a spatial adaptation in non-OA knees.

The results of the evaluation were in agreement with previous studies assessing anatomically standardized CTh maps in healthy knees [35], and sBMD in cadaveric knees [24]. In addition, the precision represented 1.7 to 9.8 times the amplitude of differences achieving statistical significance between non-OA and K/L 2, 3 or 4 knees. As such, the evaluation results indicate that the pipeline is applicable *in vivo* and in a sample representative of the general population.

This study presents several limitations, including its cross-sectional, retrospective design. In addition, the evaluation relied on a resegmentation of the same scan, because subjecting individuals to repeated CT scans would have represented unnecessary and unethical risks [43]. Lastly, although the evaluation relied on a small sample size, it is consistent with previous evaluations of computational anatomy in the knee or hip joint [24,35,44,45]

5. Conclusion

In conclusion, this study used computational anatomy algorithms to characterize spatial patterns in bone and cartilage properties within the distal femur and proximal tibia. The methods were shown to be reproducible, and offer promising possibilities to improve our understanding of bone alterations in the context of integrated OA research.

References

1. Rabenda, V.; Manette, C.; Lemmens, R.; Mariani, A.M.; Struvay, N.; Reginster, J.Y. Direct and indirect costs attributable to osteoarthritis in active subjects. *J. Rheumatol.* **2006**, *33*, 1152-1158.
2. Reginster, J.Y. The prevalence and burden of arthritis. *Rheumatology (Oxford)* **2002**, *41 Supp 1*, 3-6.
3. Loeser, R.F.; Goldring, S.R.; Scanzello, C.R.; Goldring, M.B. Osteoarthritis: a disease of the joint as an organ. *Arthritis Rheum* **2012**, *64*, 1697-1707, doi:10.1002/art.34453.
4. Conaghan, P.G.; Kloppenburg, M.; Schett, G.; Bijlsma, J.W.J. Osteoarthritis research priorities: a report from a EULAR ad hoc expert committee. **2014**, *73*, 1442-1445, doi:10.1136/annrheumdis-2013-204660 %J Annals of the Rheumatic Diseases.
5. Edd, S.N.; Omoumi, P.; Andriacchi, T.P.; Jolles, B.M.; Favre, J. Modeling knee osteoarthritis pathophysiology using an integrated joint system (IJS): a systematic review of relationships among cartilage thickness, gait mechanics, and subchondral bone mineral density. *Osteoarthritis Cartilage* **2018**, *26*, 1425-1437, doi:10.1016/j.joca.2018.06.017.
6. Andriacchi, T.P.; Favre, J.; Erhart-Hledik, J.C.; Chu, C.R. A Systems View of Risk Factors for Knee Osteoarthritis Reveals Insights into the Pathogenesis of the Disease. *Annals of Biomedical Engineering* **2015**, *43*, 376-387, doi:10.1007/s10439-014-1117-2.
7. Madry, H.; Luyten, F.P.; Facchini, A. Biological aspects of early osteoarthritis. *Knee Surg Sports Traumatol Arthrosc* **2012**, *20*, 407-422, doi:10.1007/s00167-011-1705-8.
8. Radin, E.L.; Rose, R.M. Role of subchondral bone in the initiation and progression of cartilage damage. *Clinical orthopaedics and related research* **1986**, 34-40.
9. Imhof, H.; Sulzbacher, I.; Grampp, S.; Czerny, C.; Youssefzadeh, S.; Kainberger, F. Subchondral bone and cartilage disease: a rediscovered functional unit. *Investigative radiology* **2000**, *35*, 581-588.
10. Findlay, D.M.; Kuliwaba, J.S. Bone–cartilage crosstalk: a conversation for understanding osteoarthritis. *Bone research* **2016**, *4*, 16028.

11. Goldring, S.R.; Goldring, M.B. Changes in the osteochondral unit during osteoarthritis: structure, function and cartilage-bone crosstalk. *Nat Rev Rheumatol* **2016**, *12*, 632-644, doi:10.1038/nrrheum.2016.148.
12. Andriacchi, T.P.; Koo, S.; Scanlan, S.F. Gait mechanics influence healthy cartilage morphology and osteoarthritis of the knee. *J Bone Joint Surg Am* **2009**, *91 Suppl 1*, 95-101, doi:10.2106/JBJS.H.01408.
13. Bobinac, D.; Spanjol, J.; Zoricic, S.; Maric, I. Changes in articular cartilage and subchondral bone histomorphometry in osteoarthritic knee joints in humans. *Bone* **2003**, *32*, 284-290, doi:10.1016/s8756-3282(02)00982-1.
14. Dore, D.; Quinn, S.; Ding, C.; Winzenberg, T.; Jones, G. Correlates of subchondral BMD: a cross-sectional study. *J Bone Miner Res* **2009**, *24*, 2007-2015, doi:10.1359/jbmr.090532.
15. Cao, Y.; Stannus, O.P.; Aitken, D.; Cicuttini, F.; Antony, B.; Jones, G.; Ding, C. Cross-sectional and longitudinal associations between systemic, subchondral bone mineral density and knee cartilage thickness in older adults with or without radiographic osteoarthritis. *Ann Rheum Dis* **2014**, *73*, 2003-2009, doi:10.1136/annrheumdis-2013-203691.
16. Babel, H.; Omoumi, P.; Andriacchi, T.P.; Jolles, B.M.; Favre, J. New insight on the subchondral bone and cartilage functional unit: bone mineral density and cartilage thickness are spatially correlated in non-osteoarthritic femoral condyles. *Osteoarthritis Cartilage Open* **2020**, 100079.
17. Omoumi, P.; Babel, H.; Jolles, B.M.; Favre, J. Relationships between cartilage thickness and subchondral bone mineral density in non-osteoarthritic and severely osteoarthritic knees: In vivo concomitant 3D analysis using CT arthrography. *Osteoarthritis Cartilage* **2019**, *27*, 621-629, doi:10.1016/j.joca.2018.12.014.
18. Omoumi, P.; Babel, H.; Jolles, B.M.; Favre, J. Quantitative regional and sub-regional analysis of femoral and tibial subchondral bone mineral density (sBMD) using computed tomography (CT): comparison of non-osteoarthritic (OA) and severe OA knees. *Osteoarthritis Cartilage* **2017**, *25*, 1850-1857, doi:10.1016/j.joca.2017.07.014.
19. Favre, J.; Erhart-Hledik, J.C.; Blazek, K.; Fasel, B.; Gold, G.E.; Andriacchi, T.P. Anatomically Standardized Maps Reveal Distinct Patterns of Cartilage Thickness With Increasing Severity of Medial Compartment Knee Osteoarthritis. *J Orthop Res* **2017**, *35*, 2442-2451, doi:10.1002/jor.23548.
20. Wirth, W.; Eckstein, F. A technique for regional analysis of femorotibial cartilage thickness based on quantitative magnetic resonance imaging. *IEEE Trans. Med. Imaging* **2008**, *27*, 737-744, doi:10.1109/TMI.2007.907323.
21. Favre, J.; Scanlan, S.F.; Erhart-Hledik, J.C.; Blazek, K.; Andriacchi, T.P. Patterns of femoral cartilage thickness are different in asymptomatic and osteoarthritic knees and can be used to detect disease-related differences between samples. *J Biomech Eng* **2013**, *135*, 101002-101010, doi:10.1115/1.4024629.
22. Pedoia, V.; Lee, J.; Norman, B.; Link, T.M.; Majumdar, S. Diagnosing osteoarthritis from T2 maps using deep learning: an analysis of the entire Osteoarthritis Initiative baseline cohort. *Osteoarthr Cartilage* **2019**, *27*, 1002-1010.
23. Kokkotis, C.; Moustakidis, S.; Papageorgiou, E.; Giakas, G.; Tsaopoulos, D.E. Machine learning in knee osteoarthritis: A review. *Osteoarthritis and Cartilage Open* **2020**, 100069.
24. Babel, H.; Omoumi, P.; Cosendey, K.; Cadas, H.; Jolles, B.M.; Favre, J. Three-Dimensional Quantification of Bone Mineral Density in the Distal Femur and Proximal Tibia Based on Computed Tomography: In Vitro Evaluation of an Extended Standardization Method. *J Clin Med* **2021**, *10*, 160, doi:10.3390/jcm10010160.
25. Babel, H.; Wageli, L.; Sonmez, B.; Thiran, J.-P.; Omoumi, P.; Jolles, B.; Favre, J. A Registration Method for Three-Dimensional Analysis of Bone Mineral Density in the Proximal Tibia. *J. Biomech. Eng.* **2020**, 10.1115/1.4048335, doi:10.1115/1.4048335.
26. Bowes, M.A.; McLure, S.W.; Wolstenholme, C.B.; Vincent, G.R.; Williams, S.; Grainger, A.; Conaghan, P.G. Osteoarthritic bone marrow lesions almost exclusively colocate with denuded cartilage: a 3D study using data from the Osteoarthritis Initiative. *Ann Rheum Dis* **2016**, *75*, 1852-1857, doi:10.1136/annrheumdis-2015-208407.
27. Hunter, D.; Nevitt, M.; Lynch, J.; Kraus, V.B.; Katz, J.N.; Collins, J.E.; Bowes, M.; Guermazi, A.; Roemer, F.W.; Losina, E. Longitudinal validation of periarticular bone area and 3D shape as biomarkers for knee OA progression? Data from the FNIH OA Biomarkers Consortium. *Annals of the rheumatic diseases* **2016**, *75*, 1607-1614.
28. Neogi, T.; Bowes, M.A.; Niu, J.; De Souza, K.M.; Vincent, G.R.; Goggins, J.; Zhang, Y.; Felson, D.T. Magnetic Resonance Imaging–Based Three-Dimensional Bone Shape of the Knee Predicts Onset of Knee Osteoarthritis: Data From the Osteoarthritis Initiative. **2013**, *65*, 2048-2058, doi:https://doi.org/10.1002/art.37987.
29. Babel, H.; Omoumi, P.; Andriacchi, T.; Jolles, B.; Favre, J. Decreased adaptation of cartilage thickness (CTh) and bone mineral density (sBMD) spatial variations in osteoarthritic versus non-osteoarthritic knees **2021**.
30. Felson, D.T.; McAlindon, T.E.; Anderson, J.J.; Weissman, B.W.; Aliabadi, P.; Evans, S.; Levy, D.; LaValley, M.P. Defining radiographic osteoarthritis for the whole knee. *Osteoarthr Cartilage* **1997**, *5*, 241-250.
31. Omoumi, P.; Michoux, N.; Roemer, F.W.; Thienpont, E.; Berg, B.V. Cartilage thickness at the posterior medial femoral condyle is increased in femorotibial knee osteoarthritis: a cross-sectional CT arthrography study (Part 2). *Osteoarthr Cartilage* **2015**, *23*, 224-231.

32. Moyer, R.; Wirth, W.; Duryea, J.; Eckstein, F. Anatomical alignment, but not goniometry, predicts femorotibial cartilage loss as well as mechanical alignment: data from the Osteoarthritis Initiative. *Osteoarthritis Cartilage* **2016**, *24*, 254-261, doi:10.1016/j.joca.2015.08.016.
33. Koo, S.; Gold, G.E.; Andriacchi, T.P. Considerations in measuring cartilage thickness using MRI: factors influencing reproducibility and accuracy. *Osteoarthritis Cartilage* **2005**, *13*, 782-789, doi:10.1016/j.joca.2005.04.013.
34. Lee, S.-I. Developing a bivariate spatial association measure: an integration of Pearson's r and Moran's I. *Journal of geographical systems* **2001**, *3*, 369-385.
35. Favre, J.; Babel, H.; Cavinato, A.; Blazek, K.; Jolles, B.M.; Andriacchi, T.P. Analyzing Femorotibial Cartilage Thickness Using Anatomically Standardized Maps: Reproducibility and Reference Data. *Journal of Clinical Medicine* **2021**, *10*, 461.
36. McGraw, K.O.; Wong, S.P. Forming inferences about some intraclass correlation coefficients. *J Psychological methods* **1996**, *1*, 30.
37. Koo, T.K.; Li, M.Y. A Guideline of Selecting and Reporting Intraclass Correlation Coefficients for Reliability Research. *J Chiropr Med* **2016**, *15*, 155-163, doi:10.1016/j.jcm.2016.02.012.
38. Genovese, C.R.; Lazar, N.A.; Nichols, T. Thresholding of statistical maps in functional neuroimaging using the false discovery rate. *Neuroimage* **2002**, *15*, 870-878, doi:10.1006/nimg.2001.1037.
39. Omoumi, P.; Babel, H.; Jolles, B.M.; Favre, J. Cartilage can be thicker in advanced osteoarthritic knees: a tridimensional quantitative analysis of cartilage thickness at posterior aspect of femoral condyles. *The British journal of radiology* **2018**, *91*, 20170729.
40. Sharma, L. The role of varus and valgus alignment in knee osteoarthritis. *Arthritis & Rheumatism* **2007**, *56*, 1044-1047.
41. Saari, T.; Carlsson, L.; Karlsson, J.; Kärrholm, J. Knee kinematics in medial arthrosis. Dynamic radiostereometry during active extension and weight-bearing. *J. Biomech.* **2005**, *38*, 285-292, doi:https://doi.org/10.1016/j.jbiomech.2004.02.009.
42. Hunter, D.J.; Sharma, L.; Skaife, T. Alignment and osteoarthritis of the knee. *JBJS* **2009**, *91*, 85-89.
43. Brenner, D.J.; Hall, E.J. Computed tomography—an increasing source of radiation exposure. *N. Engl. J. Med.* **2007**, *357*, 2277-2284.
44. Carballido-Gamio, J.; Bonaretti, S.; Saeed, I.; Harnish, R.; Recker, R.; Burghardt, A.J.; Keyak, J.H.; Harris, T.; Khosla, S.; Lang, T.F. Automatic multi-parametric quantification of the proximal femur with quantitative computed tomography. *Quantitative imaging in medicine and surgery* **2015**, *5*, 552-568, doi:10.3978/j.issn.2223-4292.2015.08.02.
45. Li, W.J.; Kezele, I.; Collins, D.L.; Zijdenbos, A.; Keyak, J.; Kornak, J.; Koyama, A.; Saeed, I.; LeBlanc, A.; Harris, T., et al. Voxel-based modeling and quantification of the proximal femur using inter-subject registration of quantitative CT images. *Bone* **2007**, *41*, 888-895, doi:10.1016/j.bone.2007.07.006.